AMERICAN UNIVERSITY OF BEIRUT

DEVELOPMENT OF ANTENNAS AND SOURCES FOR HIGH POWER MICROWAVE APPLICATIONS

by
HILAL M. EL MISILMANI

A dissertation
submitted in partial fulfillment of the requirements
for the degree of Doctor of Philosophy
to the Department of Electrical and Computer Engineering
of the Faculty of Engineering and Architecture
at the American University of Beirut

Beirut, Lebanon
April 2015

AMERICAN UNIVERSITY OF BEIRUT

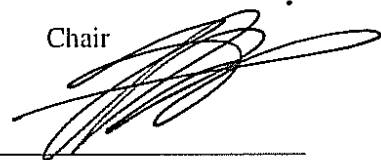# DEVELOPMENT OF ANTENNAS AND SOURCES FOR HIGH POWER MICROWAVE APPLICATIONS

by
HILAL M. EL MISILMANI

Thesis Committee:

Prof. Ali El-Hajj, Professor	Chair
AUB, Electrical and Computer Engineering	
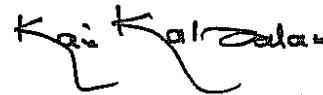
Prof. Karim Kabalan, Professor	Advisor
AUB, Electrical and Computer Engineering	

Prof. Joseph Costantine, Assistant Professor	Member of Committee
AUB, Electrical and Computer Engineering	

Prof. Youssef Nasser, Senior Lecturer	Member of Committee
AUB, Electrical and Computer Engineering	

Prof. Soubhi Abou Chahine, Professor   Member of Committee

Beirut Arab University

Prof. Christos G. Christodoulou, Professor   Member of Committee

University of New Mexico
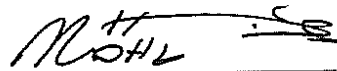
Dr. Mohammed Al-Husseini, Senior Researcher   Member of Committee

Beirut Research and Innovation Center

Date of dissertation defense: April 23rd, 2015

AMERICAN UNIVERSITY OF BEIRUT

THESIS, DISSERTATION, PROJECT
RELEASE FORM

Student Name: __El Hisimani_____Hilal_____H.__
    Last .   First   Middle

◯ Master's Thesis   ◯ Master's Project   ● Doctoral Dissertation

☐   I authorize the American University of Beirut to: (a) reproduce hard or electronic copies of my thesis, dissertation, or project; (b) include such copies in the archives and digital repositories of the University; and (c) make freely available such copies to third parties for research or educational purposes.

☒   I authorize the American University of Beirut, **three years after the date of submitting my thesis, dissertation, or project,** to: (a) reproduce hard or electronic copies of it; (b) include such copies in the archives and digital repositories of the University; and (c) make freely available such copies to third parties for research or educational purposes.

_____   __May 4, 2015__
Signature   Date

Acknowledgements

Five years ago I joined the graduate program at the American University of Beirut with one objective: receiving a PhD degree. Alhamdulillah. Today is the moment I was waiting for and dreaming of: successfully defending and submitting my PhD dissertation. This accomplishment would not have been possible without the guidance and blessing of Allah and the support of special people.

First and foremost I want to thank my advisor Dr. Karim Kabalan. It has been an honor to be his student throughout my Master's and PhD studies. I appreciate all his contributions of time, ideas, helpful and invaluable assistance, guidance and inspiration, and funding to make my graduate experience productive and stimulating. The joy and enthusiasm he has for his research was contagious and motivational for me, even during tough times of my PhD pursuit.

I would like to express my gratitude and deep appreciation as well to my PhD dissertation committee members for their continuous support, cooperation, assistance, and valuable contributions.

My deepest gratitude is also due to my dear friend, a member of my PhD dissertation committee, and my colleague in the Electromagnetics and Radio Frequency research group, Dr. Mohammed Al-Husseini, whose knowledge, helpful and invaluable assistance, have been priceless all over my thesis and research work.

Finally, to the ones who have always inspired and supported me to the fullest in all my pursuits, raised me with a love of science, and encouraged me to do my best and never quit, to my parents and family members, thank you for believing in me. And most of all for the love of my life, my wife to be, thank you for your faithful support, encouragement and patience during the tough time of my PhD journey.

What I've learned from this journey is that you always need to focus on your goals in your life, no matter what obstacles you face and difficulties you encounter. You need to wake up each day with one goal: get better every single day. You can continue sleeping with your dreams, or you can wake up and chase them! In short, if you want something, go get it, the future is promised to no one. Just remember, you can do anything you set your mind to!

An Abstract of the Dissertation of

HILAL M. EL MISILMANI   for   Doctor of Philosophy

                                             Major: Electrical and Computer Engineering

Title: Development of Antennas and Sources for High Power Microwave Applications

High Power Microwave (HPM) technology has lately been the great interest of many researchers in the area. An HPM system comprises a high power generator and a high power capable antenna. The generator has to produce the needed high voltage pulse. This pulse in turn has to be converted to a RF signal and coupled to an RF antenna part required to radiate the signal to its intended destination. This technology has found its interest in various applications ranging from commercial to military applications, such as radar and communication systems, law enforcement, materials processing, and environmental protection.

The aim of this thesis is to investigate the major parts of a High Power Microwave system, and to highlight the design and development of high power capable antennas for such applications. The generator part has to develop the needed high voltage pulse which will be converted later on to RF signal to be fed to the proper high power capable antenna. The latter has to be designed in a certain way to radiate the generated wave in a pencil shape pattern, with high gain and low sidelobe levels.

The thesis is organized as follows: The idea behind the use of HPM and its widely known applications is introduced in Chapter 1. This chapter begins with a brief introduction on the high power microwave sources and states the main objectives of the thesis. The major components of a high power microwave system are the identified and described in Chapter 2, before delving into the core of the thesis aiming at designing and implementing high power capable antennas in the second part of the thesis. The first type of antennas studied and improved is the Vlasov antenna in Chapter 3, for which an improved shape with curved cuts for High Power Microwaves applications is proposed, leading to higher gain, decreased half power beamwidth, and decreased sidelobe level. In addition, two optimized reflectors, one with enhanced position, and the second with additional shape enhancement having curved edges, are also proposed,

with the ability to radiate the maximum radiation back to the waveguide axis and further decrease the HPBW. The second type of antenna studied in this thesis and it is the main focus of this work is the Slotted Waveguide Antenna (SWA). A simple procedure for designing such SWAs with specified sidelobe level ratios (SLRs) is presented in Chapter 4, for which some general guidelines for the slots width, length and longitudinal positions are first given. Then, the offsets of the slots positions with respect to the waveguide centerline, which determine the SLR, are then obtained from well-known distributions. Illustrative examples showing the distribution coefficients, slots displacements, resulting patterns and S_{11} plots are also given. A prototype antenna was fabricated and tested, and the results are presented. Chapter 5 studies the SWA in the presence of a coaxial feed, and also serves as an introduction to two-dimensional SWA array systems. Next, the design of 2D SWA array system is described in two different approaches. The first one uses inclined coupling slots in an added SWA used as the main feeder to other SWA modules serving as branches. This is presented in Chapter 6. The procedure is explained through two examples designs of 8×8-elliptical-slot SWA arrays with SLR higher than 20 dB. Adding our contributions on the SWA design procedures, the second approach is illustrated in Chapter 7, for which an inventive and simple procedure for the design of a 2D slotted waveguide antenna having a desired sidelobe level ratio and a pencil shape pattern is presented using longitudinal elliptical slots in both branches and feeder SWAs. This is done for the radiating SWAs as well as the feed SWA. Two examples of SWA systems with 8×8 elliptical slots and 10×10 are designed using this procedure for an SLR higher than 20 dB. Finally, Chapter 8 summarizes the work done in the thesis and the future extensions and interesting research directions that can be employed to further improve the designed antennas.

Contents

List of Figures

List of Tables

Chapter 1

Introduction

Although nuclear Electromagnetic Pulse (EMP) was known since the very first days of nuclear weapons testing, the high effects of such pulses were obscured until 1962, when a thermonuclear weapon test in space, called the Starfish Prime test, took place in the pacific ocean and considered an important scientific event. The Starfish Prime test knocked out some of the electrical and electronics component, damaged and ultimately disabled of at least six orbiting satellites, and disrupted the radio transmission for very wide ranges, as far as 897 miles away from the nuclear explosion, for several hours [1, 2]. It was then suggested that, if such a such a pulse can be generated without a nuclear explosion, through a High Power Microwave system (HPM), it can be used intentionally, as a nonlethal weapon, to disturb or destroy electronic equipment without damaging the infrastructure or hurting people [3, 4]. Consequently, HPM systems are usually referred to as Intentional Electromagnetic Interference or IEMI. This HPM attack or IEMI can be either: a hard kill where the HPM pulse induces currents high enough to melt the metal on a circuit board or a voltage that will result in a flashover in sensitive electrical components and hence the electrical components are physically damaged; or a soft kill where the components are disabled with malfunction as a result

1

of applying the same order of voltage as the operating voltage to a semiconductor component.

In the recent years, High Power Microwave technology has emerged as a new technology offering new applications or innovative approaches and advances in existing applications. The microwave power level is increasing as a result of either pushing conventional microwave mechanism devices in new directions or employing new interaction mechanisms. Nowadays, HPM technology is well known in both military and commercial applications, such as radar systems, broadcasting systems, power beaming, fusion heating, directed energy weapons, and communication systems, with its future use is directed towards combat operations, law enforcement, environmental protection and materials processing [5–11]. Among these applications, the highest power requirements are for earth-to-space power beaming and directed energy weapons, with the most stressful applications in terms of volume and mass requirements are the military ones, for which, the most significant HPM weapons programs are in the United States of America, Russia, United Kingdom, France, Sweden, Germany, China, Japan, and India [3].

Another important application for HPM is its use in the remote activation of improvised explosive devices (IEDs) [12, 13], rather than using the conventional dangerous, slow and expensive mine neutralization techniques [14]. This system comprises a high-power electromagnetic generator and a high-power capable antenna. The high-power microwaves could be directed towards the target landmine/ERW to heat it or induce large currents in its detonator wires (if it contains them), leading to its detonation. This application might be useful also for any war zone situation for which usually many areas are contaminated with mines and explosive remnants of war (ERW) as a legacy of different conflicts.

In this thesis, a system of High Power Microwave is investigated, for which

2

the process of pulse generation and wave radiation through a new designed HPM capable antenna are studied. Two high power microwave capable antenna types are researched and improved. These are the Vlasov antenna [15], and the slotted waveguide array antenna [16]. These two types are the most adequate for this application and the best configuration for each of these antennas are investigated. The focus of the thesis is on improving the antennas gain, beam pointing ability and power handling capability.

High Power Microwave is defined as devices that exceed 100 MW in peak power, and span the centimeter- and millimeter-wave range of frequencies between 1 and 300 GHz, with some devices reaching a power of 15 GW, as with the Multiwave Cerenkov generators (MWCGs). A simple HPM system can be represented by the block diagram shown in Fig. 1.1. The flow of power and energy is from left to right, from the prime power generator at the input side to radiation of microwaves from the antenna at the output side to the final target. The major components needed are defined in the following:

1. A prime power: used at the input side to generate and feed a relatively low power electrical input in a long-pulse or continuous mode

2. A pulsed power: used to take the low power/long-pulse electrical power generated from the prime power, store it, and then switch it out in high power electrical pulses of shorter duration

3. A microwave source: used to transform the short-duration high power electrical pulses generated from the pulsed power to electromagnetic waves

4. A mode converter: used when a conversion of microwave generated from the microwave source is needed to couple the output of the source to the antenna

5. An antenna: used at the final stage to radiate and direct the microwave electro-

3

magnetic output, in a well-defined direction and a higher intensity beam

Figure 1.1: High power microwave system

The design of a HPM system is extremely iterative and complicated, for which the output requirements of the system affect several components used in the HPM chain and limit the usage of special components, out of these requirements we mention: the peak energy per pulse needed to be delivered to the target, the pulse repetition rate within a burst of pulses, the length of the burst of pulses, the burst repetition rate, the system volume and mass, the gain of the antenna, the frequency range of the radiated microwave, the beam pointing capability of the antenna. Several choices are available for each of the 5 components, for which the use of each choice will affect other choices in other blocks. Going into the choice in each block, under each component a set of choices are also found, some of which have sub-branches for different part choices. These all choices contribute to the design calculations. For this, the optimization of such systems should be done on the overall system, as distinct from the optimization of every element and part of the system.

As a consequence of this complexity and wide range of solutions, this thesis concentrates on the antenna part used in such systems, with a brief overview on the HPM components preceding the antenna block and preparing the pulse needed to be radiated. The major achievements of the thesis can be summarized as follows:

1. Improvement of the Vlasov antenna widely used in HPM systems in terms of breakdown capability and beam pointing angle for which conventional Vlasov antenna suffer from rotated propagation angle

2. Detailed design procedure on a how to design a one-dimensional Slotted Waveg-

4

uide Antenna with specified sidelobe level ratios in a simpler and direct way in comparison to the conventional equations

3. The use of the proposed design method to design two-dimensional Slotted Waveguide Antenna Arrays with inclined coupling slots rotated in specific angles according to the desired distribution

4. Finally, the proposed design method of the one-dimensional Slotted Waveguide Antenna is used to propose a new design of a two-dimensional Slotted waveguide Antenna Array using the same design concept in both components: the feeder and the branches. The final design achieves a gain of 25.3 dB, with sidelobe level ratios of 27.4 and 27.7 dB in E- and H-plane respectively, and half power beamwidth of $10°$ and $9.4°$ in E- and H-plane respectively, using only 10 SWA elements, in addition to a main SWA feeder

Chapter 2

High Power Microwave Systems

Before delving into the core objective of the thesis in designing suitable HPM antennas, it is important to develop a systems perspective toward high power microwave (HPM). For this, this chapter starts with a brief overview of the first three components in a HPM system, the prime power, the pulsed power and the microwave source. The final output of these three components is microwave pulses with durations of several to tens of microseconds, and peak powers of several hundreds of megawatts. Despite the very high peak power values, the average power is the kilowatt range, due to the short pulse duration. The generator should have a repetition frequency, meaning that it should be capable of re-producing the same microwave pulse every time period. Conventional high voltage generators are physically very large devices, they have slow rise-time output voltage pulse, they suffer from poor energy transfer efficiency, and they are expensive to construct and not particularly portable. In order to address the problems of load matching, energy transfer efficiency and rise-time, pulse forming network (PFN) generators have been used, as discussed in the next section. Nowadays, much high energy research equipment is operated in a pulsed mode. The reason behind working in pulsed mode is mainly to keep heat dissipation down and use high energy

that often occurs at short time scales. The final output of such systems is rectangular with well-defined output impedance which enables accurate matching of the source and load. This results in high energy transfer efficiency to the load. Following the brief description of the prime power, the pulsed power and the microwave source components, the pulse forming network (PFN) and pulse forming Line (PFL), in addition to Blumlein TL are investigated in details to have some profound knowledge on the basic mechanism of such systems.

2.1   Prime Power

The main objective of this block in a HPM system is to feed the system generating at the input a relatively low power electrical input in a long-pulse or continuous mode. The important parameters of this block are the average power, the repetition rate, and the output voltage. The average power and the repetition rate define the energy per pulse generated at the input. Several options could be employed to provide continuous prime power output, which will eventually fed as an input to the pulse power. Out of these options, a common choice is to use a generator powered by an internal combustion engine, such as the diesel alternator or the turbo alternator, but it is also possible to drive systems with batteries for long periods, such as the AgZn secondary battery or the Lithium chloride battery. In either case, either an alternating current (AC) internal combustion generator or a direct current (DC) battery provides long-pulse or continuous power. This in its turn is converted to a DC output that functions as input to the pulsed power. As for the switch used at the output, such as the spark gap, magnetic, or solid-state switches, they depend on the repetition rate for peak power.

If the system is working in burst mode, the energy has to be stored before any conversation. This will limit the first subcomponent choices of prime power to

internal combustion prime movers choices generating AC output, such as the Turbine, Diesel, Turbine-alternator, or Diesel-alternator, which should be followed in this mode by an added interface, such as the Hydraulic pump/motor/controller, Electric motor/controller, or an AC/DC converter, followed by an energy store and electrical source block, such as the Flywheel/alternator, Pulsed alternator, or High-rate secondary battery. The final output is then converted to DC to be fed to the pulse power block.

Hence, comparing the continuous and burst-mode systems in the prime power block, the key difference is the added energy storage in the burst one. The average power is much higher in the continuous mode.

2.2   Pulsed Power

The main objective of this block in a HPM system is to take the low power/long-pulse electrical power generated from the prime power, store it, and then switch it out in high power electrical pulses of shorter duration. The existing choices for this block are the modulators, Marx generators, Pulse Forming Lines (PFLs) and Pulse Forming Networks (PFNs), and inductive energy storage in combination with opening switches.

Taking the output from the prime power, the pulse power output is fed into either another pulsed power component for further pulse power compression, or directly to a microwave source, or to an impedance and voltage transformer, with the series of pulsed power components being the most typical type used. As a typical example of such connection, a Marx generator is used first to provide the input to a further stage of electrical pulse compression, such as the Pulse Forming Line. For the direct connection type, a Marx generator could be connected directly to a driving antenna (with or without a mode converter before the antenna depending on the type of the antenna

used).

Taking as input parameters generated by the prime power: the voltage, average power and repetition rate, the pulsed power output parameters should indicate: the output voltage, impedance, and pulse length, in addition to the rise and fall times needed to meet the resonance conditions necessary for the microwave source to generate the microwaves.

Hence, because of the importance of Marx generator, PFLs and PFNs in such systems, both components are investigated in Sections 2.5, 2.4.1 and 2.4 respectively.

2.3   Microwave Source

The main objective of this block in a HPM system is to transform the short-duration high power electrical pulses generated from the pulsed power to electromagnetic waves. It is usually the most complex component of the HPM system. Taking the output from the pulsed power, the microwave source outputs the following essential parameters: the peak microwave frequency, the frequency range, pulse length, and output waveguide mode (necessary to decide whether a mode converter is needed before the radiating antenna).

Several choices for microwave source are found, such as: magnetron, virtual cathode oscillator (vircator), reltrons, reflex triode, relativistic diffraction generator (RDG), gyrotron, multiwave cerenkov generator (MWCG), multiwave diffraction generator (MWDG), relativistic klystron, traveling wave tube (TWT), backward wave oscillator (BWO), cyclotron autoresonant maser (CARM), free-electron laser (FEL). Among these choices, the most commercially available types are the magnetrons, vircators, BWOs, klystrons, reltrons, and gyrotrons. A basic investigation of magnetrons is conducted in Section 2.6.

9

The microwave source can have several supporting equipment such as, a vacuum pump, a magnet, a cooling system, a collector to capture the beam, and a master oscillator.

An intensive care should be given on the design of the interface between the pulsed power and the microwave source. This comes from the importance of having the impedances of the pulsed power and the microwave source to be well-matched in order not to lose serious energy and power efficiency.

2.4   Pulse Forming Network

A pulse forming network (PFN) is an electric circuit that accumulates electrical energy over a comparatively long time, and then releases the stored energy in the form of a relatively square pulse of a brief duration for various pulsed power applications. Energy storage components such as capacitors, inductors or transmission lines are charged in a PFN by means of a high voltage power source. After charging, they rapidly discharged into a load via a high voltage switch, such as a spark gap or hydrogen thyratron. PFNs are used to produce precise nanosecond-length pulses of electricity, with repetition rates ranging from single pulses to about 10^4 pulses per second.

Mainly, a PFN consists of a series of high voltage energy storage capacitors and inductors interconnected as a "ladder network". The components behave similarly to a length of transmission line. For this, a PFN is sometimes called an "artificial, or synthetic, transmission line". Initially, the capacitors are used to store the electrical energy by a high voltage DC power supply. When the PFN is discharged, the capacitors discharge in sequence. This produces an approximately rectangular pulse, which is conducted to the load through a transmission line. To prevent losses due to energy reflection, the PFN must be impedance matched to the load impedance.

2.4.1 Transmission line PFN

To show a simple PFN, a transmission line (TL) PFN network is described here, shown in Fig. 2.1. In this simple charged transmission line pulse generator, a length of TL is connected through a switch to a matched load RL at one end, and to a DC voltage source V at the other end to through a resistor R_S. R_S is large compared to the characteristic impedance Z_0 of the line [17]. The pulse generation is as follows:

- Initially, the switch is open:

    - When the power supply is connected it slowly charges up the capacitance of the line through R$_S$

- After charging, the switch is closed:

    - the charge stored in the line begins to discharge through the load with a current of $V/2Z_0$

    - a voltage equal to V/2 is applied to the load

    - a voltage step travels up the line toward the source [18]

    - since the source end is behaving as open circuit, the step voltage is reflected toward the load [17]
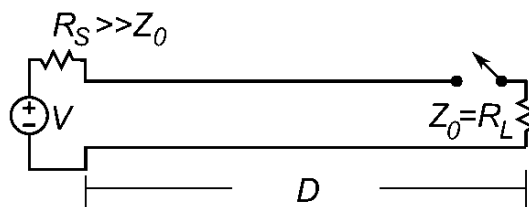
Figure 2.1: Simple charged transmission line PFN [19]

The result is that a pulse of voltage is applied to the load with a duration equal to 2D/c where D is the length of the line and c is the propagation velocity of the pulse

11

in the line [17]. A disadvantage of this simple PFN pulse generators is that the voltage stored on the line is divided equally between the load resistance and the characteristic impedance of the line as a result of the matching between the transmission line and the load resistance R_L. Hence, the voltage pulse applied to the load is only one-half the power supply voltage [17, 18].

For high power application, PFNs generally use specialized transmission lines consisting of pipes filled with oil or deionized water as a dielectric to handle the high power dissipation [18].

2.4.2 Basic Blumlein T.L. Concept

To solve the above problem and produce an output pulse equal to the power supply voltage V, Blumlein TL was invented by Alan Blumlein and is widely used today in PFN [17]. In the Blumlein generator, shown in Fig. 2.2, the load is connected in series between two transmission lines. The load R_L is made equal to twice the characteristic impedance Z_0 of the line. The mode of operation is as following:
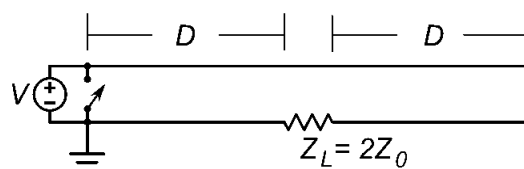
Figure 2.2: Blumlein transmission line

- Initially, the switch is open:

  - the two transmission lines are charged by a DC power supply at one end [17]

- After charging, the switch is closed:

  - since $R_L = 2Z_0$ the voltage step is half reflected and half transmitted

– two symmetrical opposite polarity voltage steps propagate away from the load, creating between them a voltage drop of $V/2 - (-V/2) = V$ across the load

– the voltage steps reflect from the ends and return, ending the pulse

The pulse duration is equal to $2D/c$ in this case.

2.4.3   Parallel-Plate Blumlein Line (PPBL)

2.4.3.1   PPBL Configuration
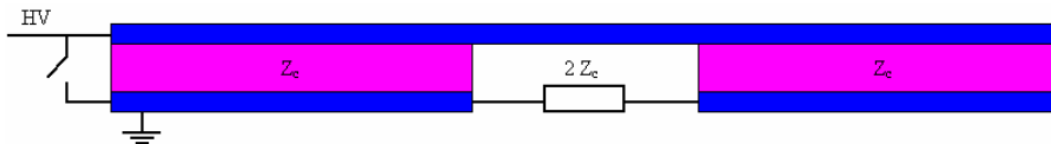
Figure 2.3: Basic form of a parallel-plate Blumlein-configuration

The basic form of a Parallel Plate Blumlein (PPBL) is shown in Fig. 2.3. It consists of two transmission lines with an additional load connected between them. The two lines have equal lengths and characteristic impedances, which are determined by:

- the width of the plates (blue-colored),

- the height of the dielectric material (pink-colored),

- the permittivity of the dielectric.

The load impedance is designed to be $2 \times Z_c$ of the single line

The upper conductor plate is constantly connected to a HV source. The bottom plate of the line next to the voltage source is grounded, whereas the bottom plate of the other line is "floating". The switch used to trigger the pulse-forming process is placed between the charged plate and the grounded plate of the line next to the source

13

2.4.3.2 PPBL Mechanism
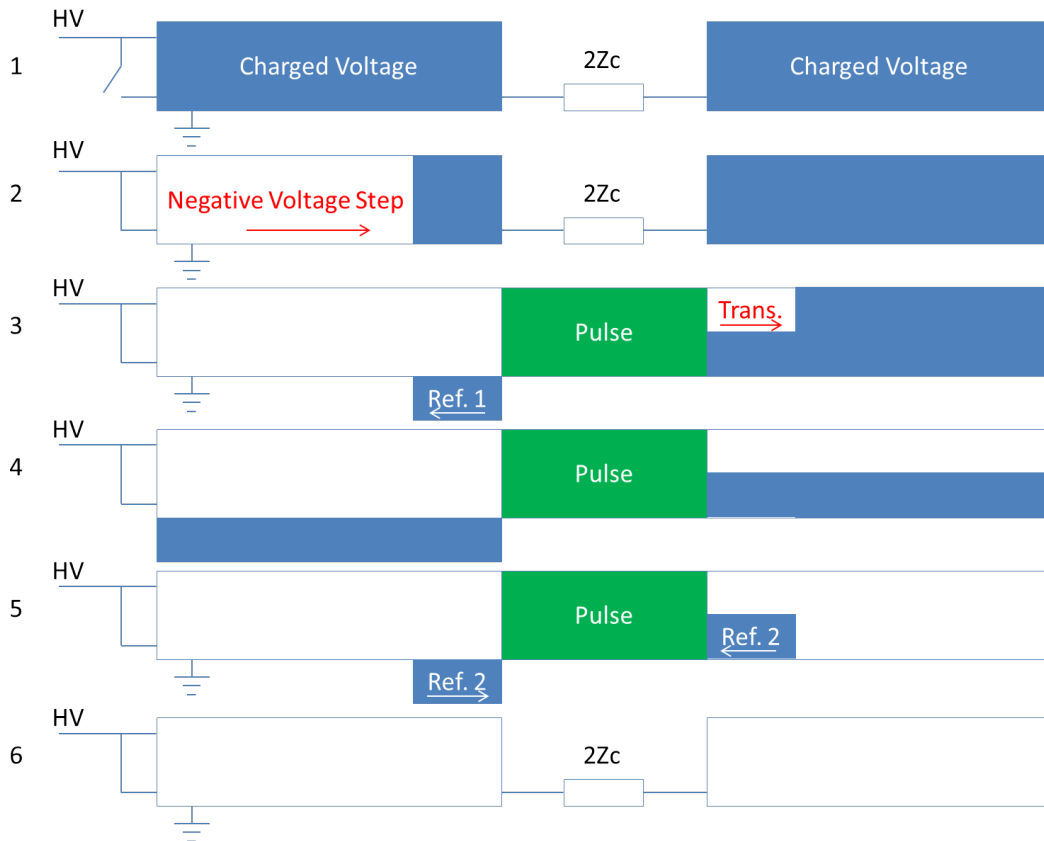
Figure 2.4: PPBM Mechanism

The mechanism of the Parallel Plate Blumlein to generate the pulse is summarized as per below, and shown in Fig. 2.4.

1. Switch is Open: both lines get precharged, through the upper conductor, to a desired voltage value

2. Switch is Closed: Negative voltage step starts propagating along the line annihilating the initial voltage

3. When the propagating negative voltage step effect reaches the load: a portion of the impinging wave reflects from the load, while another portion passes through

the load propagating towards the end of the second T.L. This is the period when the pulse is created across the load

4. The waves propagating towards the end of each line face a short circuit end on the side of the switch and an open circuit on the other side

5. Two waves of equal magnitudes but opposite polarities are now traveling back towards the load

6. When these two waves hit the load again, they cancel each other and the voltage across the load → mechanism ends with a pulse that lasted double the transit time along a single T.L.

2.4.4   Compact PPBL

2.4.4.1   Compact PPBL Configuration

This basic configuration of Blumlein transmission line discussed previously possess a large system with an undesired size to be added to a complete HPM system. An adequate miniaturization of this system has been presented in [20], for which a compact PPBL has been proposed, as shown in Fig. 2.5. Inspecting the figure, L is the length of the Blumlein, w is the width, d is the thickness of the dielectric, and t is the thickness of the conductor plates.
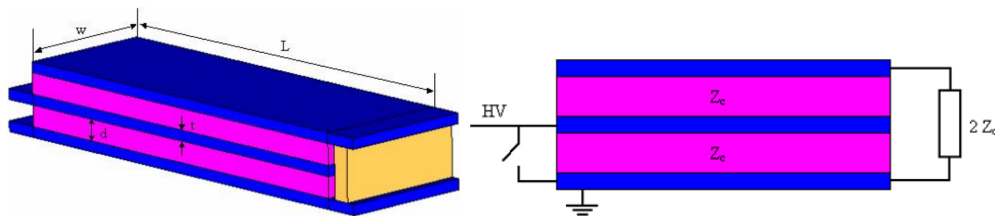
Figure 2.5: Compact PPBL Configuration [20, 21]

2.4.4.2 Compact PPBL Design

The presented design in [20] proposed the following two equations that control the design process: the equation of the characteristic impedance Z_c of one of the transmission lines constituting the Blumlein given by:

$$Z_c = \frac{\eta_0 d}{\sqrt{\varepsilon_r}\omega} \tag{2.1}$$

where ε_r is relative permittivity of the dielectric, and $\eta_0 = 120\Omega$ is the free-space impedance.

and the equation of the duration of the pulse τ given by:

$$\tau = \frac{2L\sqrt{\varepsilon_r}}{c} \tag{2.2}$$

where c is the velocity of light.

The design objective is the following, for a desired load impedance, a pulse of a desired duration is needed to be generated. In this sense, if the duration of the pulse τ is desired to be long, the PPBL length L has to be long according to Equation 2.2. However, this can be avoided if the relative permittivity of the material ε_r is sufficiently high.

2.4.4.3 Compact PPBL Properties

According to Equation 2.2, one can keep the value of the pulse duration constant by shortening the length of the Blumlein L and increasing the value of the relative permittivity ε_r in a proportional way. Although that is theoretically true, it was shown in [20] through taking different values of L and ε_r that give the same pulse duration τ, that this highly affects the shape of the pulse generated and hence degrade the overall performance. This is shown in Fig. 2.6, by applying the values of L and ε_r listed in

Table 2.1.

Table 2.1: Example of Tradeoffs for Unchanged Pulse Duration

Line length	Dielectric permittivity	Line width	Pulse duration	Line impedance
L	ε_r	W	τ	Z_c
L/2	$4\varepsilon_r$	W	τ	$Z_c/2$
L/4	$16\varepsilon_r$	W	τ	$Z_c/4$

As can been, although the three suggested values give theoretically the same value of pulse duration τ, the pulse changed its form between the three studied examples, for which one is nicely shaped (Curve #1), one somewhat degraded (Curve #2), and one very deformed (Curve #3).
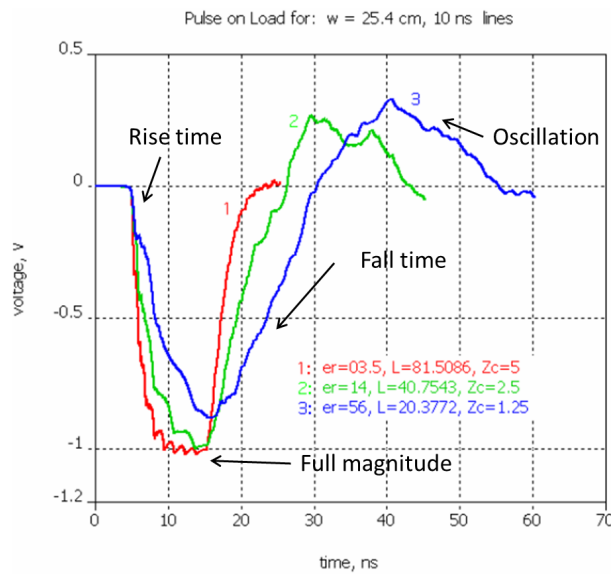
Figure 2.6: Three pulse forms, each supposed to have an equal pulse duration [20]

Observing Fig. 2.6, the following deviations are seen:

- An increased rise/fall time

- An excessive duration of the pulse

17

- An additional oscillation at the end of the pulse for which the pulse is supposed to decay to zero

- A decrement in the voltage full magnitude before decaying

The effects seen are the result of changing three values in the calculation of the pulse duration τ, the length of the Blumlein L, the relative permittivity ε_r and the characteristic impedance Z_c. Hence, at least one of these parameters is highly causing the degradation of the pulse generated. For this, keeping Z_c and ε_r constant with values equal to the values used to generated the degraded pulse (Curve #3) in Fig. 2.6, and changing only the value of L, it is seen that it is still possible to generate a good pulse (Curve #3), as shown in Fig. 2.7, noting that Curve #1 in this case is Curve #3 in Fig. 2.6. Hence, neither Z_c, nor ε_r, is responsible for the degradation of the pulse.
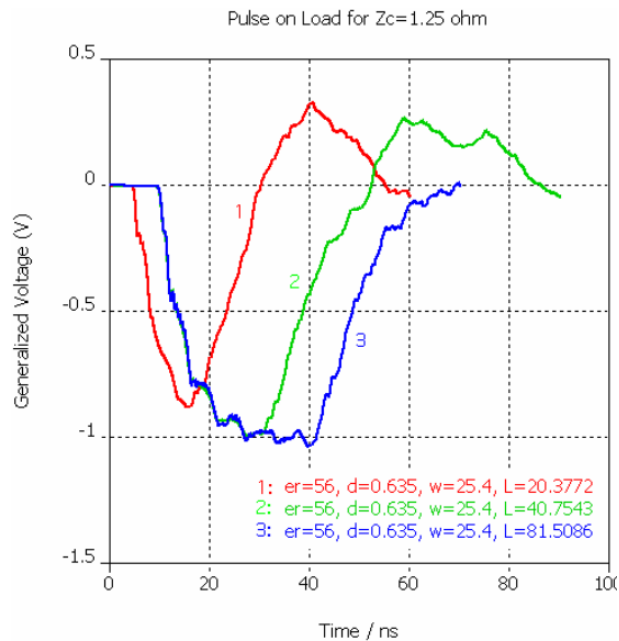
Figure 2.7: Testing which parameter is related to pulse degradation [20]

Observing Fig. 2.7, one can conclude that increasing the value of the Blumlein length L is the one responsible of obtaining a nicely shaped pulse. However, as

indicated in [20], generating such good pulse is not independently related to the value of *L* but to its ratio with respect to the line width *w*, as seen in Fig. 2.8. Inspecting the Figure, the cases with a good-shaped pulses are Curved #1, #4 and #5. The design of these curves possess different combinations of Blumlein length *L* and width *w*, but with an equal ratio of *L/w*. Hence, in the design process of such transmission lines, a care should be given to this ratio in the design of a desired pulse duration, for which a minimal value of this ratio exists, as will be discussed further.
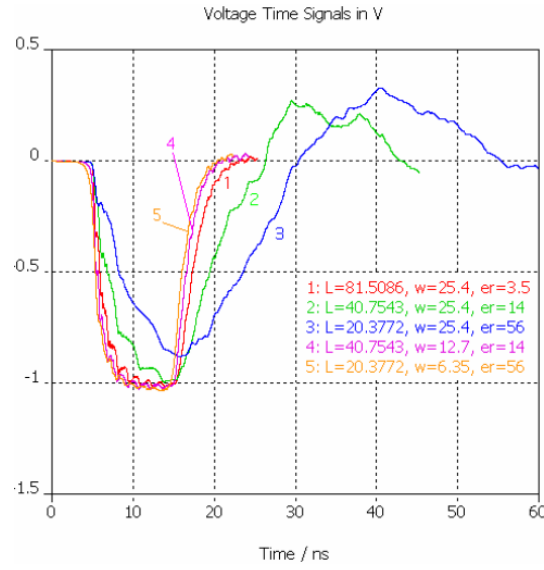
Figure 2.8: Indication that L/w matters for pulse form, rather than just L [20]

A further optimization of the Blumlein T.L. proposed in [20] is explained as follows. Rearranging Equations 2.1 and 2.2, two equations can be obtained:

$$\sqrt{\varepsilon_r} = \frac{\eta_0 d}{Z_c \omega} \tag{2.3}$$

$$\sqrt{\varepsilon_r} = \frac{2L\tau}{c} \tag{2.4}$$

Equating the two Equations 2.3 and 2.4, the ratio L/W can be written as:

$$L/W = \frac{c}{2\eta_0}\tau Z_c \mid_d \tag{2.5}$$

Since Equation 2.5 clearly shows that L/W is independent of ε_r, and since c and η_0 are constant, L/W can be expressed as a function of (Z_c, τ) for a certain value of d, though ε_r still has some effect on the generated pulse as will be seen further.

With this definition, within any range of Z_c and τ, and for some fixed value of d, all values of L/W lie on a surface, as shown in Fig. 2.9. An example is shown on the figure for which Z_c is 5, τ is 10, and L/W is 3.13.
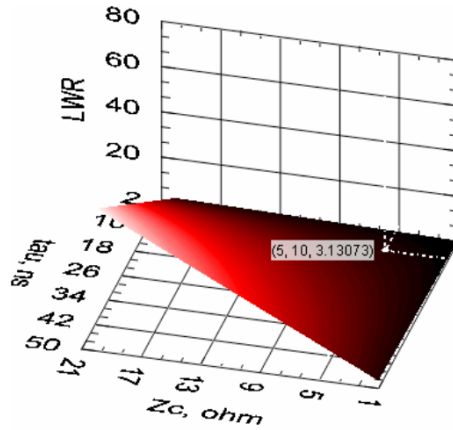
Figure 2.9: Surface of all solutions to LWR, for some range of Z_c and τ [20]

Taking several values of L/W, it was shown that there exist some minimal range of L/W values that generate some good pulses: less than this range a deformation of the pulse is resulted, higher than this range an oscillation and overshoot in the pulse is resulted [22]. This deformations and oscillations are shown in Figs. 2.10(a) and 2.10(b) respectively.

Hence, two threshold can be defined to confine the range of L/w values that generate well-shaped pulses, as shown in Fig. 2.11. L/w values that lie below the low threshold will generate a deformed pulse, whereas L/w values that lie above the

20
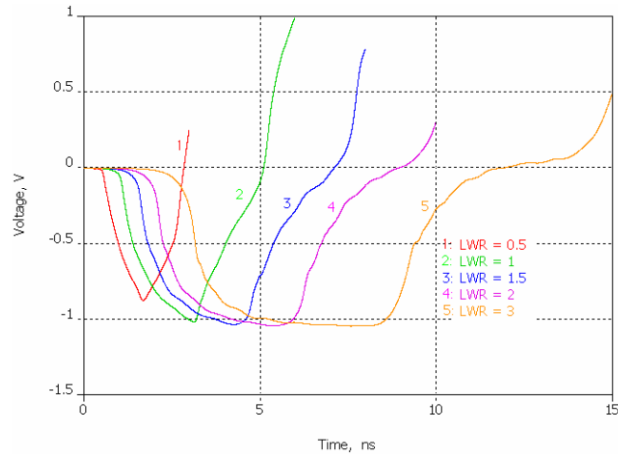
(a)
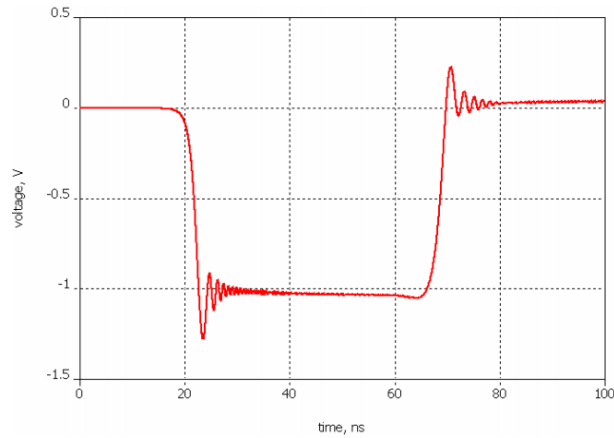
(b)

Figure 2.10: a) low LWR with equal Z_c, and unequal L settings; (b) high LWR [20]

high threshold will generate a pulse with oscillations. These threshold in their turn are not fixed, but depend on the values of width w and relative permittivity ε_r, and this is where ε_r plays a role in the form of the generated pulse, though, w has a stronger impact on the value of the thresholds than ε_r [20].

2.4.5 Microstrip Blumlein Configuration

A different configuration of Blumlein T.L has been presented by S. Romeo & *al.* in [23], for which a microstrip line configuration with meander-shaped conducting strips
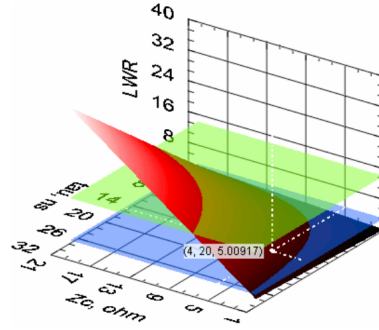
Figure 2.11: Two thresholds limiting the surface of LWR solutions

has been realized. The conducting strip has a width w placed on a dielectric substrate of thickness h and located on a ground plane. At low frequencies, typically below a few gigahertz, the fundamental propagation mode is a quasi-TEM mode [24].

In the design of such transmission lines, the main design parameters to be considered for each transmission line are the following:

1. The characteristic impedance,

2. and the electrical time delay $\tau/2$, where τ, in the double-switch Blumlein, representing the longest possible pulse duration

Assuming the propagation mode as quasi-TEM mode, the characteristic impedance Z_c and of the mictristrip-line can be written as [25]:

$$
Z_0 = \begin{cases} \dfrac{60}{\sqrt{\varepsilon_{eff}}} ln\left(\dfrac{8h}{w} + \dfrac{w}{4h}\right), & \text{for } \frac{w}{h} \leq 1 \\[4mm] \dfrac{120\pi}{\sqrt{\varepsilon_{eff}}\left(\frac{w}{h} + 1.393 + 0.667ln\left[\frac{w}{h} + 1.444\right]\right)}, & \text{for } \frac{w}{h} \geq 1 \end{cases}
\tag{2.6}
$$

with:

$$
\varepsilon_{eff} = \frac{\varepsilon_r + 1}{2} + \frac{\varepsilon_r - 1}{2}\frac{1}{\sqrt{1 + 12\frac{h}{w}}}
\tag{2.7}
$$

22

and w being the width of the strips, h is the thickness of the dielectric substrate, and ε_r is the relative permittivity of the dielectric substrate.

Inspecting Equations 2.6 and 2.7, it is seen that, in order to obtain a specific Z_c, the width w, the material and the thickness of the dielectric layer, have to be considered. Hence, the design formula can be written as [25]:

$$\frac{w}{h} = \begin{cases} \dfrac{8e^A}{e^{2A-2}}, & \text{for } \frac{w}{h} < 2 \\ \dfrac{2}{\pi}\left(B - 1 - ln(2B-1) + \dfrac{\varepsilon_r - 1}{2\varepsilon_r}C\right), & \text{for } \frac{w}{h} > 2 \end{cases} \tag{2.8}$$

where:

$$A = \frac{Z_0}{60}\sqrt{\frac{\varepsilon_r + 1}{2}} + \frac{\varepsilon_r - 1}{\varepsilon_r + 1}\left(0.23 + \frac{0.11}{\varepsilon_r}\right) \tag{2.9}$$

$$B = \frac{377\pi}{2Z_0\sqrt{\varepsilon_r}} \tag{2.10}$$

$$C = ln(B-1) + 0.39 - \frac{0.61}{\varepsilon_r} \tag{2.11}$$

And finally to set the desired value of the length of each Blumlein, the following equations can be used:

$$L = v_f\frac{\tau}{2} = \frac{c}{\sqrt{\varepsilon_{eff}}}\frac{\tau}{2} = \frac{c}{\sqrt{\varepsilon_r}}\frac{\tau}{2} \tag{2.12}$$

with:

$$v_f = \frac{c}{\sqrt{\varepsilon_{eff}}} \tag{2.13}$$

where v_f is the phase velocity, c is the speed of light in vacuum, and $\frac{\tau}{2}$ being

the electrical delay introduced by each line in this case. Since h/w is very small, ε_{eff} given in Equation 2.7, can be approximated to the ε_r of the dielectric material.

Since, several substrates are already found in the fabrication process, hence h and ε_r are already known. This leaves only the width w of the tracks to be calculated in order to get the desired characteristic impedance Z_c of the line.

2.5   Marx Generator

2.5.1   Basic Concept of a Marx Generator

Described by Erwin Otto Marx in 1924, Marx generator is an electrical circuit that generates a high-voltage pulse from a low-voltage DC supply. In general, its mode of operation consists of charging a number of capacitors in parallel, then suddenly connecting them in serious, producing the high-voltage pulse. Other Marx generators use charging inductors instead of resistors [26]. In general, the principle of operation of Mark generator is as follows [27–29]:

Initially, the switches are open, N capacitors (C) are charged in parallel to a voltage V by a high voltage DC power supply through the resistors R_C, as shown in Fig. 2.12(a). The switches are spark gaps having voltage V across them. Since these gaps have a breakdown voltage greater than V, they all behave as open circuits while the capacitors charge. The last gap is used to isolate the output of the generator from the load. In order to generate the pulse, the first spark gap is triggered. Its breakdown closes the gap placing the first two capacitors in series. This applies a voltage of about $2V$ across the second gap [17]. Consequently, the second gap breaks down and the third capacitor is added in series to what could be called stack or chain of capacitors. This phenomena continues till reaching the last gap that connects the output of the series

24

chain of capacitors to the load, as shown in Fig. 2.12(b). Ideally, the output voltage will be equal to the number of capacitors times the charging voltage, i.e. $N \times V$. However, in practice, the output value is less. The charge on the capacitors limits the available charge. For this, the output behaves as a pulse as the capacitors discharge through the load. At some point, the discharge stops, the spark gaps stop conducting and the high voltage supply begins charging the capacitors again, and the procedure restarts.

(a)

(b)
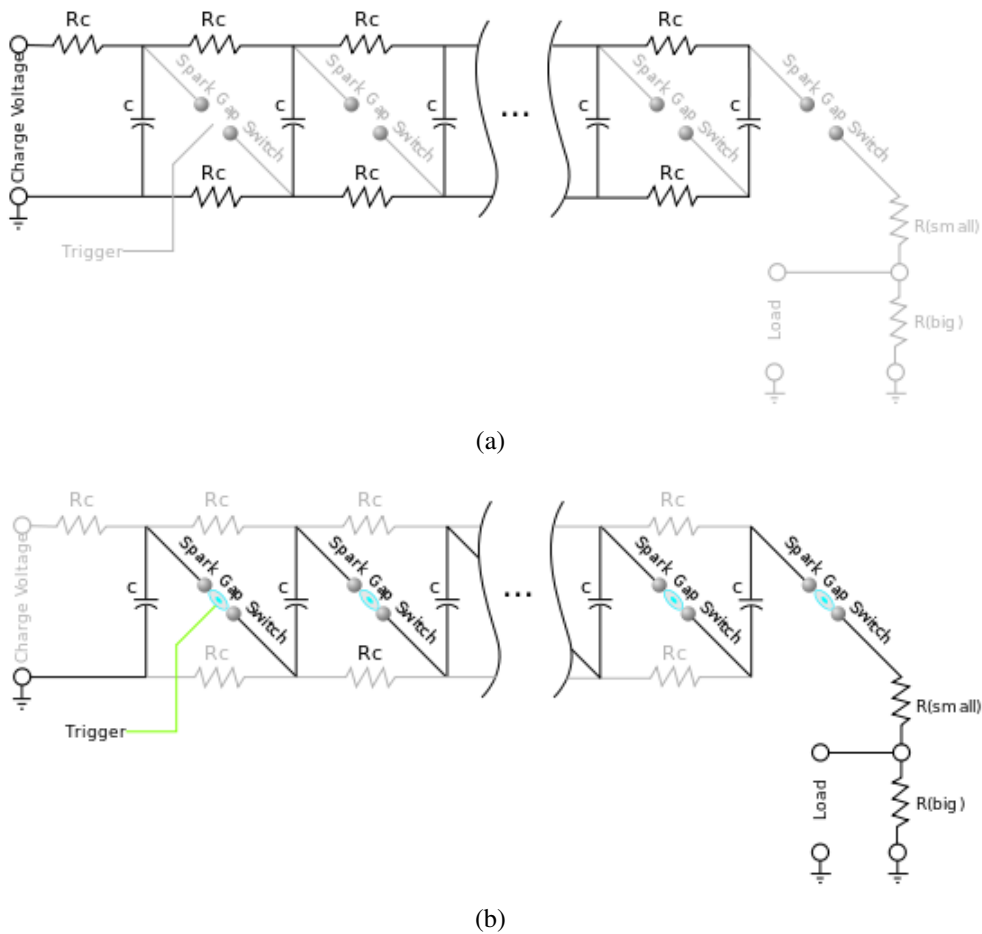
Figure 2.12: Marx generator mode of operation, (a) charging, (b) discharging

The principle of multiplying voltage by charging capacitors in parallel and discharging them in series is also used in the voltage multiplier circuit, the difference is that the voltage multiplier is powered with alternating current, and produces a steady

25

DC output voltage, while the Marx generator produces a pulse. An example of Marx generator in action is shown in Fig. 2.13.

Figure 2.13: Marx generator in action, 600K volts derived from 6 C cell batteries [30]

2.5.2 Marx Generators Structures Overview

Conventional high voltage Marx generators or impulse generators suffer from the large size, and hence the rise-time of the output voltage pulse tends to be slow. Moreover, the capacitors in such structures derive an output pulse profile which is double exponential. This will result in poor energy transfer efficiency, as well as a difficulty in portability and an expensive system to construct.

To solve some of the issues rose with the use of conventional Marx generators, pulse forming network Marx generators have been introduced, with the advantage of producing a square output pulse as each stage is comprised of a high voltage transmission line. In this case, the source impedance of the generator is well known which enables good source to load matching with excellent energy transfer efficiency.

Based on the concept of pulse forming network Marx generator, Li *et al.* have studied in [31] two design that generate a rectangle-pulse Marx generator. In the

first design, the circuit is arranged according to the classical Marx generator scheme. The second design is constructed as an LâĹŠC Marx generator in which the voltage multiplication is based on the polarity reversal of half of the capacitors, with only one command switch and one isolating switch is needed, as shown in Fig. 2.14.

(a)
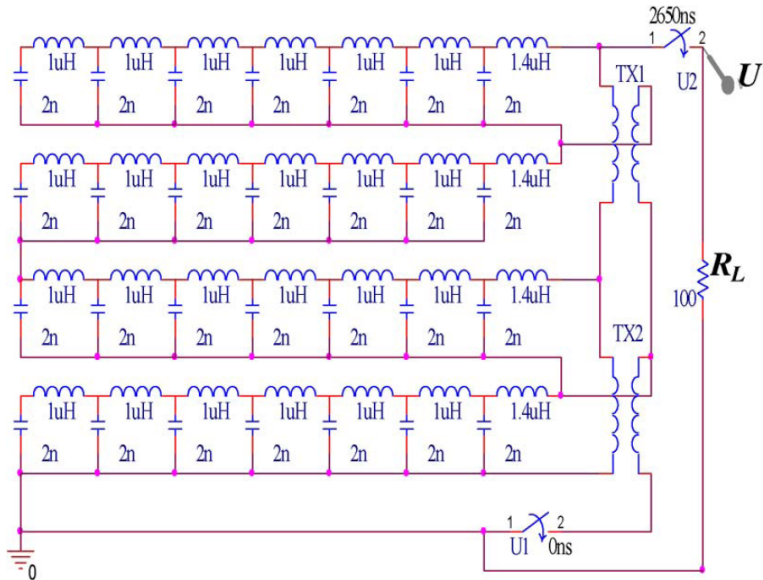
(b)

Figure 2.14: Marx generators designs [31]

The four PFNs have been tested, for which each PFN is composed of inductors and capacitors with the proposed schemes consisting of several identical interconnected according to Marx generator scheme, resulting in similar results of a pulse of 500ns duration and 65ns rising-time. The resulting pulses for both designs are shown in Fig. 2.15.
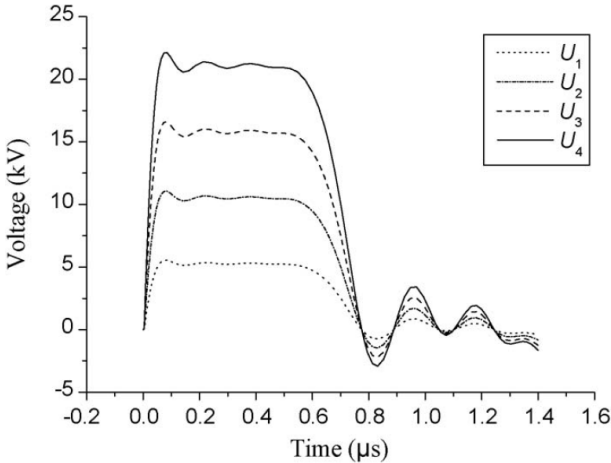
(a)
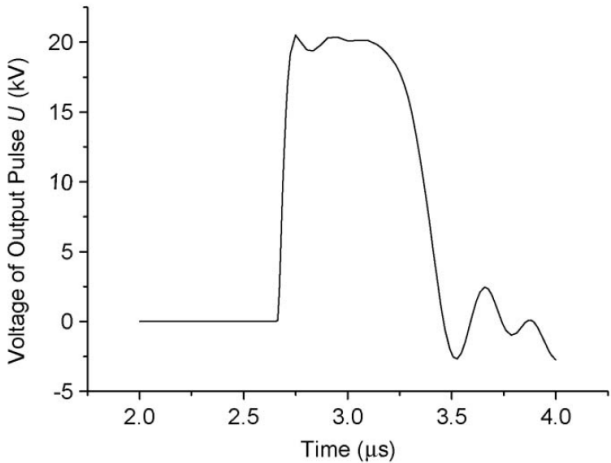
(b)

Figure 2.15: Resulting pulses of both Marx generator designs [31]

For both schemes of the PFN Marx generators proposed, it is good to note the equations relating the output pulse to the parameters of the pulse forming networks.

28

Assuming that *k* is the number of sections in one pulse forming network, with *C* and *L* being the capacitance and inductance of the individual capacitor and inductor in the pulse forming network section respectively, the pulse duration can be written as [31]:

$$\tau = 2k\sqrt{LC} \tag{2.14}$$

Taking that the number of pulse forming networks is *n*, the characteristic impedance of the pulse forming network Marx generator can be given by:

$$Z_M = n\sqrt{\frac{L}{C}} \tag{2.15}$$

Finally, assuming that the charging voltage of capacitors is U_0, the voltage across the match load can be written as:

$$U_L = \frac{nU_0}{2} \tag{2.16}$$

Hence, the pulsed power on the match load is calculated as:

$$P_L = \frac{nU_0^2}{4\sqrt{L/C}} \tag{2.17}$$

However, these systems also require high cost due to the large number of components required for each section, and this will be larger with the increment of desired output pulse voltage.

Turnbull *et al.* have proposed in [32] an inexpensive and compact pulse forming network Marx generator. The generator is made up of five stages, constructed with commercially available high voltage coaxial cables replacing the discrete high voltage inductors and capacitors which normally make up each stage. This construction has the advantage of being easy to be assembled, compact and inexpensive. However,

29

it is suitable for moderate to low energy applications, such as general HV testing of capacitive loads and high speed triggering. Their design is shown in Fig. 2.16.
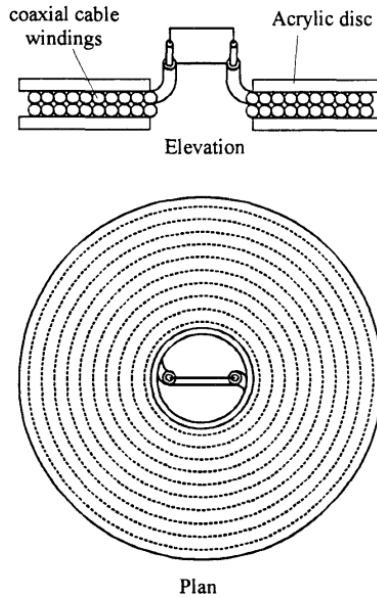
Figure 2.16: A schematic diagram of one stage of the PFN Marx generator [32]

The performance of the 5-stage pulse forming network Marx generator has been further investigated by MacGregor *et al.* in [33]. The output voltage pulse of their proposed system had a rectangular profile, with a rise-time of $\simeq 30$ ns and a duration of $\simeq 100$, a maximum output voltage of 200 kV and an output impedance of 125 ω. The PFN Marx generator assembly is shown in Fig. 2.17.

2.5.3 Further Enhancement and Design Notes of Marx Generators

As can be concluded from the design of the various Marx generators, the proper performance of such generators depends upon selection of capacitor and the timing of the discharge. To improve the switching times, two methods can be used. The first one considers doping of the electrodes with radioactive isotopes casium 137 or nickel 63, and the second one regards orienting the spark gaps so that ultraviolet light from a

30
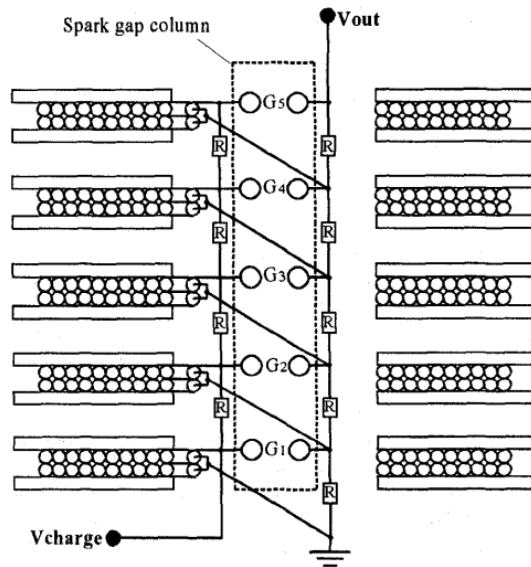
Figure 2.17: Schematic diagram of the PFN Marx generator assembly [33]

firing spark gap switch illuminates the remaining open spark gaps [34]. In addition, immersing the Marx generator in transformer oil or a high pressure dielectric gas such as sulfur hexafluoride (SF6) is often used to insulate the high-voltage produced.

Another care should also be taken for the initial trigger of the first switch, for which it may be allowed to spontaneously break down (sometimes called a self-break) during charging if the absolute timing of the output pulse is unimportant; or intentionally triggered once all the capacitors in the Marx bank have reached full charge. This could be done either by reducing the gap distance, by pulsing an additional trigger electrode (such as a Trigatron), by ionizing the air in the gap using a pulsed laser, or by reducing the air pressure within the gap [35]. For stage voltages less than 500 volts, avalanche diodes can replace the spark gap. In this case, no extra ionization is needed, and the charge carriers easily leave the electrodes.

Furthermore, the charging resistors, R_C, need to be properly sized for both charging and discharging. The resistors are mainly made from plastic or glass tubing filled with dilute copper sulfate solution which overcomes many of the problems ex-

31

perienced by more-conventional solid resistive materials that have a tendency to lower their resistance over time under high voltage conditions. Inductors are sometimes used instead of resistors for improved efficiency and faster charging as in [31].

2.6   Magnetrons

After addressing the Marx generator to be used as a high voltage generator, and the Blumlein transmission line to be used as a high voltage microwave generator to shape the pulse generate, Magnetrons are used to convert the microwave generated into a radio frequency signal to be fed to the antenna. They offer high energy conversion efficiency (around 75%) at a low cost [36]. Magnetrons were invented during World War II, when their small size, high power and short wavelength made them ideal for use in radar [36].

2.6.1   Concept of Magnetrons

In general, a magnetron is a diode vacuum tube used as a high power microwave oscillator. It consists of a cylinder cathode placed at the center and a coaxial anode between which the direct current potential generate an electric field. An external magnet is used to apply an additional magnetic field. The potential energy of an electron cloud near the cathode is converted into a radio frequency energy in a series of cavity resonators [37]. An example of Magnetrons is shown in Fig. 2.18(a). Magnetrons are thus capable of generating extremely high frequencies and also short bursts of very high power. They are mainly used in radar systems and in microwave ovens.

The basic concept of the magnetron is as follows: Electrons leave the cathode and are accelerated toward the anode, due to the dc field established by the voltage applied, which in our case is the high pulse generated. The presence of a strong magnetic
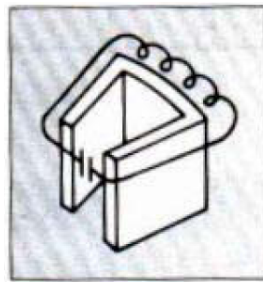
(a)
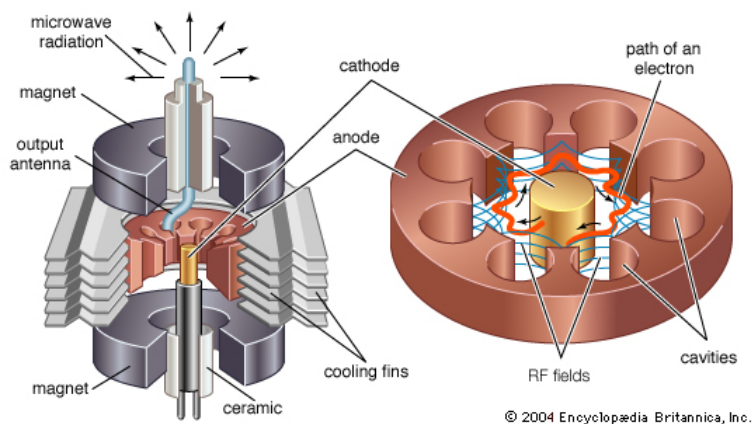
(b)

Figure 2.18: (a) Magnetron resonator, (b) basic magnetron structure [36]

field in the region between cathode and anode produces a force on each electron which is mutually perpendicular to the dc field and the electron velocity vectors, thereby causing the electrons to spiral away from the cathode in paths of varying curvature, depending upon the initial electron velocity at the time it leaves the cathode [37]. A sketch of the basic magnetron structure is shown in Fig. 2.18(b).

In our case, the magnetron is operated with very short pulses of applied voltage generated using the high voltage generators discussed earlier. This generates a short pulse of high power microwave energy to be radiated through the coupled antenna.

2.6.2 Challenges in Magnetrons

Using magnetrons at high microwave frequencies can result into different discrepancies:

1. The magnetron may suffer from frequency instability in its transmitted frequency, which might not only be varying from pulse to pulse but also within an single transmitted pulse [38]

2. The magnetron might possess a wide frequency spectrum, which will spread the energy over a wide range. This might add some noises to the receiver side which should have a wide range of selectivity of receive the transmitted frequencies. This might reduce the overall performance of the system [38]

3. A special safety care should be taken to prohibit any radiation hazard from the magnetrons that could harm the users, especially in our case for which it should radiate high power microwaves

2.7 Radiating the Microwaves

2.7.1 Mode Converter

After generating the needed microwaves out of the microwave source, what is left is to radiate these microwaves using a suitable antenna. The connection between the microwave source and the antenna is governed by the output parameters of the microwave source. The most widely found output of these sources is in the waveguide mode. This mode has to be compatible with desired antenna. If the antenna operates in a different

mode, a mode converter is needed to convert the output mode into the suitable one at the antenna. Mode conversion has been known as mode transformation [39], and it deals with the conversion from TE to TM or other TE modes, or from circular to rectangular waveguides, or directly from a waveguide mode to a radiating mode. The early method was based on projecting an electrode from one waveguide into another; however such method could result into abrupt transition and will breakdown at high powers.

Direct conversion from waveguide to radiating waves can be achieved using Vlasov convertor [40]. The TE mode is reflected from a curved conductor to produce a Gaussian-shaped beam at an angle of the waveguide axis.

2.7.2   Antenna

The antenna constitutes the last component in the HPM system. After receiving the microwaves from the source, and after any mode conversion if needed, the antenna radiates the microwaves to the intended target. The output characteristics of the antenna are the, frequency, the antenna gain, the angular beam width, the sidelobe levels, and power. These characteristics determine the output beam propagation characteristics. A suitable antenna should have the ability to concentrate the radiated power in a particular direction. Two major types of antennas are found, the narrowband antennas, and wideband antennas. This thesis concentrates on the narrowband ones. In practice, a few choices of conventional antennas have been used in narrowband HPM. The gain of these antennas are shown in Table 2.2. Parabolic dish antennas are abundant in conventional microwave applications, but have found little interest in narrowband HPM because of the high field found in the centralized feed. Impulse Radiating Antenna (IRA) and Flat Parabolic Surface (FLAPS) antenna are variants of the dish antennas, and they are widely used in ultrawideband HPM.

Table 2.2: Narrowband Principal Antenna Types [3]

Antenna	Gain	Note
Pyramidal and TEM horn	$2\pi ab/\lambda^2$	a,b are the sides
Conical horn	$5D^2/\lambda^2$	D is the diameter
Parabolic dish	$5.18D^2/\lambda^2$	
Vlasov	$[6.36D^2/\lambda^2]/cos\theta$	θ is the angle of slant-cut
Biconic	$120[cot\alpha/4]$	α is the bicone opening angle
Helical	$[148NS/\lambda]D^2/\lambda^2$	N is the number of turns, S is the spacing between the turns
Array of horns	$9.4AB/\lambda^2$	A, B are the sides of the array

Out of the listed antennas, the Vlasov antenna is considered a great candidate and a well-suited antenna to lunch narrowband HPM radiation. It is considered a very good match to the cylindrically symmetric microwave sources (MILO, Vircator, Cerenkov, etc.), and hence no need for additional mode converter before the antenna. However, a main shortcoming of this type of antennas is the rotated propagation angle. This type of antennas is investigated in this thesis and improved in terms of high power capability, beamwidth, and most importantly the propagation angle rotation, in Chapter 3.

Antenna arrays have been developing in the last years. Out of these arrays, the Slotted Waveguide Antennas (SWA) is taking a major interest, with its major ability of beam pointing. In addition, it can be directly connected to reltrons microwave source, without the need for additional mode converter. This type of antennas is investigated in the rest of the thesis, for which the design procedure of a one-dimensional SWA and two-dimensional SWA is explained with some major improvements in the design and results in terms of gain and sidelobe level ratio, in Chapters 4, 5, 6, and 7.

Chapter 3

Vlasov Antenna for High Power Microwave Applications

High power microwave (HPM) systems generate extremely high intensity pulses of electromagnetic energy (1 GW or greater) and are useful for applications ranging from radar to electronic warfare. Because of their extremely high voltage levels and power densities, these systems require special type of antennas. These antennas need to be directive for less energy loss, and to be able to withstand high power. HPM antennas tend to be large, and they often contain oil or gas insulation and vacuum to control breakdown. The main focus of this thesis is to investigate two HPM capable antennas, the Vlasov antenna and the Slotted Waveguide Antenna (SWA), and tend to improve these antennas in terms of gain, sidelobe level ratio (SLR), performance, and radiation characteristics.

This chapter presents the work done in designing a novel Vlasov antenna with curved cut shape and improved reflector position and geometry suitable for high power microwave applications. The curved shape of the proposed cut totally eliminates the sharp edges and angles present in Vlasov antennas with step and bevel cuts. Further-

more, with the proposed reflector configuration, the wave is radiated in the direction of the axis of the waveguide. A Vlasov antenna, designed for operation at 3 GHz, is used to compare the three cut types. An additional comparison is conducted to validate the concept of the enhanced reflector position, using the bevel-cut antenna and the improved cut. The proposed antenna results in increased antenna gain and in good performance in terms of sidelobe levels and half-power beamwidth, with maximum radiation directed toward the axis of the waveguide center.

3.1 Introduction

High Power Microwave (HPM) sources, such as the backward-wave Oscillator (BWO), the gyrotron, and the vircator (virtual cathode oscillator), generate power in cylindrically symmetric transverse electric TE_{0n} or transverse magnetic TM_{0n} modes. The sidelobe generation, gain reduction, and inefficient power loading on the antenna aperture, make these modes unsuitable for driving conventional antennas. This gave the idea of using mode converters at the output of these sources to convert these modes into a plane-parallel linearly polarized beam.

A Vlasov antenna [40–42], which is one of the most known mode converters used, is composed of a cylindrical waveguide with a shaped end, which can directly radiate energy from cylindrically symmetric modes in circular waveguides, without the need for an additional mode converter. The two well-known Vlasov antenna types come with a step cut and with a beveled cut [15]. The first type, a waveguide aperture with a step cut, originally suggested by Vlasov, has sharp edges and therefore may suffer from electrical breakdown when radiating HPM [43]. The beveled cut, was suggested by Nakajima [44] to avoid the sharp points of the step cut, leading to a more suitable shape for usage in HPM applications.

A comparison of the performance of bevel-cut and step-cut Vlasov antennas in HPM is conducted by B. G. Ruth *et al.* in [45], concluding that the bevel cut has better performance in such applications. A series of Vlasov-type high power microwave launchers have been investigated with several slant-cut angles in [46]. Additional experimental results and and theoretical investigation of TE_{0n} and TM_{0n} mode Vlasov launchers have been presented in [47, 48]. Other studies focused on increasing the gain of bevel-cut and step-cut Vlasov antennas. R. K. Dahlstrom *et al.* added a reflector to a bevel-cut Vlasov antenna to increase its gain and better direct the main beam [49]. M. Fazaelifar and M. R. Fatorehchy proposed in [50] two methods for increasing the gain of a bevel-cut antenna, one using a parabolic cylinder reflector, and the second using a horn. Moreover, X. Zhang *et al.* studied the step cut in the presence of a parabolic reflector [51]. Other work discussed the use of dual-reflector in the presence of Vlasov antennas [52, 53]. Improved beam focusing of high powered microwaves radiating from a Vlasov antenna has been also achieved by applying a flare to the launcher aperture [54]. Moreover, Sealy *et al.* investigated the use of corrugations with the flare to enhance the pattern performance [55]. Other studies used Vlasov antennas as a component in several systems [56–58]. However, a Vlasov antenna with either the bevel- or step-cut has its own maximum radiation shifted by some angle with respect to the axis of the waveguide. The work by the authors in [59] focused on optimizing the reflector position to bring back the maximum radiation along the axis of the waveguide antenna.

In this part of the thesis, we first design a bevel-cut Vlasov antenna operating at 3 GHz with the aim of obtaining maximum gain. Next, a step-cut version is designed to have radiation in the same direction as the bevel-cut counterpart, and a comparison of the performance of both is conducted. Later, a new cut shape, better suitable for the use of Vlasov antennas in HPM applications is presented and its advantages are re-

ported. Furthermore, the optimized reflector position for Vlasov antennas is presented, which will help, with the proper rotation angle, to orient the generated waves along the +Z direction, which is the axis of the waveguide in our case. In addition, with our proposed configuration, the reflector is directly attached to the waveguide structure, decreasing the size of the usual Vlasov antennas with reflectors, and eliminating the need of extra components to hold the waveguide and reflector together. The proposed reflector is applied to a bevel-cut and step-cut Vlasov antennas, and then further enhanced with curved edges to be applied to the curved cut to evaluate its performance.

3.2 Vlasov Antennas

Both step- and bevel-cut Vlasov antennas are the result of shaping the end part of a circular waveguide. For operation at 3 GHz, the used circular waveguide has a radius of 45 mm and a length of 300 mm.

(a) Bevel-cut design   (b) Step-cut design
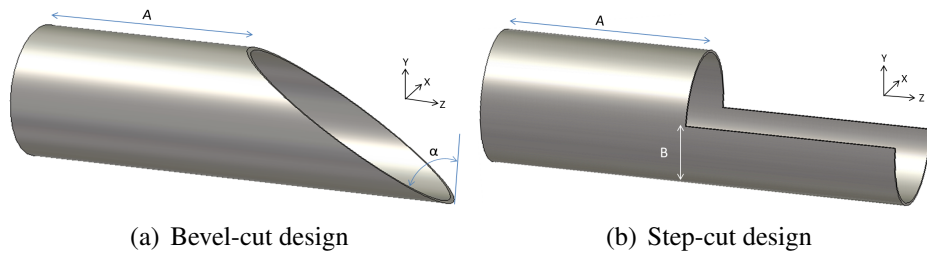
Figure 3.1: Configurations and parameters of bevel- and step-cut Vlasov antennas

3.2.1 Vlasov with Bevel Cut

A Vlasov antenna with a beveled cut is shown in Fig. 3.1(a). The cut angle α is the single parameter available for optimization, and it has the main effect on the gain and radiation patterns of the antenna. The angle that maximizes the gain of the antenna is given by [15]:

$$\alpha = sin^{-1}((\rho_{0n}\lambda)/(2\pi a)), \tag{3.1}$$

where ρ_{0n} is the n-th root of the equation $J_0(\rho_{0n}) = 0$, λ is the wavelength, a is the inner radius of the waveguide, and J_0 is the Bessel function of the first kind and zeroth order.

For the TM_{01} circular waveguide designed for 3 GHz, $a = 4.5$cm and $\lambda = 10$cm. Also, $\rho_{01} = 2.405$, so the bevel cut will be calculated as follows:

$$\alpha = sin^{-1}((2.405 \times 10)/(2\pi \times 4.5)) = 58.32°. \tag{3.2}$$

The highest gain according to the equation is obtained at a cut angle of $58.32°$. This result has been verified by simulations using ANSYS HFSS. For this angle, the resulting peak gain is 10.9 dB. The gain patterns, computed in CST MWS for both $\phi = 0°$ and $\phi = 90°$ planes are shown in Fig. 3.2. Maximum radiation is obtained in the $\theta = 32°, \phi = 90°$ direction.

(a) $\phi = 0°$ plane (b) $\phi = 90°$ plane
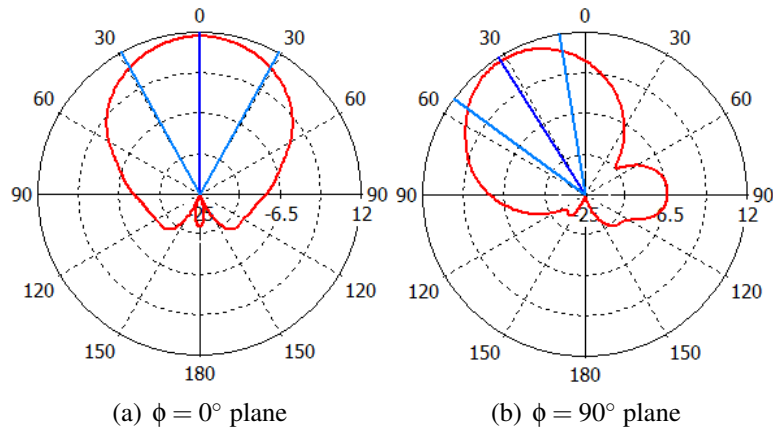
Figure 3.2: Gain patterns of bevel-cut design (using CST)

3.2.2 Vlasov with Step Cut

A Vlasov antenna with a step cut is shown in Fig. 3.1(b). The step cut is determined by the two parameters, A and B, as indicated. The value of A is fixed at 148.5 mm, which is the same value obtained with the bevel cut after finding the angle α. For comparison purposes, the step-cut Vlasov is designed so that it has the same direction of maximum radiation obtained with the beveled cut. For this purpose, via CST simulations, B is found to be 25 mm. It was noticed that, as the value of B decreases, the angle of maximum radiation increases. The gain patterns of the step-cut Vlasov antenna, in the $\phi = 0°$ and $\phi = 90°$ planes, are shown in Fig. 3.3(a) and 3.3(b) respectively. As is the design aim, the main lobe peaks at $\theta = 32°$.

(a) $\phi = 0°$ plane   (b) $\phi = 90°$ plane
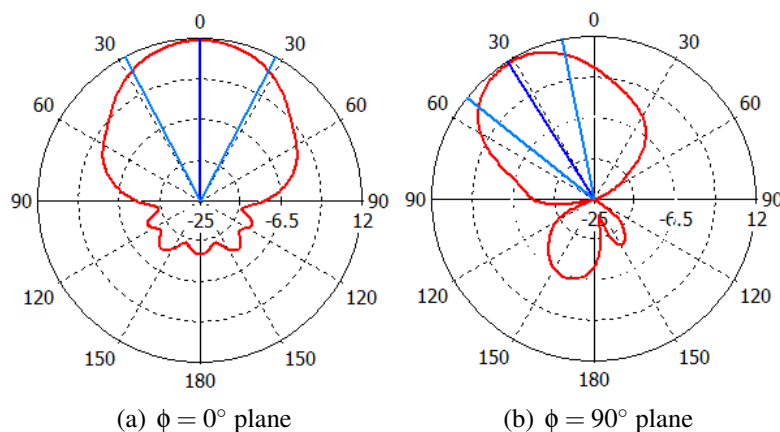
Figure 3.3: Gain patterns of step-cut design (using CST)

Comparing the two Vlasov antenna types, it is verified that the step cut gives better performance in term of maximum gain and half-power beamwidth (HPBW). However, the beveled cut results in lower side lobes, and this comes in addition to its suitability for HPM applications.

3.3   Improved Cut

The conventional Vlasov antennas may suffer from electric breakdown when they radiate at HPM. Although the beveled cut was introduced to avoid the sharp edges present in the step cut, it results in a decreased gain and an increased HPBW of the antenna. A new cut shape, introduced by the authors in [60], is shown in Fig. 3.4. This shape, totally based on curves, goes ahead of the beveled cut in removing the sharp edges and corners, and is as a result better suitable for applications involving HPM.

(a) 3D view   (b) Parametrized dimensions
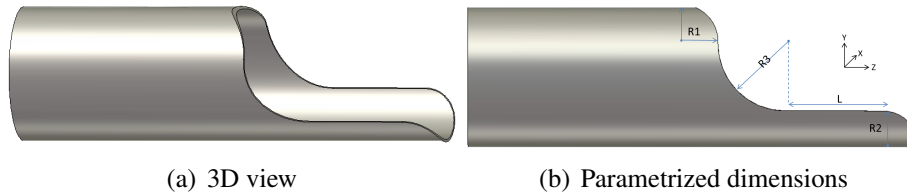
Figure 3.4: Vlasov antenna with proposed cut

In this design, we have the flexibility to optimize several parameters to reach the desired gain, HPBW, and direction of maximum radiation. These are the radius of Curve 1 (R1), the radius of Curve 2 (R2), the radius of Curve 3 (R3), and the separation between Curves 2 and 3, noted by L on Fig. 3.4.

To compare it with the step- and bevel-cut versions, a Vlasov antenna based on the same waveguide and on the proposed cut is designed so that it has the maximum radiation in the same $\theta = 32°, \phi = 90°$ direction. Table 3.1 lists the obtained parameters of the new design. The resulting patterns are shown in Fig. 3.5.

Table 3.1: Parameters of the Proposed Vlasov Antenna

Parameter	Value (mm)	Parameter	Value (mm)
Waveguide Radius	45	R2	24.5
Waveguide Length	300	R3	41
R1	24.5	L	65

(a) φ = 0° plane   (b) φ = 90° plane
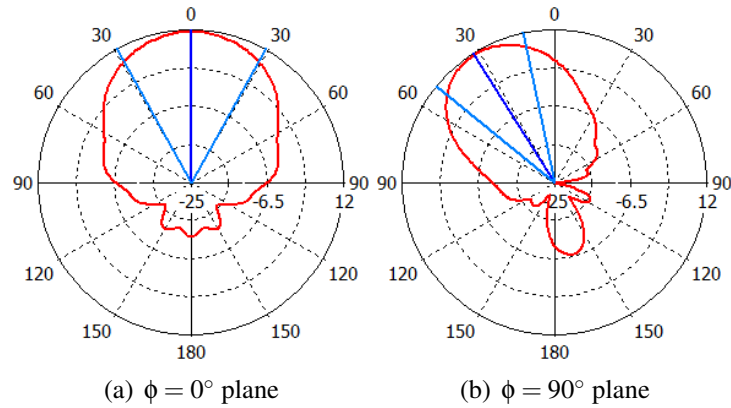
Figure 3.5: Gain patterns of the proposed Vlasov antenna (using CST)

The gain patterns resulting from the step, the beveled and the proposed Vlasov cuts are compared in Fig. 3.6. The obtained peak gain values are given in Table 3.2. Both CST and HFSS reveal that the proposed Vlasov antenna has a higher peak gain, which overcomes the decreased gain issue that the bevel cut has.

(a) φ = 0° plane   (b) φ = 90° plane
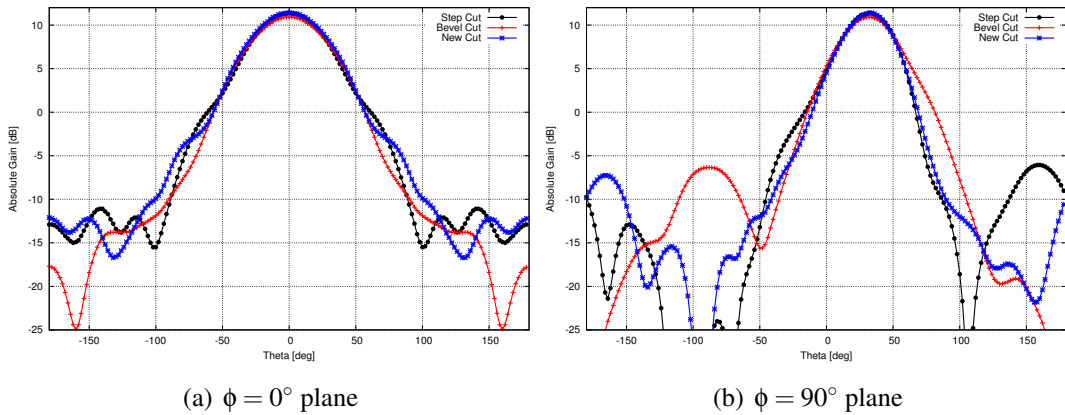
Figure 3.6: Comparison of the gain patterns of the step, the beveled and the proposed Vlasov cuts

The compared HPBW and sidelobe level ratio (SLR) results, computed in CST, are listed in Table 3.2. In addition to totally eliminating the sharp edges and corners that limit the performance of the antenna at high powers and providing higher peak gains, the results have shown that the proposed cut gives a smaller HPBW and a

44

Table 3.2: Compared Peak Gain, HPBW and Sidelobe Level Ratio (SLR)

Antenna	Gain (dB)		HPBW°		SLR (dB)	
	CST	HFSS	$\phi = 0°$ plane	$\phi = 90°$ plane	$\phi = 0°$ plane	$\phi = 90°$ plane
Bevel Cut	10.88	10.30	58.4	44.5	24.7	17.2
Step Cut	11.33	10.64	55	40.1	22.4	17.5
Curved Cut	11.40	10.74	58	39	23.5	18.6

(a) S11 using CST

(b) S11 using HFSS
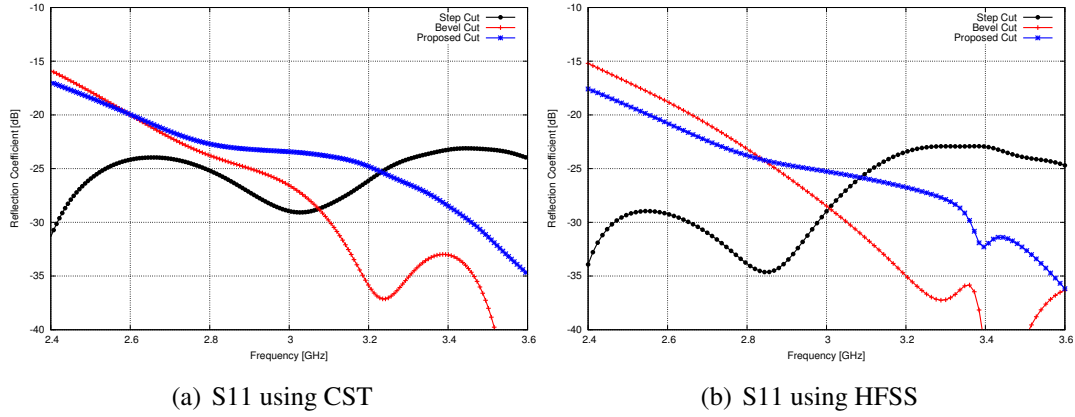
Figure 3.7: Comparison of the reflection coefficient, using both CST and HFSS

better SLR in the $\phi = 90°$ plane, a better SLR compared to the step cut in the $\phi = 0°$ plane, and a slightly narrower beam in the $\phi = 0°$ plane when compared to the bevel cut. These observations are also verified using HFSS simulations.

The reflection coefficient plots, for the three cut types, are given in Fig. 3.7. As shown, the three antennas operate at and around 3 GHz with very low S11 values.

3.4 Vlasov with Reflector

Vlasov antennas radiate waves with maximum radiation obtained in a shifted direction. This was proven through our simulations in Section 3.2, for which the three designed antennas radiate in the shifted directions corresponding to $\theta = \theta_m = 28°$ and $\phi = 90°$, computed using HFSS. However, it is preferred to have the maximum radiation of the

antenna directed in a well-known and easy to locate direction. This refers to the axis of the waveguide in our case. In addition, the HPBW in $\phi = 0°$ plane is large for the three radiated antennas, and it is hard to highly increase the gain of these antennas. In order to achieve rotating the maximum point of radiation of any of the Vlasov antennas and the curved-cut shape antenna and decrease the HPBW in $\phi = 0°$ plane, an optimized reflector is proposed in the following work. The reflector has the shape of a half-hollow cylinder. A conventional reflector is used with the step- and bevel-cut antennas designed. Whereas for the optimized curved-cut shape proposed in Section 3.3 an optimized reflector having also curved edges instead of the sharp corners of the conventional reflector is proposed. In both cases, the two reflectors have several parameters that affect the radiation: the starting point of the reflector, the radius of the reflector, the length of the reflector and the angle of rotation of the reflector with respect to the waveguide axis. All these parameters have been optimized to obtain the desired radiation patterns.

3.4.1 Bevel-Cut Vlasov Antenna with Reflector

3.4.1.1 Design and Simulations
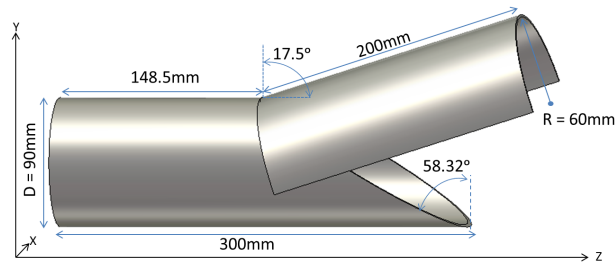
Figure 3.8: Bevel-cut Vlasov antenna with reflector

Using the bevel-cut antenna design in Section 3.2.1, the maximum radiation is obtained in the shifted direction corresponding to $\theta = \theta_m = 28°$ and $\phi = 90°$, computed

46
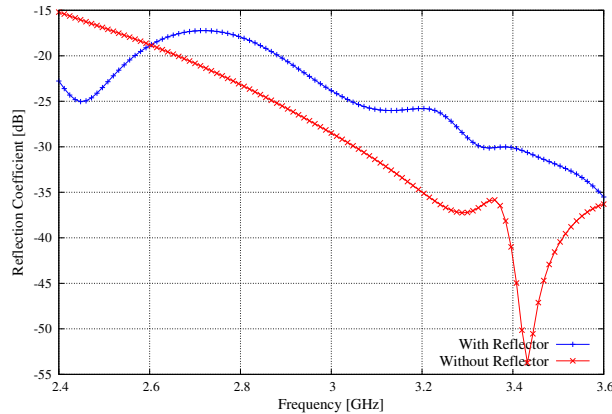
Figure 3.9: Reflection coefficient computed using HFSS, with no-reflector case shown in red (dashed), and with reflector in blue

using HFSS. A conventional reflector having the shape of a half hollow cylinder is then attached to the bevel-cut Vlasov antenna as shown in Fig. 3.8. The added reflector has the optimized values of 60 mm for the cylinder radius and a length of 200 mm. Upon rotating the reflector by a specific angle, it is seen that as the angle increases the shift angle approaches to origin. The initial bevel-cut Vlasov antenna gives a maximum computed gain of 10.3 dB, with the maximum radiation along the $\theta = 28°$ and $\phi = 90°$ direction. The optimized reflector angle for perfect direction along the +Z axis is seen at angle of 17.5°. For this angle, the maximum radiation is back along the axis of the waveguide, i.e. $\theta = 0°$ and $\phi = 90°$. The bevel-cut antenna operates at 3 GHz as shown in the reflection coefficient plot (S_{11}) in Fig. 3.9. It has a gain of 10.9 dB and a reduced HPBW, as indicated in Figures 3.10(a) and 3.10(b). It is shown that, for the case with the reflector, the maximum radiation is redirected along the axis of the waveguide.

3.4.1.2   Verification of the Results Using CST

The same design simulated in Section 3.4.1 using HFSS has been also tested using CST. The gain patterns in the two cases (without and with reflector) are shown in Fig. 3.11. As can be seen, the maximum gain of the antenna is redirected along the axis

(a) Red in the plane formed by the
X-axis and the point of maximum
radiation ($\theta = \theta_m, \phi = 90°$), blue
in $\phi = 0°$ plane

(b) $\phi = 90°$ Plane
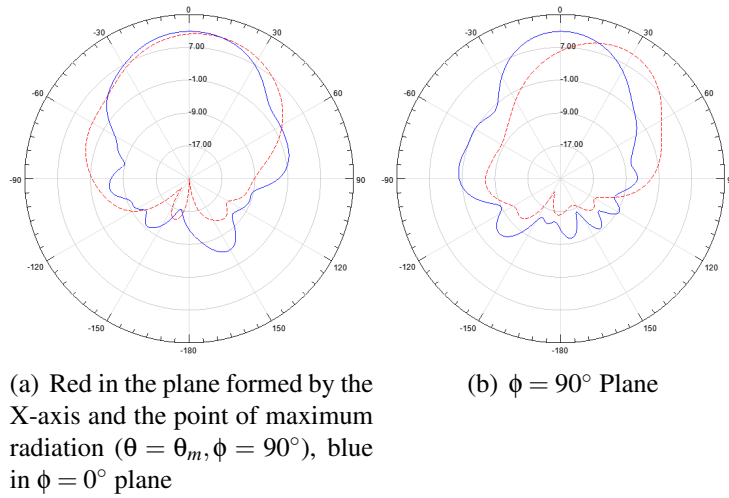
Figure 3.10: Simulated gain patterns computed using HFSS, with initial bevel-cut results shown in red (dashed) and proposed design results in blue

of the waveguide. The 3D gain patterns comparing the two cases, are shown in Fig. 3.12. Furthermore, the peak gain has increased from 10.88 to 12 dB, and the HPBW has decreased in the plane of interest, i.e. $\phi = 0°$ plane, from 58.4° to 41.7°.

3.4.2 Step-cut Vlasov Antenna

3.4.2.1 Design and Simulations

Again, using the step-cut antenna design in Section 3.2.2, the maximum radiation is obtained in the shifted direction corresponding to $\theta = \theta_m = 28°$ and $\phi = 90°$, computed using HFSS. The same reflector used in Section 3.4.1 is then attached to the step-cut antenna as shown in Fig. 3.13. Here, L is the distance between the waveguide port and the start of the reflector. The gain patterns of the designed step-cut antenna are shown in Fig. 3.14. By inspecting Fig. 3.14(b), the concept of rotating the reflector is validated and maximum radiation is obtained back along the waveguide axis for a rotation angle of 17.5° similar to the one used for the bevel-cut case. The design has been also simulated using CST showing the same results with an increment in gain

48

(a) $\theta = \theta_m, \phi = 90°$ plane   (b) $\phi = 90°$ plane

(c) $\phi = 0°$ plane   (d) $\phi = 90°$ plane
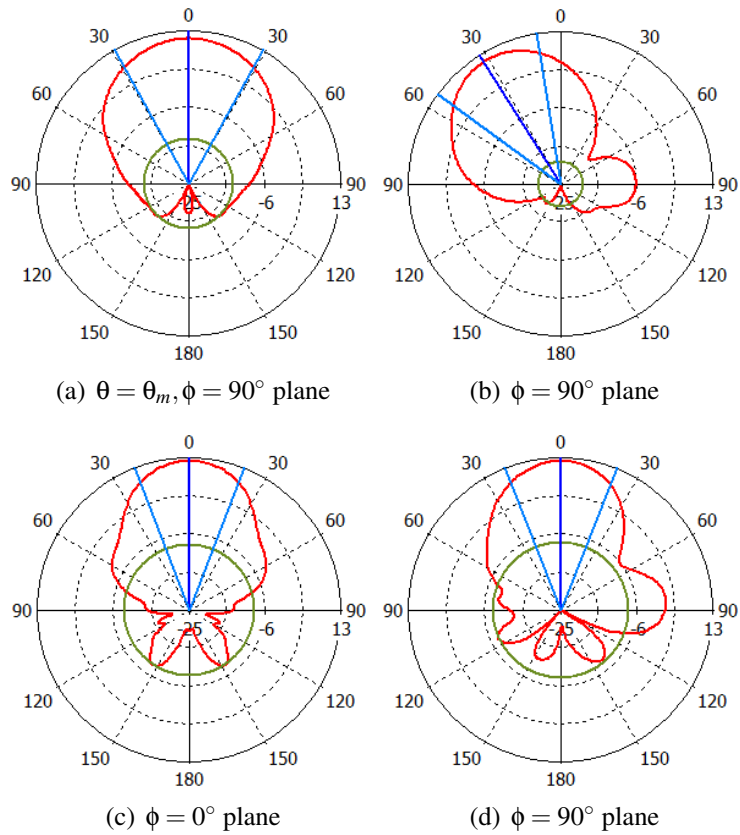
Figure 3.11: Bevel cut simulated gain patterns using CST : (a) & (b) without adding the reflector, (c) & (d) after adding the reflector

(a) Without reflector   (b) With reflector
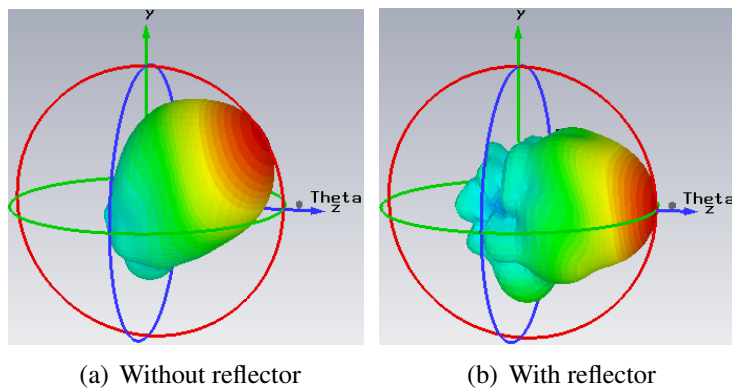
Figure 3.12: Bevel cut 3D gain patterns using CST: (a) without reflector and (b) with reflector

from 11.33 dB to 11.86 dB with a large decrement in HPBW in the plane of interest ($\phi = 0°$) from 55° to 41° with negligible changes in the $\phi = 90°$ plane.
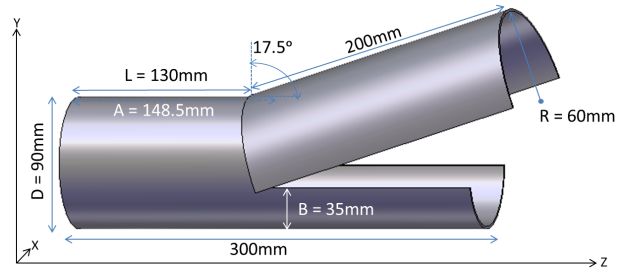
Figure 3.13: Step-cut Vlasov antenna with a reflector
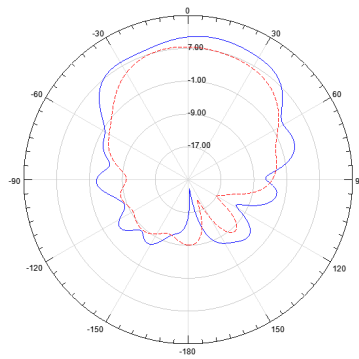
(a) Red in $\theta = \theta_m, \phi = 90°$ plane, blue in $\phi = 0°$ plane
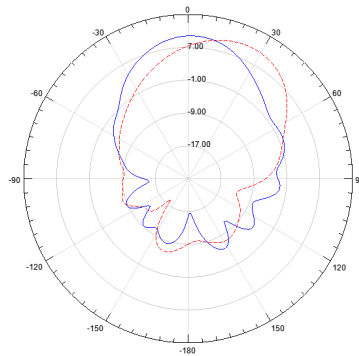
(b) $\phi = 90°$ plane

Figure 3.14: Step cut simulated gain patterns, with initial step-cut results shown in red (dashed) and proposed design results in blue

3.5 Improved Curved Cut with Optimized Reflector Position

After modifying the cut of the Vlasov antenna in order to optimize its performance as described in Section 3.3, in this section the optimized reflector proposed in Section 3.4 will be used to validate the concept of rotating the reflector in order to radiate the wave generated along the +Z direction on the novel cut shape. However, in order to also avoid having sharp corners in the reflector, an optimized one is proposed here to be attached to the curved-cut shape antenna. Fig. 3.15 shows the proposed combined antenna joining the curved-cut antenna and the curved-edges reflector with its optimized parameters. The parameters of the curved-cut antenna are the same used in the previous design in Section 3.3 and are listed in Table 3.1. In order to get the optimized values of the reflector radius and length indicated, the following parametric study has been done.
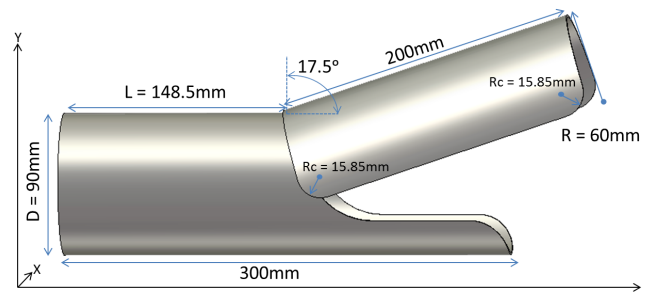
Figure 3.15: Enhanced Vlasov cut with a rotated optimized reflector with curved edges

51

3.5.1 Parametric Study

3.5.1.1 Radius Study

In order to choose the appropriate value of the reflector radius, the radius has been varied from 40 mm to 70 mm. The realized gain value at each value of radius is shown in Fig. 3.16(a), and the gain pattern in the plane of interest ($\phi = 90°$) at each radius value is also shown in Fig. 3.16(b).

Inspecting Fig. 3.16(a), it is seen that the realized gain in the plane of interest ($\phi = 90°$) increases as the radius of the reflector increases, till reaching a maximum value at a radius of 65 mm. However, inspecting the gain pattern in the $\phi = 90°$ plane in Fig. 3.16(b), it is seen that at this radius the SLLs and HPBW are higher than those with the second maximum value of gain at a radius of 60 mm. Hence a radius of 60 mm is suggested to be the optimized value taking into account the value of gain, SLLs and HPBW.

3.5.1.2 Length Study

In order to choose the appropriate value of the reflector length, the radius has been varied from 150 mm to 220 mm. The realized gain value at each value of length is shown in Fig. 3.17(a), and the gain pattern in the plane of interest ($\phi = 90°$) at each length value is also shown in Fig. 3.17(b).

Inspecting Fig. 3.17(a), it is seen that the realized gain in the plane of interest ($\phi = 90°$) increases as the length of the reflector increases, till reaching an approximate maximum value at a length of 200 mm, after which the value of gain might increase but in very small steps compared to the increase in the length. In addition, inspecting the gain pattern in the $\phi = 90°$ plane 3.17(b), it is seen that at this chosen value of length the SLLs and HPBW are better than those with the higher values. Hence a length of
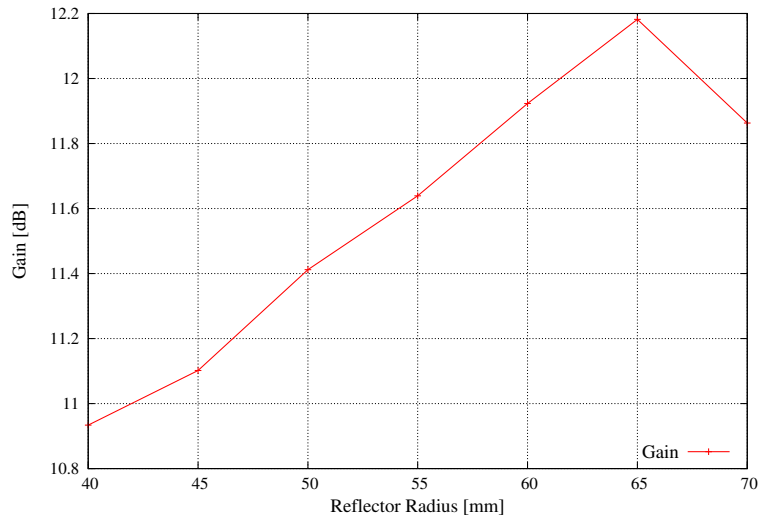
(a)
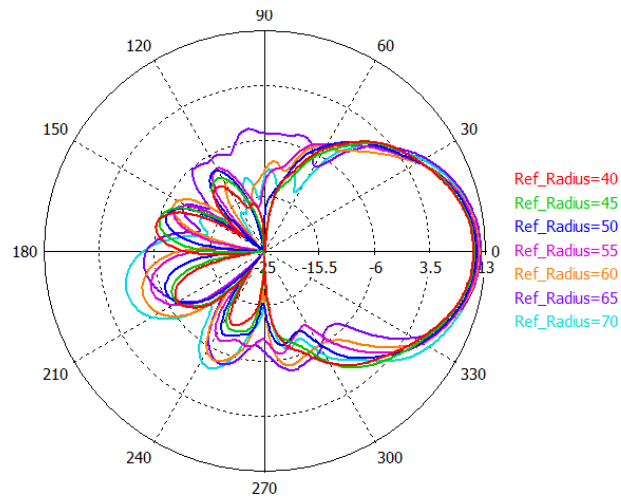
(b)

Figure 3.16: Simulated gain patterns computed using CST: (a) realized gain values, (b) 2D gain patterns

200 mm is suggested to be the optimized value taking into account the value of gain, SLLs, HPBW, and antenna structure size.
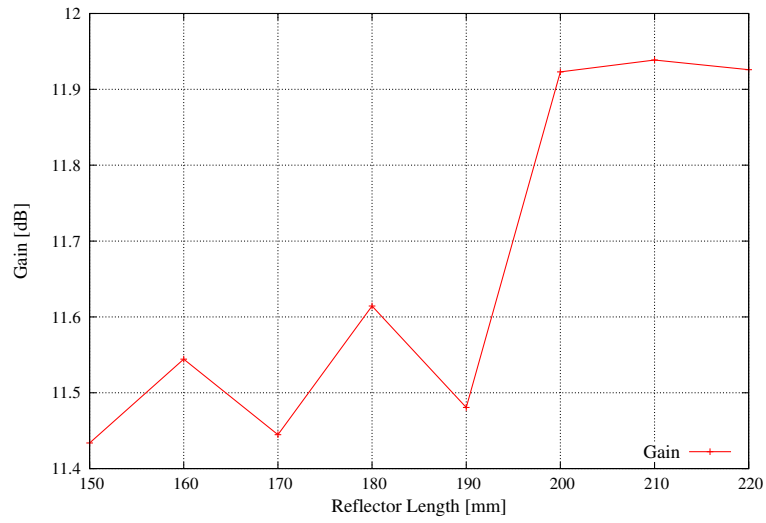
(a)
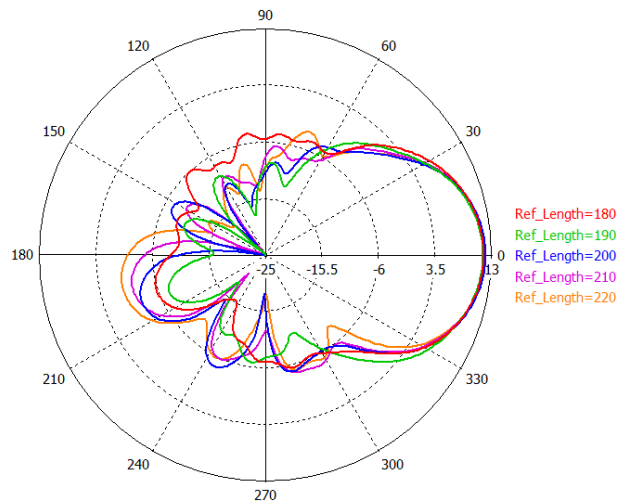
(b)

Figure 3.17: Simulated gain patterns computed using CST: (a) realized gain values, (b) 2D gain patterns

3.5.2 Simulations and Results

Taking into account the optimized values of the reflector parameters, the proposed combined antenna suitable for high power microwave applications has been simulated using CST with the radiation pattern results shown in Fig. 3.18.

The maximum radiation of the curved-cut antenna without using the reflector

(a) $\phi = 0°$ plane   (b) $\phi = 90°$ plane
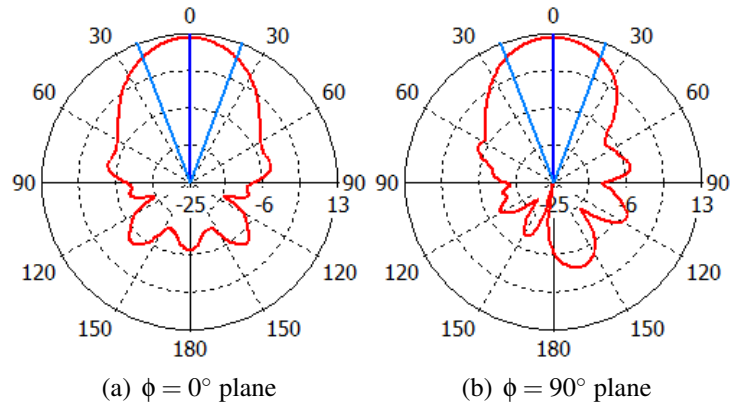
Figure 3.18: Gain patterns of the proposed curved-cut antenna with the optimized reflector position and shape, computed using CST

was shifted in the direction corresponding to $\theta = \theta_m = 28°$ and $\phi = 90°$, as depicted in Section 3.3. Inspecting Fig. 3.18, the concept of rotating the reflector is validated and the radiation in $\phi = 90°$ plane is now directed towards the +Z plane, as can be seen in Fig. 3.18(b). In addition, the proposed combined antenna also increases the gain of the antenna from 11.4 dB to 11.92 dB and decreases its HPBW in the $\phi = 0°$ plane from 58° to 41°, with minor changes in the $\phi = 90°$ plane. The same result has been also achieved using HFSS with an increment in gain from 10.7 dB to 11.00 dB as shown in Fig. 3.19.
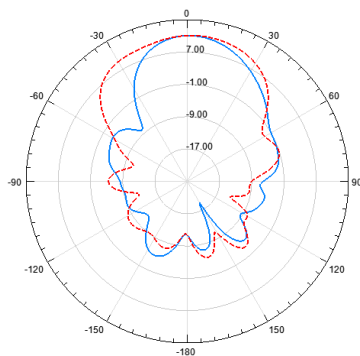
Figure 3.19: Gain patterns of the proposed curved-cut antenna with the optimized reflector position and shape, computed using HFSS: red (dashed) in $\phi = 0°$ plane, blue in $\phi = 90°$ plane

55

Combining all the simulations of the three designed antennas, with and without having the enhanced suitable reflector, Table 3.3 compares the radiation characteristics of the various cases studied. As listed, in addition to bringing back the maximum radiation along the axis of the waveguide, the proposed combined antenna also increases the gain of the antenna and decreases its HPBW.

Table 3.3: Comparison of the Radiation Characteristics of the Three Designed Antennas, With and Without Having the Enhanced Suitable Reflector, Computed Using CST

Antenna	Reflector	HPBW°		Gain (dB)
		$\phi = 0°$ plane	$\phi = \phi_m°$ plane	
Bevel-cut	Without	58.4	44.5	10.88
	With	41.7	42.9	12
Step-cut	Without	55	40.1	11.33
	With	42	43	11.86
Curved-cut	Without	58	39	11.40
	With	41.1	41	11.92

3.5.3 Observations

Several simulations have been done to study the effect of each parameter of the Vlasov antenna with curved-cut and improved reflector position and shape on the radiation performance. The following observations have been inspected:

- As the starting point of the reflector goes backward to the start of the Vlasov antenna, the gain decreases and the HPBW highly increases. This change also affects the point of maximum radiation which will be rotated by a certain degree from the axis of the waveguide.

- As the rotation angle of the reflector increases, the gain slowly increases with minor variations in HPBW. However, this change also affects the point of maximum radiation which will be rotated by a certain degree from the axis of the

waveguide.

- As the radius of the reflector decreases, the gain slowly decreases and the HPBW increases.

Hence, care should be taken in choosing the optimized values for each of these parameters in order to attain the desired performance.

One example on the use of such optimizations is to extend the reflector length to 250 mm, decrease the angle of rotation to 15°, and increase the starting point of the reflector (noted by L) to 151 mm. Applying these changes, the gain will increase to 12.42 dB, the HPBW in the $\phi = 90°$ plane will decrease to 37°, with the HPBW in the $\phi = 0°$ kept constant at 41.1°.

3.6 Conclusion

The Vlasov antenna, originally designed with a step cut made to one end of a circular waveguide, has been improved by Nakajima who implemented it using a beveled cut. The latter cut gets rid of the sharp corners present in the former one, which makes the antenna supportive of higher microwave powers, but this comes at the cost of reduced antenna gain and broader beam widths. In addition, the maximum radiation of these two antennas is shifted by some angle in the $\phi = 90°$ plane, assuming the antenna is directed along the +Z axis. In this part of the thesis, an improved shape with curved cuts for High Power Microwaves applications has been suggested, leading to higher gain, decreased HPBW, and decreased side lobes levels. Furthermore, two optimized reflectors, one with enhanced position, and the second with additional shape enhancement having curved edges, are proposed, with the ability to radiate the maximum radiation back to the +Z axis and further decrease the HPBW. This concept has been validated using the bevel- and step-cut Vlasov antenna, and with the new curved cut proposed in

this thesis.

Most of the work in this chapter has been published by the author in [59–61].

Chapter 4

One-dimensional Slotted Waveguide Antenna for High Power Microwave Applications

The next part of the thesis addresses the Slotted Waveguide Antenna (SWA) systems. It starts with investigating a resonant one-module SWA, for which the procedural steps for designing resonant SWAs with longitudinal slots cut in the broad-wall are outlined. Then, this SWA is transferred from waveguide fed SWA into a coaxial fed SWA where some calculations and design enhancement need to be established to assure correlation between the simulated designs and fabricated and tested ones. Furthermore, the resulting coaxial fed SWA is used in an array of multiple coax-fed SWAs in the objective to check for radiation enhancement in case of a 2D system. Since this proved necessity in term of increasing the gain and decreasing the SLLs needed in such applications, the rest of the thesis concerns the design of 2D SWA systems. Two different feeding mechanisms are proposed. The feeding mechanism for each design, the excitation co-efficients and slots displacements, the spacing between the slots, and the SWA modules

arrangement are all outlined to reach to the best performing array design.

Slotted waveguide antenna (SWA) arrays offer clear advantages in terms of their design, weight, volume, power handling, directivity, and efficiency. For broadwall SWAs, the slot displacements from the wall center-line determine the antenna's sidelobe levels. This chapter presents a simple inventive procedure for the design of broad-wall SWAs with desired SLRs. For a specified number of identical longitudinal slots, and given the required SLR and operating frequency, this procedure finds the slots length, width, locations along the length of the waveguide, and displacements from the center-line of the waveguide. Compared to existing methods, this procedure is much simpler as it uses a uniform length for all the slots and employs closed-form equations for the calculation of the displacements. A computer program has been developed to perform the design calculations and to generate the needed slots data. Illustrative examples, based on Taylor, Chebyshev, and the binomial distributions are given. In these examples, elliptical slots are considered, since their rounded corners are more robust for high power applications. A prototype SWA has been fabricated and tested and the results are in accordance with the design objectives.

4.1   Introduction

Rectangular slotted Waveguide Antennas (SWAs) [62] radiate energy through slots cut in a broad or narrow wall of a rectangular waveguide. This means the radiating elements are an integral part of the feed system, which is the waveguide itself, leading to a simple design not requiring baluns or matching networks. The other main advantages of SWAs include relatively low weight and small volume, their high power handling, high efficiency, and good reflection coefficient [63]. For this, they have been ideal solutions for many radar, communications, navigation, and high power microwave ap-

plications [64].

SWAs can be resonant or non-resonant depending on the way the wave propagates inside the waveguide, which is a standing wave in the former case and a traveling-wave in the latter [65, 66]. The traveling-wave SWA has a larger bandwidth, but it requires a matched terminating load to absorb the wave and prevent it from being reflected, which reduces its efficiency. It also has the shortcoming of the dependency of the main beam direction on the operating frequency. Resonant SWAs, on the other hand, have the end of the waveguide terminated with a short circuit, which results in a higher efficiency due to no power loss at the waveguide end. In addition, the main beam is normal to the array independently of the frequency, but these advantages come at the cost of a narrower operation band.

The design of a resonant SWA is generally based on the procedure described by Stevenson and Elliot [65, 67–70], by which the waveguide end is short-circuited at a distance of a quarter-guide wavelength from the center of the last slot, and the inter-slot distance is one-half the guide wavelength.

4.2 Slotted Waveguide Antenna Theory

The conventional cut-slots found in SWAs are rectangular slots with configurations shown in Fig. 4.1. The three types are: longitudinal slots, inclined slots, and edge-slots (or inclined slots in narrow-wall).

With axes chosen as shown in Fig. 4.1, field components for a TE_{10} mode,
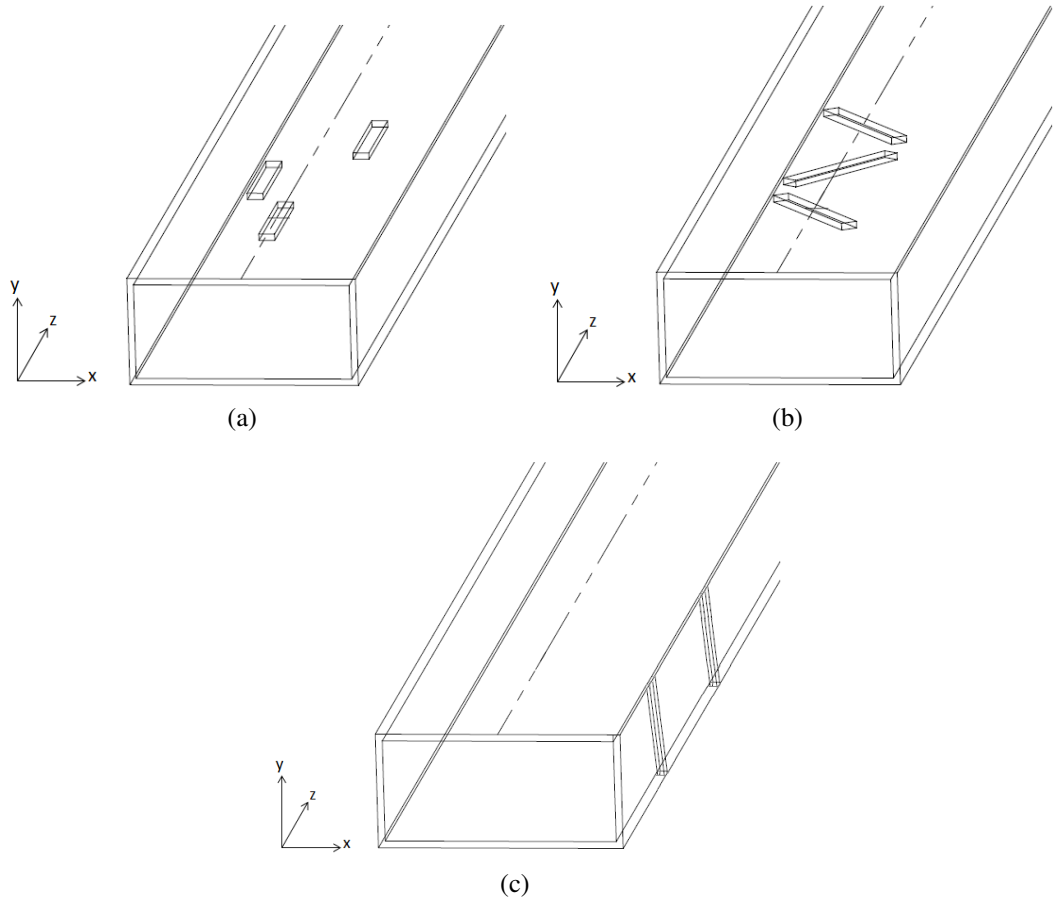
Figure 4.1: Types of slots: (a) longitudinal slots in broad-wall, (b) inclined slots in broad-wall, (c) edge slots (or inclined slots in narrow-wall)

traveling in the positive z-direction, can be written as:

$$
\begin{aligned}
H_x &= \frac{-E_0}{2\pi f\mu}\sqrt{k^2 - \left(\frac{\pi}{a}\right)^2}\, sin\left(\frac{\pi x}{a}\right)\exp^{-j\sqrt{k^2-\left(\frac{\pi}{a}\right)^2}z} \\
H_z &= \frac{jE_0}{2af\mu}cos\left(\frac{\pi x}{a}\right)\exp^{-j\sqrt{k^2-\left(\frac{\pi}{a}\right)^2}z} \\
E_y &= E_0 sin\left(\frac{\pi x}{a}\right)\exp^{-j\sqrt{k^2-\left(\frac{\pi}{a}\right)^2}z}
\end{aligned}
\tag{4.1}
$$

where f is the frequency of interest, k is the wavenumber and E_0 is a constant related to the fed power into the waveguide.

Theoretically, and as in the cavity-backed slot antenna, each slot could be

independently fed with a voltage source applied across each slot. However, the resulting system is very difficult to construct, complicated, and large in size. Instead, the common feeding method of these slots is the waveguide itself, which is used as the transmission line to feed the elements.

The radiated wave from each slot is determined through the shape of each, its position with respect to the waveguide center-line and the radiated wall chosen, and its orientation. Nevertheless, the shape of the waveguide and frequency of operation also play a major role in the radiation process. This is studied in the following.

Back to the E- and H-field equations, with the presence of magnetic fields electric currents are produced on the surface. Using the resulting surface current density J, given in Equation 4.2, the induced currents on the top wall (broad-wall) of the waveguide (where the slot cuts are found), can be solved to give Equations 4.3.

$$J = \widehat{n} \times H \tag{4.2}$$

On the top wall of the waveguide (where the slots are), the induced currents will be:

$$
\begin{aligned}
J_x &= \frac{-jE_0}{2f\mu a} cos(\frac{\pi x}{a}) \exp^{-j\sqrt{k^2 - \frac{\pi^2}{a}}z} \\
J_z &= \frac{-E_0}{2\pi f\mu} \sqrt{k^2 - \frac{\pi^2}{a}} sin(\frac{\pi x}{a}) \exp^{-j\sqrt{k^2 - \frac{\pi^2}{a}}z}
\end{aligned}
\tag{4.3}
$$

4.2.1 Longitudinal Slots

If a narrow slot is cut in one of the waveguide walls such that its long dimension runs parallel to a current line as seen in Fig. 4.1(a), the z-component of the current will not be disturbed, the x-component of the current is the one responsible for the

radiation. If the slot is placed on the center-line of the waveguide, i.e. first slot, this will cause negligible perturbation, and no radiation is occurring. This is demonstrated by taking the equation of the current density in the x-component given in Equation 4.3 and replacing x by $\frac{a}{2}$ (center-line of the waveguide), which will result into zero current density, i.e. no current and hence no radiation. This slot (slot 1) can be useful in Electric field measurements inside the waveguide. A vertical probe can be inserted inside the waveguide through this slot to sample the field [71].

If this slot is displaced from the center-line as shown in Fig. 4.1(a), second slot, this will interrupt x-directed current. The x-directed current will not be zero and will need to travel around the slot, and hence radiation will occur.

In this case, the more the displacement, the greater is the interruption. Thus, the distance from the edge of the waveguide determines the magnitude of the current and hence the power radiated from this slot which can be altered by moving the slots closer or farther from the edge. Doing so, a phased array can be designed with varying excitation to each slot.

4.2.2   Inclined Slots

If the slot in Fig. 4.1(a) is rotated at an angle about the center-line as shown in Fig. 4.1(b), it will interrupt z-directed current. The x-component is disturbed as well, however the currents have opposite magnitudes on either side of the center-line and hence tend to cancel out the radiation. The power radiated in this type of slots is controlled by the inclination angle from the center-line.

4.2.3 Edge-slots or Slots on the Narrow Wall

The third widely known type of slots is the edge slots or inclined slots in the narrow wall, shown in Fig. 4.1(c). This type of slots interrupts y-directed current. As with the inclined slots in Fig. 4.1(b) the more the inclination, the greater is the interruption. This type of slots has been used as both radiating slots or coupling slots to another antenna systems [72–74].

The common feature of the three types of slots is the ability to control the amount of radiation. This is done either through the choice of amount of slots displacements from the waveguide edges, as in Fig. 4.1(a), or inclination as in Figs. 4.1(b) and 4.1(c). This feature is the key to our work for which we need to control the radiation to obtain a pencil shape pattern with low SLLs, relatively low HPBW and high gain.

4.3 Equivalent Circuit

Assuming the slots are those of longitudinal ones, used for radiations, which is the most widely known configuration of a SWA, it is seen that the waveguide itself acts as a transmission line. Taking a transverse electric field in each slot, the TE_{10} mode scattering is taken to be symmetrical and hence each slot could be represented as a shunt element on an equivalent transmission line. Method of Moments (MoM) solutions indicate that this is a good assumption if the slots are narrow, if the b dimension of the waveguide is not too small, and if the slot offsets are not too large [69]. The theory of the conventional MoM approach is described by the author in Appendix

The slots can be viewed as parallel (shunt) admittances. The end of the

waveguide is short circuited, with the other end used as an input port. A schematic of this system can be drawn as shown in Fig. 4.2. The separation between the slots is noted by d_s, and that between the last slot and the short circuit end is d_c.
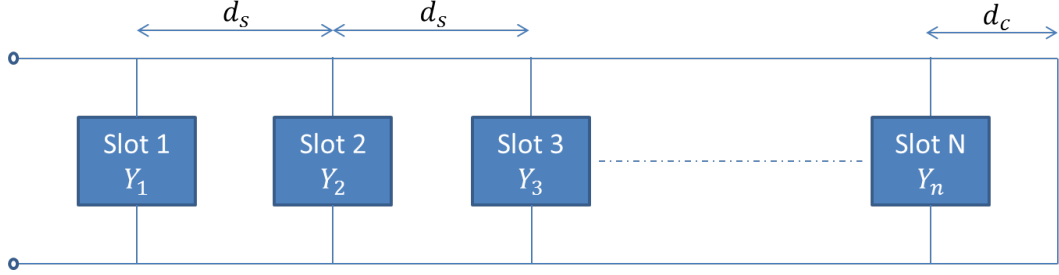
Figure 4.2: Slotted Waveguide Antenna equivalent circuit

Transmission line theory states that the impedance of a short circuit a quarter-wavelength down a transmission line is an open circuit. Hence, in this case the distance between the last slot and the end d_c is often chosen to be a quarter guide wavelength, or $\lambda_g/4$. The guide wavelength is defined as the distance between two equal phase planes along the waveguide. It is a function of the operating wavelength (or frequency) and the lower cutoff wavelength, and is calculated according to the following equation:

$$\lambda_g = \frac{\lambda_0}{\sqrt{1 - \left(\frac{\lambda_0}{\lambda_{cutoff}}\right)}} = \frac{c}{f} \times \frac{1}{\sqrt{1 - \left(\frac{c}{2a.f}\right)}} \tag{4.4}$$

where λ_0 is the free-space wavelength, c is the speed of light, and f is the operation frequency.

In order to have the input impedance the same viewed a half guide wavelength away, the separation between the slots d_s is designed to be $\lambda_g/2$. In this way, all the slots can be viewed as being in parallel. As a result, the input impedance and

66

admittance for an N element Slotted Waveguide Antenna can be calculated as:

$$Y_{in} = \sum_{1}^{N} YZ_{in} = \frac{1}{\Sigma_1^N Y}$$

(4.5)

If the slots have the same admittance, and hence the same displacements from the edges, the input impedance and admittance for an N element Slotted Waveguide Antenna can be written as:

$$Y_{in} = NY_{slot}$$
$$Z_{in} = \frac{1}{NY_{slot}}$$

(4.6)

4.4 Objective

For rectangular slots, the slot length should be about half the free-space wavelength. However, since sharp corners aggravate the electrical breakdown problems, slot shapes that avoid sharp corners are more suitable, especially for high power microwave applications. Elliptical slots are thus an excellent candidate for such applications [75, 76].

The resulting sidelobe level ratio (SLR) for antenna arrays is related to the excitations of the individual elements. In SWAs, the excitation of each slot is proportional to its conductance. For the case of longitudinal slots in the broad-wall of a waveguide, the slot conductance varies with its displacement from the broadface center-line [67]. Hence, for each desired SLR, a suitable set of slots displacements should be determined.

In his well-known procedure, Elliott has proposed two main equations that should be solved simultaneously to determine the values of the displacement and length for each slot. These two equations are based on Stevenson equations and Babinet's principle, and also rely on Tai's formula [77] and Oliner's length adjustment

factor [78], in addition to Stegen's assumption of the universality of the resonant slot length [79]. In brief, the existing resonant SWA design procedures are complex, and mostly rely on numerically solving several equations to deduce both the displacement and length of each slot. This thesis presents a simplified procedure by which all the slots have the same uniform length, and closed-form equations are used to determine the slots non-uniform displacements, for a desired SLR. The other parameters such as the slots inter-spacing along the length of the waveguide, and their distances from both the feed port and the shorted end, are obtained from the guidelines set by Elliott and Stevenson.

For rectangular slots, the slot length is about half the free-space wavelength. However, for elliptical slots, as the ones used in this work, the exact length is to be optimized. For a desired SLR, the conductances of the slots are obtained from a certain distribution, Chebyshev, Taylor, or Binomial; then an equation that relates these conductances to the displacements from the center-line is used to deduce these displacements. A computer program written in Python has been developed to perform the design calculations and output the resulting slots dimensions and coordinates. Several examples are given to illustrate the presented procedure. An *S*-band SWA with 10 elliptical slots is used for these examples. For each example, results for the obtained displacements, reflection coefficients and radiation patterns are presented. A prototype SWA with 7 elliptical slots, operating at a frequency of 3.4045 GHz, has been designed, fabricated, and measured, and the results show good analogy with the simulated ones.

4.5 Configuration and General Guidelines

For the illustrative examples, an *S*-band WR-284 waveguide with dimensions $a = 2.84''$ and $b = 1.37''$ is used. The design is done for the 3 GHz frequency. Ten elliptical slots are made to one broad-wall. The waveguide is shorted at one end and fed at the other.

4.5.1 Slots Longitudinal Positions

As a summary, the are general rules for the longitudinal positions of the slots on the broad-wall:

- The center of the first slot, *Slot* 1, is placed at a distance of quarter guide wavelength ($\lambda_g/4$), or $3\lambda_g/4$, from the the waveguide feed,

- The center of the last slot, *Slot* 10, is placed at $\lambda_g/4$, or $3\lambda_g/4$, from the waveguide short-circuited side,

- The distance between the centers of two consecutive slots is $\lambda_g/2$.

Calculating the guide wavelength λ_g using Equation 4.4, and taking the free-space wavelength calculated at 3 GHz, $\lambda_g = 138.5$ mm.

Based on the above guidelines, the total length of the SWA is $5\lambda_g$, as shown in Fig. 4.3.

4.5.2 The Slot Width

The width of each elliptical slot, which is 2 times the minor radius of the ellipse, is fixed at 5 mm. This is calculated as follows: for *X*-band SWAs, the width of a rectangular slot the mostly used in the literature is $0.0625''$, corresponding to $a = 0.9''$.
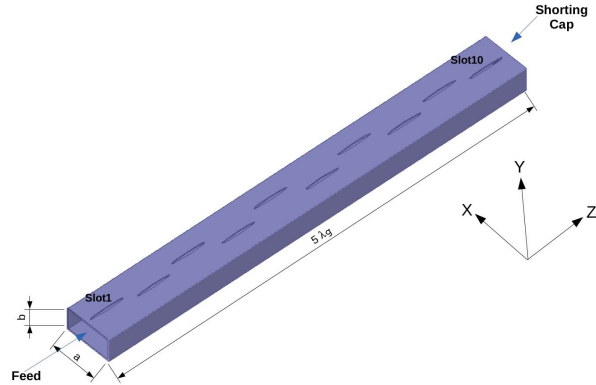
Figure 4.3: Slotted waveguide with 10 elliptical slots

By proportionality, the width of the elliptical slot for this *S*-band SWA is computed as follows:

$$SlotWidth = a \times \frac{0.0625}{0.9} = 2.84 \times \frac{0.0625}{0.9} = 0.197'' = 5mm$$

4.5.3   The Slot Displacement

A slot displacement refers to the distance between the center of a slot and the center-line of the waveguide broadface, as illustrated in Fig. 4.4.

With uniform slot displacements, all slots are at the same distance from the center-line. This is similar to the case of antenna arrays with discrete elements having equal excitation, which results in an SLR around 13 dB. Lower SLLs are obtained upon using non-uniform slot displacements. In both the uniform and non-uniform displacement cases, the slots should be placed around the center-line in an alternating order. This is done to ensure that all slots radiate in phase and hence result in higher efficiency of the antenna.

The value of the uniform slot displacement that leads to a good reflection
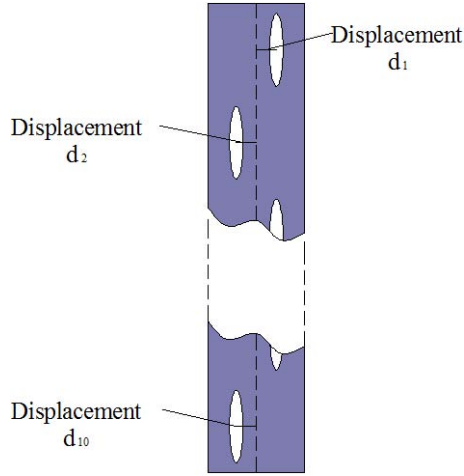
Figure 4.4: Slotted waveguide with 10 elliptical slots

coefficient is given by [80, 81]:

$$d_u = \frac{a}{\pi} \sqrt{\arcsin\left[\frac{1}{N \times G}\right]} \qquad (4.7)$$

where:

$$G = 2.09 \times \frac{a}{b} \times \frac{\lambda_g}{\lambda_0} \times \left[\cos(0.464\pi \times \frac{\lambda_0}{\lambda_g}) - \cos(0.464\pi)\right]^2 \qquad (4.8)$$

In Equation (4.7), N is the number of slots, which is equal to 10. In Equation (4.8), $\lambda_0 = 100$ mm at 3 GHz. Combining Equations (4.7) and (4.8), d_u is found to be 7.7 mm.

4.5.4 The Slot Length

For rectangular slots, the length is usually $0.98 \times \lambda_0/2 \simeq \lambda_0/2$. Because of the narrower ends of elliptical slots, their length (double the major radius) is expected to be slightly larger than $\lambda_0/2$. The optimized elliptical slot length is determined as follows:

the SWA, having 10 slots, is modeled assuming a uniform displacement ($d_u = 7.7$ mm); this 10-slot SWA is used to obtain the optimized slot length which takes into account the effect of mutual coupling on the slot resonant length. An initial length of $0.98 \times \lambda_0/2$ per slot; the length is increased while inspecting the computed reflection coefficient S_{11} until the antenna resonates at 3 GHz with a low S_{11} value. In our case, the elliptical slot length is found to be 54.25 mm.

For these uniform displacement and slot length, the resulting sidelobe level ratio (SLR) is around 13 dB, which is as expected. The reflection coefficient S_{11} and the gain pattern in H-plane this case are given in Figs. 4.5(a) and 4.5(b), respectively. A peak gain of 16.6 dB is recorded. The half-power beamwidth (HPBW) in this plane is $7.2°$. The pattern in the E-plane is a broadside one, with a HPBW of $82.1°$, as shown in 4.6(a). These values are obtained using CST Microwave Studio, and then verified with ANSYS HFSS.
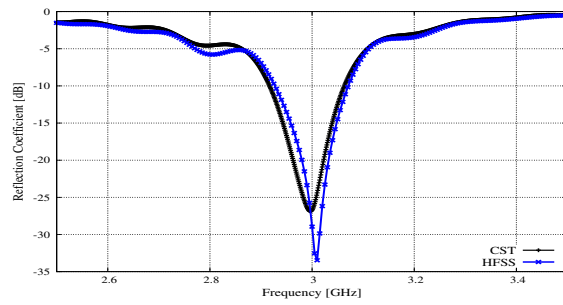
(a) S_{11} for uniform slots displacement
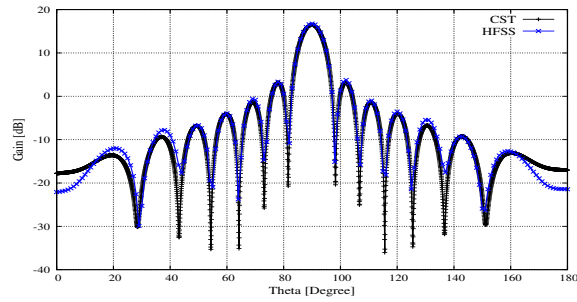
(b) 2D gain pattern: H-plane

Figure 4.5: Radiation characteristics simulated results for the case of uniform slot displacements: (a) reflection coefficient, and (b) gain pattern in the H-plane
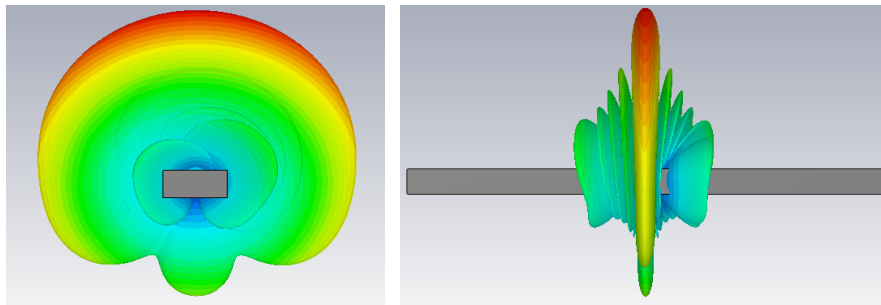
(a) 3D gain pattern: E-plane

(b) 3D gain pattern: H-plane

Figure 4.6: Simulated 3D gain patterns results for the case of uniform slot displacements: (c) in the E-plane and (d) in the H-plane

4.6 Non-uniform Displacement Calculation Procedures

The simulations performed in this part have proven that the resonating length of the elliptical slots is not very sensitive to the slots displacements calculated using the method

proposed in this part. This will be addressed again in later sections. For this, in the next calculations the length of all slots is fixed at 54.25 mm. The displacement of the nth slot is related to its normalized conductance g_n by [80, 82–84]:

$$d_n = \frac{a}{\pi} \arcsin \sqrt{\frac{g_n}{2.09 \frac{\lambda_g}{\lambda_0} \frac{a}{b} \cos^2\left(\frac{\pi\lambda_0}{2\lambda_g}\right)}} \tag{4.9}$$

$$g_n = \frac{c_n}{\sum\limits_{n=1}^{N} c_n}. \tag{4.10}$$

In Equation (4.10), N is the number of slots, and $c_n s$ are the distribution co-efficients that should be determined to achieve the desired SLR. Equation (4.10) guarantees that $\sum\limits_{n=1}^{N} g_n = 1$.

Several distributions (tapers) well-known in discrete antenna arrays can be used to generate the $c_n s$ (e.g. Taylor and Chebyshev). However, the resulting SLR of the SWA is always lower than the SLR used for the discrete array distribution. To reach the desired SWA SLR, a few iterations of the simulation setup are required, where in each the SLR of the discrete array used to generate the taper values is increased. Illustrative examples are shown below to further highlight this design procedure.

4.6.1   Example 1: 20 dB SLR with Chebyshev Distribution

In this example, the target is an SLR of 20 dB, where the $c_n s$ are selected according to a Chebyshev distribution.

4.6.1.1   Coefficients and Slots Displacements

The coefficients $c_n s$ for a Chebyshev distribution are calculated from equations in [85, 86], as given in the following. The array factor of a generalized Chebyshev array can

be written as:

$$f(u) = \prod_{n=1}^{p} \left(\frac{1}{R_n} T_{N_n-1}(\gamma_n cos\frac{u}{2}) \right)$$
$$= \frac{1}{R} \prod_{n=1}^{p} \left(T_{N_n-1}(\gamma_n cos\frac{u}{2}) \right)$$

(4.11)

where:

- T_x denotes a Chebyshev polynomial of order x,

- $\gamma_n = cosh[cosh^{-}1(R_n)/(N_n - 1)]$,

- $u = 2\pi(d/\lambda)(cos\theta - cos\theta_0)$ with d being the inter-element spacing and θ_0 the elevation angle of maximum radiation,

- R_n is the sidelobe level ratio SLR of the nth basis Chebyshev array,

- and N_n is the number of elements of the nth basis array.

For a uniform spacing and an amplitude symmetrical about the center, the array factor can be written as:

$$f(u) = \begin{cases} 2\sum_{m=1}^{N/2} I_m cos[(m-1/2)u], & \text{for N even} \\ \sum_{m=1}^{(N+1)/2} \varepsilon_m I_m cos[(m-1)u], & \text{for N odd} \end{cases}$$

(4.12)

where ε_m equals 1 for $m = 1$ and equals 2 for $m \neq 1$. Finally, the excitation coefficients

are found using:

$$I_m = \begin{cases} \dfrac{2}{NR} \displaystyle\sum_{q=1}^{N/2} f[u=p]cos[q], & \text{for N even} \\[2em] \dfrac{1}{NR} \displaystyle\sum_{q=1}^{\frac{N+1}{2}} \varepsilon_q f[u=v]cos[w], & \text{for N odd} \end{cases} \tag{4.13}$$

where:

- $p = 2\pi/N(q-1/2)$,

- $q = 2\pi/N(m-1/2)(q-1/2)$,

- $v = 2\pi/N(q-1)$,

- and $w = 2\pi/N(m-1)(q-1)$

Equation (4.13) uses Chebyshev polynomials and the computed excitation currents result in a normalized array factor.

For a 35 dB SLR Chebyshev taper, the c_ns and their corresponding slots displacements, calculated from Equation (4.13), are given in Table 4.1. The 35 dB SLR Chebyshev taper has been selected after some simulation iterations, as it provides the desired 20 dB SLR for the SWA. A 20 dB SLR Chebyshev taper leads to SWA SLR lower than the 20 dB goal.

It is clear from Table 4.1 that the slots near the two waveguide ends are closest to the broadface center line, whereas those toward the waveguide center have the largest displacement. This property applies to all the examples.

4.6.1.2 Results

For the previously determined slot parameters (length, width, and coordinates), the SWA computed results show a resonance at 3 GHz, an SLR of 20 dB, and a peak

Table 4.1: 35 dB SLR Chebyshev Taper Coefficients and Corresponding Slots Displacements Leading to an SWA of SLR of 20 dB

Slot Number	Chebyshev Coefficient	Displacement (mm)
1	1	3.74
2	2.086	5.42
3	3.552	7.11
4	4.896	8.4
5	5.707	9.11
6	5.707	9.11
7	4.896	8.4
8	3.552	7.11
9	2.086	5.42
10	1	3.74

gain of 16.1 dB. The H-plane HPBW has increased to 8.4°, compared to the uniform displacement case, as shown in Fig. 4.7. The broadening of the main beam is expected since the sidelobes have been forced to go lower.
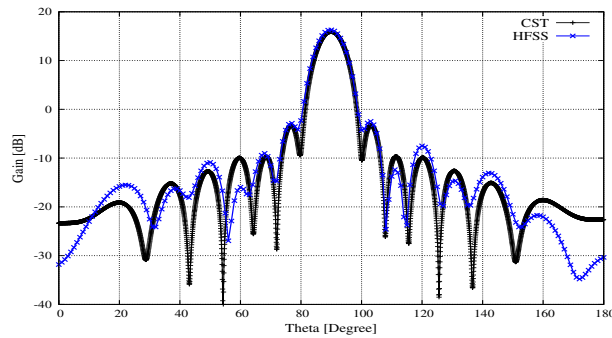
Figure 4.7: Antenna's H-plane gain pattern for the case of non-uniform slot displacement with Chebychev distribution for an SLR of 20 dB

4.6.2 Example 2: 20 dB SLR with Taylor (One-Parameter) Distribution

In this example, the SWA is designed to have an SLR of 20 dB, where the c_ns will be obtained from a Taylor one-parameter distribution [87].

77

4.6.2.1 Coefficients and Slots Displacements

The c_ns for a Taylor one-parameter distribution can be computed using the equations in [88] or [89], as given in the following. The excitation coefficients, $I_n(z')$, for continuous line distribution of length l, are equal to:

$$
I_n(z') = \begin{cases} J_0\left[j\pi B\sqrt{1 - \left(\dfrac{2z'}{l}\right)^2} \right], & \text{for } -l/2 \leqslant z' \leqslant +l/2, \\[3ex] 0, & \text{elsewhere} \end{cases}
\tag{4.14}
$$

For the discrete case [89], the current magnitudes of an N-element linear array with symmetric excitation are equal to:

$$
a_m = \begin{cases} I_0\left[\beta\sqrt{1 - \left(\dfrac{m - 0.5}{M - 0.5}\right)^2} \right], & \text{for N = 2M} \\[3ex] I_0\left[\beta\sqrt{1 - \left(\dfrac{m - 1}{M - 1}\right)^2} \right], & \text{for N = 2M - 1} \end{cases}
\tag{4.15}
$$

where:

- $1 \leq m \leq M$,

- a_1 is the excitation of the array's center element(s),

- and a_M is that of the two edge elements.

For a 20 dB SLR SWA, a 30 dB SLR Taylor (one-parameter) taper is required. The resulting coefficients, and the corresponding slots displacements are listed in Table 4.2.

Table 4.2: 30 dB SLR Taylor (One-Parameter) Coefficients and Corresponding Slots Displacements Leading to an SWA SLR of 20 dB

Slot Number	Taylor-based Coefficient	Displacement (mm)
1	1	3.493
2	2.467	5.518
3	4.137	7.194
4	5.597	8.419
5	6.449	9.070
6	6.449	9.070
7	5.597	8.419
8	4.137	7.194
9	2.467	5.518
10	1	3.493
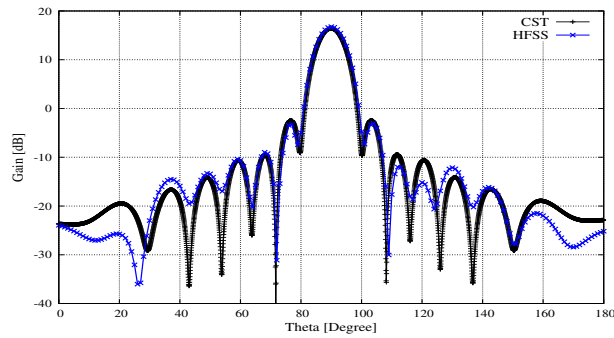
Figure 4.8: Antenna's H-plane gain pattern for the case of non-uniform slot displacement with Taylor (one-parameter) distribution for an SLR of 20 dB

4.6.2.2 Results

For the slots displacements in Table 4.2, the antenna keeps its resonance at 3 GHz, shows an SLR of about 20 dB, and has a peak gain of 16 dB. The H-plane HPBW is 8.5°, as shown in Fig. 4.8. It is to note that for the same SLR of 20 dB, the determined Chebyshev and Taylor (one-parameter) coefficients have led to almost identical radiation patterns, HPBW and gain parameters.

4.6.3 Example 3: 30 dB SLR with Taylor (One-Parameter) Distribution

In this example, a Taylor (one-parameter) distribution is used to obtain an SWA SLR of 30 dB. For this, the taper coefficients for a 40 dB SLR Taylor (one-parameter) distribution are required, and these are listed in Table 4.3 alongside their corresponding slots displacements. The results show an antenna resonance at 3 GHz, and a peak gain of 15.3 dB. The 30 dB SLR has been attained, and the H-plane HPBW has increased to $10°$. The H-plane gain pattern is shown in Fig. 4.9.

Table 4.3: 40 dB SLR Taylor (One-Parameter) Coefficients and Corresponding Slots Displacements Leading to an SWA SLR of 30 dB

Slot Number	Taylor-based Coefficient	Displacement (mm)
1	1	1.631
2	6.611	4.215
3	16.828	6.785
4	28.573	8.937
5	36.519	10.181
6	36.519	10.181
7	28.573	8.937
8	16.828	6.785
9	6.611	4.215
10	1	1.631
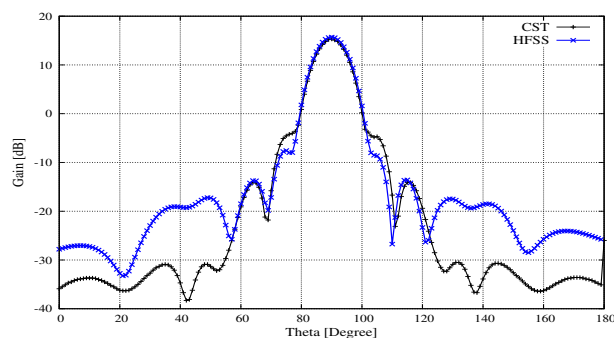
Figure 4.9: Antenna's H-plane gain pattern for the case of non-uniform slot displacement with Taylor (one-parameter) distribution for an SLR of 30 dB

4.6.4 Example 4: Binomial Excitation

Although it is not directly possible to use a binomial distribution to control the SLR, it is interesting to use the c_ns from a Binomial distribution and observe the resulting SWA SLR. The binomial coefficients are obtained from the binomial expansion:

$$(1+x)^{m-1} = 1 + (m-1)x + \frac{(m-1)(m-2)}{2!}x^2 \frac{(m-1)(m-2)(m-3)}{3!}x^3 + \dots \quad (4.16)$$

For the case of 10 slots, the binomial coefficients and the resulting slots displacements are listed in Table 4.4. For these displacements values, the obtained SLR is 33.5 dB, and the peak gain is 15 dB. The H-plane HPBW increases to 11.1°, as shown in Fig. 4.10.

Table 4.4: Binomial Coefficients and Corresponding Slots Displacements

Slot Number	Binomial Coefficient	Displacement (mm)
1	1	0.964
2	9	2.900
3	36	5.847
4	84	9.069
5	126	11.268
6	126	11.268
7	84	9.069
8	36	5.847
9	9	2.900
10	1	0.964

4.6.5 Reflection Coefficients

The S_{11} plots for the four examples are shown in Fig. 4.11. For all the studied examples where all the slots have a fixed length of 54.25 mm, the SWAs retain resonance at 3
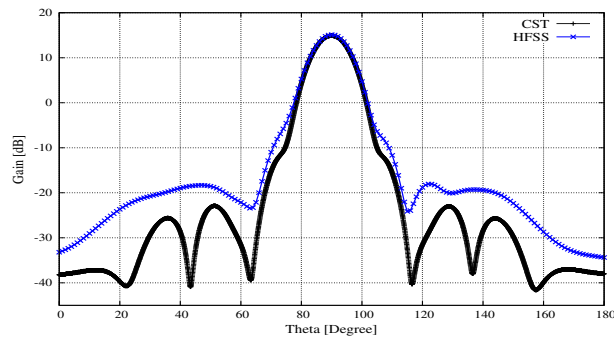
Figure 4.10: Antenna's H-plane gain pattern for the case of non-uniform slot displacement with binomial distribution

GHz, despite the different slots displacements used. This is evident by comparing the S_{11} plot for the case of uniform displacements in Fig. 4.5(a) to those of the four SWA examples in Fig. 4.11, where the resonating length of the elliptical slots proved insensitive to the slots displacement.
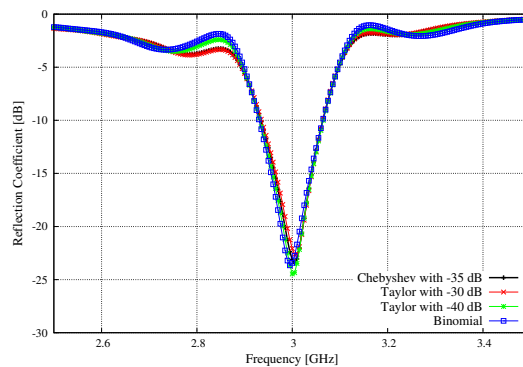
Figure 4.11: Reflection coefficient plots for the four illustrated examples in case of non-uniform displacements (using CST)

4.7   Computer Program

A computer program written in Python has been written to generate the slots displacements for a desired SLR. The program takes as input the design frequency, waveguide dimensions *a* and *b*, the number of slots, and the lowest allowable SLR. It computes

and outputs λ_0, λ_g, the total needed waveguide length, the resonant length of a rectangular slot (which serves as a starting point in optimizing the length of any used slot shape), the width of the slot (which is kept the same for any slot type), the taper coefficients (Chebyshev or Taylor), and the corresponding slots displacements. The units are indicated on the program graphical user interface (GUI). A screenshot of the program output is given in Fig. 4.12. This program was used for the examples in Section 4.6, and for the design in Section 4.8. Improvements to the program interface are still being done.
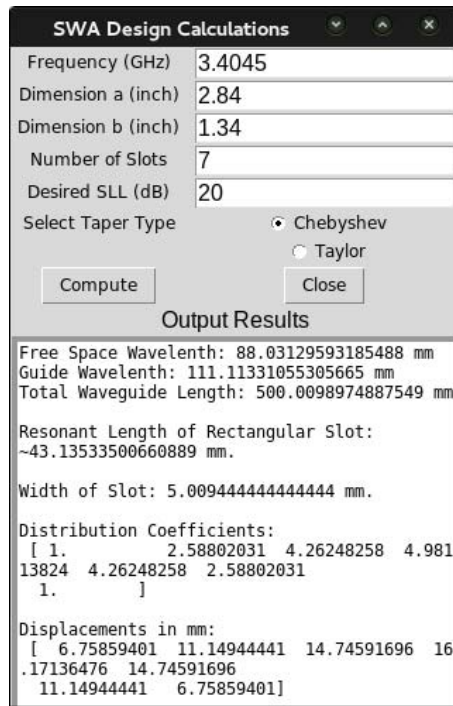
Figure 4.12: A screenshot of the python program output

4.8 Fabrication and Measurements

In order to validate the procedure illustrated in this part of the thesis, a prototype SWA array has been fabricated and tested. The waveguide in hand has a length of 50 cm.

This length is not enough to fit 10 slots respecting the different slot distance and length guidelines, so the design has been made with 7 slots, of elliptical shape. To avoid the two edge slots intersecting the waveguide flanges, the distance between each of these two slots and the nearby waveguide edge has been increased from $\lambda_g/4$ to $3\lambda_g/4$, leading to a total SWA length of $4.5\lambda_g$. This change was accounted for in the Python computer program, which was used for this design. To keep the waveguide length of 50 cm, the SWA is designed for a frequency of 3.4045 GHz. At this frequency, $\lambda_g = 111.11$ mm, and $4.5\lambda_g = 50$ cm. After initially designing the SWA with the correct uniform distribution displacement, the elliptical slot length has been optimized to get to this resonance frequency. It is found equal to 48 mm. With this optimized length, and for a slot width of 5 mm, the SWA has later been designed to radiate with a sidelobe level ratio of more than 20 dB. A Chebyshev distribution of -35 dB has been used to calculate the excitation coefficients in this case. These coefficients and the corresponding slot displacements are listed in Table 4.5.

Table 4.5: Normalized Chebyshev Taper Coefficients and Corresponding Slots Displacements

Slot Number	Chebyshev Coefficient	Displacement (mm)
1	1	6.759
2	2.588	11.149
3	4.262	14.746
4	4.981	16.171
5	4.262	14.746
6	2.588	11.149
7	1	6.759

The design of the fabricated antennas and a photo of the fabricated prototype are shown in Fig. 4.13. The reflection coefficient plot in Fig. 4.15 shows a comparison between the results computed using both CST and HFSS software, and two measured results. During Measurement 1, the slots make on the antenna were mistakenly covered

by scotch tape that was used to handle the antenna on the rotating table. In addition, the antenna itself had some protrusions on the corners of the elliptical slots, which were filed for Measurement 2, resulting in a perfect elliptical shape of the slot. Snapshots taken through Measurements 1 and 2 showing the antenna covered and handled on the rotating table are shown in Figs. 4.14. The compared gain patterns computed in both HFSS and CST and measured are also shown in Fig. 4.16. Inspecting the S_{11} and pattern Figs., credible analogy has been revealed despite the slight difference, which is due to the other inaccuracies in the fabrication. An SLR of more than 20 dB has been achieved, with a gain of around 14.5 dB, validating the design procedure illustrated.

(a)   (b)
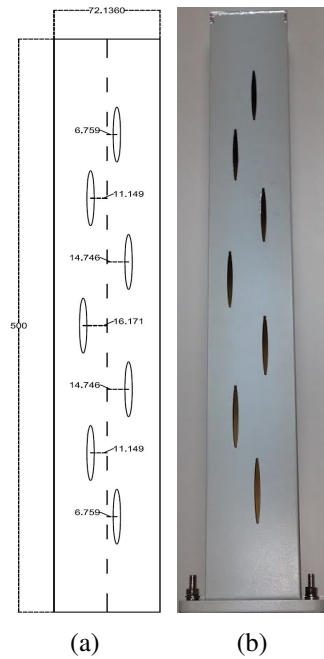
Figure 4.13: SWA: (a) designed (dimensions in mm), (b) fabricated

(a)   (b)
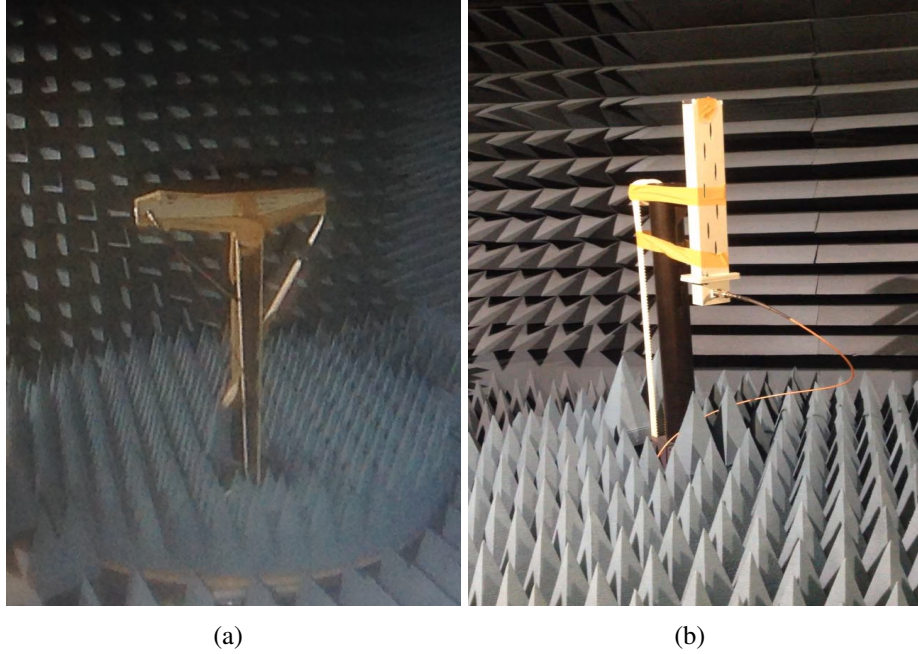
Figure 4.14: SWA: (a) Measurement of gain pattern in the H-plane in Measurement 1,
(b) Measurement of gain pattern in the E-plane in Measurement 2
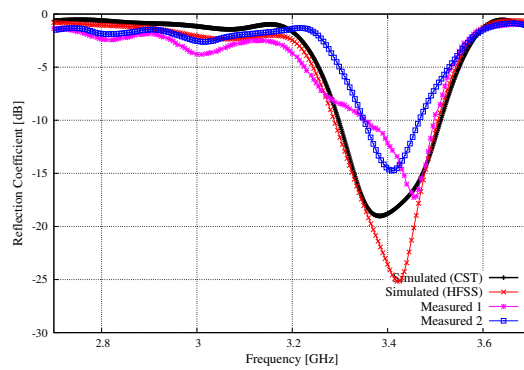
Figure 4.15: The compared measured and simulated reflection coefficient results

(a)   (b)
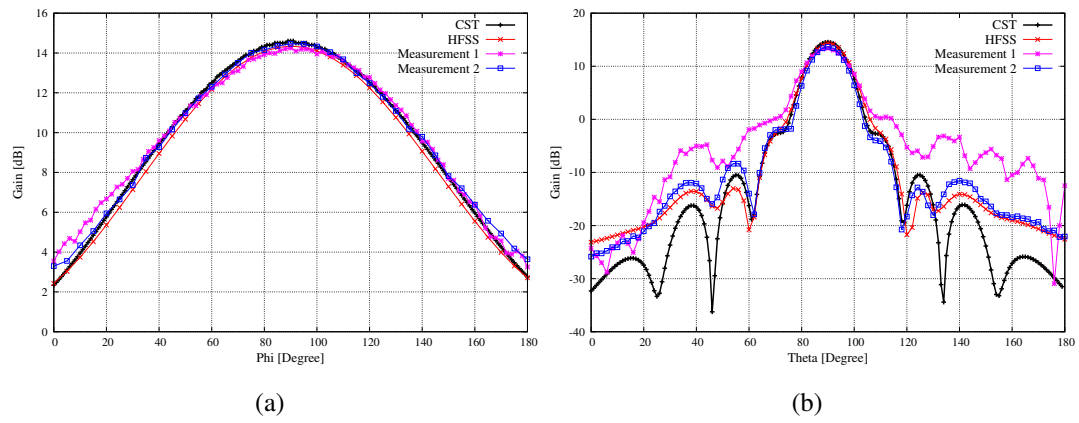
Figure 4.16: The compared simulated gain pattern results using HFSS and CST: (a)
E-plane, (b)H-plane

4.9   Breakdown Capability

Electrical breakdown (also called dielectric breakdown) refers to a rapid reduction in the resistance of an electrical insulator when the voltage applied across it exceeds the breakdown voltage. The breakdown voltage of an insulator is the minimum voltage that causes a portion of it to become electrically conductive [90]. This may be a momentary event (as in an electrostatic discharge), or may lead to a continuous arc discharge. Electrical breakdown can occur within solids, liquids, gases or vacuum, under sufficient electrical stress The specific breakdown mechanisms are significantly different for each. Within a gas, such as air for which we are interested in, electrical breakdown occurs when the dielectric strength of the gas is exceeded, hence regions of high electrical stress will cause nearby gas to partially ionize and begin conducting. Although air is normally an excellent insulator, a sufficiently high voltage of an electric field strength of about $3 \times 10^6 V/m$ can cause the air to begin to break down, and becoming partially conductive, and even reaching complete electrical breakdown if the voltage is sufficiently high [91]. This will culminate in an electrical spark or an electric arc that bridges the entire gap. There exists a non-linear relation between voltage and current before gas breakdown. A schematic is shown in Fig. 4.17, for which 4 regions are found: In region 1, there are free ions that can be accelerated by the field and induce a current, after a certain voltage these ions will be saturated and give a constant current shown in region 2, and finally Regions 3 and 4 are caused by ion avalanche as explained by the Townsend discharge mechanism, for which avalanche multiplication is caused by the ionization of molecules by ion impact [92].

For this, the proper design of the electrical system requires knowledge of the breakdown behavior. Experiments on contacts in air at micrometer gaps have shown that the contact gap crucially controls the breakdown voltage. This demands an eval-
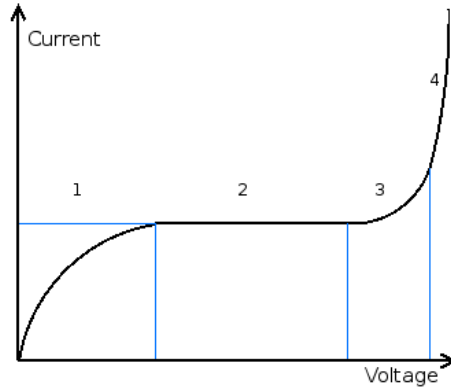
Figure 4.17: Voltage-current relation before breakdown

uation of published electrical breakdown measurements, to quantify the voltage limits and understand the breakdown behavior as a function of contact gap spacing.

Assuming a uniform Electric field distribution in the aperture of E_s, the slot voltage V_s and the radiated power P_s can be written as:

$$V_s = w_s \times E_s$$
$$P_s = V_s^2 G_s$$

(4.17)

where w_s is the slot width and G_s is the slot radiation conductance, which can be determined by duality from the equivalent resonant dipole radiation resistance, $R_d = 73.2\Omega$ by [93]:

$$G_s = \frac{1}{R_s} = \frac{4R_d}{Z_0^2} = 4\frac{73.2}{120\pi^2} = 2.06mS$$

(4.18)

The maximum allowable E_s corresponds to the onset of air breakdown, $E_{arc} = 30kV/cm$. Noting the maximum radiated power as $P_{e_{max}}$, the minimum slot width required to avoid breakdown can be calculated by:

$$w_{e_{min}} = \sqrt{\frac{Z_0^2 P_{e_{max}}}{4R_d E_{arc}^2}}$$

(4.19)

89

Hence, if one knows the maximum power needed on a slot (which will be the middle slots on the SWA), the minimum slot width $w_e^m in$ can be determined to avoid electrical breakdown at high power microwaves. In our case, the slot width is taken to be 5 cm, hence the maximum power that the slot can withstand is:

$$P_{e_{max}} = \frac{w_e^2 4 R_d E_{arc}^2}{Z_0^2} = \frac{(0.5cm)^2 \times 4 \times 73.2\Omega \times (30kV/cm)^2}{(120\pi\Omega)^2} = 4.63544 \times 10^5 W = 463kW$$

(4.20)

Hence, if this design is to be used at high power microwaves, one slot can radiate up to $463kW$ of power without electrical breakdown.

4.10   Mutual Coupling

When two antennas are placed closed to each other, some of the energy that is primarily intended for one ends up at the other, whether one and/or both are transmitting or receiving. This primarily depends on the:

1. relative separation between them

2. radiation characteristics of each

3. relative orientation of each

In our case, each slot is assumed to be a unique antenna or one element, used for transmission. Assuming N slots, and since all the elements are excited simultaneously, the radiated and rescattered fields by and from each slot must be added vectorially to arrive at the total field at any observation point. This is in agreement with the theory of far-field pattern, for which the total contribution of a particular element in the array to the far-field pattern depends not only upon the excitation furnished by its own

generator (the direct excitation) but upon the total parasitic excitation as well. This in turn depends upon the couplings from and the excitation of the other generators [94].

The wave directed from the one slot (Slot$_1$) to the second slot (Slot$_2$) and finally toward the generator is added vectorially to the incident and reflected waves of the Slot$_2$ itself, thus enhancing the existing standing wave pattern within it. For coherent excitations, the coupled wave due to Slot$_1$ differs from the reflected one in Slot$_2$ only in phase and amplitude. These two waves interact depending on the coupling between the slots and the excitation of each. The overall result is that this coupling will influence the input impedance and hence the driving impedance of the elements and usually referred to as mutual impedance variation.

The manner in which these two waves interact depends on the coupling between them and the excitation of each slot. It is evident then that the vector sum of these two waves will influence the input impedance looking in at the terminals of antenna m and will be a function of the position and excitation of antenna n. This coupling effect is commonly modeled as a change in the apparent driving impedance of the elements and it is usually referred to as mutual impedance variation. Since the driving impedance for a given slot is a function of the placement and excitation of the other slots, then optimum generator impedance that maximizes array radiation efficiency varies with array excitation. For this, our procedure is focused on calculating the elements excitations for optimized radiation. These excitation, in their turn, control the displacement of each slot, and hence the coupling between the elements. The resulting radiation, in this case, will slightly change in term of the SLR, bandwidth and resonant frequency which will be slightly lower. Because of that, mutual coupling effects are often neglected for this type of Slotted Waveguide Arrays [67,79,95–98]. In addition, internal higher order mode coupling between adjacent slots is ignored. This is an acceptable assumption since the desired array performance is modest and the *b*

91

dimension of the waveguide is not too small [69]. In our experiments on 1D and 2D SWA arrays, the effects of this mutual coupling were negligible and thus neglected in the study.

4.11 Conclusion

This part of the thesis presented a simple procedure for designing SWAs with specified SLRs. General guidelines for the slots width, length, and longitudinal positions were first given. The offsets of the slots positions with respect to the waveguide center-line, which determine the sidelobe levels, were then obtained from well-known distributions. An intuitive rule regarding the used distribution was deduced, which was to select a distribution with an SLR 15 dB higher than the desired SWA SLR. This procedure was implemented using a Python computer program. Illustrative examples showing the distribution coefficients, slots displacements, resulting patterns and S_{11} plots were given. A prototype antenna was fabricated and tested, and the results were presented.

Most of the work in this chapter has been published by the author in [99, 100].

Chapter 5

From Wave Port to Coaxial Port and Introduction to Two-dimensional Slotted Waveguide Antenna Array

In fabrication and measurement procedures, the wave port will be transformed into a coaxial port to be able to feed the fabricated system and measure its parameters. For this, in this section, we transform the designed antenna in Chapter 4 from a wave-port fed antenna to a coaxial-fed antenna. Later, this antenna is duplicated to form an array of SWAs to be studied in terms of radiation pattern characteristics.

5.1   Coaxial Cable and Antenna Design

The coaxial cable used in the design is a 50Ω coaxial cable known as LMR 400 Cable [101]. It is shown in Fig. 5.1 with its specifications listed in Table 5.1.

The SWA used is the one having the elliptical slots with non-uniform displacement, having less sidelobe levels and better capability of high power than that

93

of the SWA with rectangular slots with uniform displacement. It has the optimized elliptical slots of 10 elements designed in Example 1, 20 dB SLR with Chebyshev Distribution, illustrated in Chapter 4.
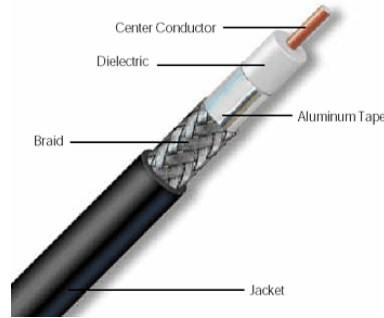
Figure 5.1: LMR 400 cable

Table 5.1: LMR 400 Cable Specifications

Part	Material	Diameter (mm)
Inner Conductor	Physical Foam Polyethylene	7.24
Dielectric	Solid Copper	2.74
First Shield Diameter	Bonded Aluminum Foil	7.39
Outer Conductor Diameter	Tinned Copper Braid	8.00
Jacket	Black PVC or Polyethylene	10.29

In our design, the jacket and braid are not used. Instead, a shield is added around the dielectric material only since the shield is surrounded by vacuum in simulation software.

In order to add the coaxial cable and give room to the probe inside the waveguide, the SWA already designed in previous section has to enlarge. To avoid losing resonance and minimize the effect of adding the probe feed, λ_g is added to the length of the waveguide, such that the probe feed is located at λ_g from the center of the last slot, or $\lambda_g/4$ from the bottom of the waveguide, as shown in Fig. 5.2. The probe length inside the waveguide has been optimized to keep resonance at 3 GHz.
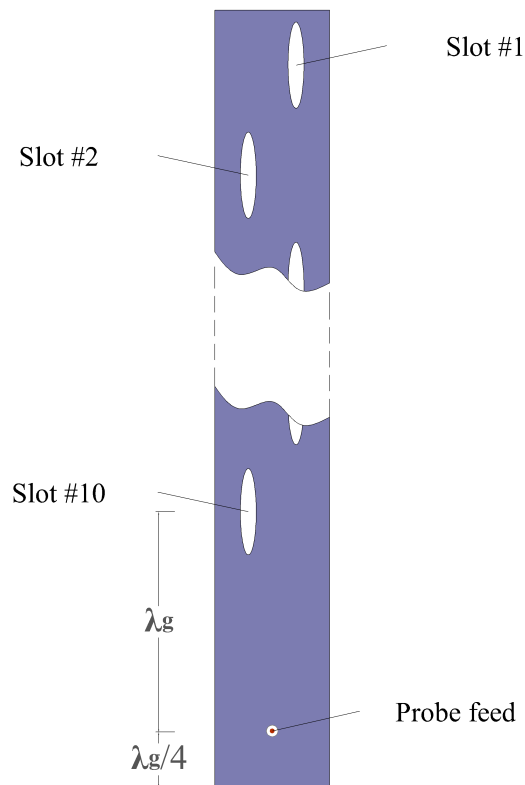
Figure 5.2: SWA with probe feed design

5.2 Simulations and Results

The reflection coefficient result in addition to 2D and 3D radiation patterns are shown in Figs. 5.3, 5.4 and 5.5. Moreover, Table 5.2 summarizes the results of simulations. As can be noticed, the antennas still resonate at 3GHz, with a total realized gain of 15.4 dB.

However, although the antennas has a relatively high gain, it suffers from the wide radiation (broadside of HPBW = 85.1°) in the plane perpendicular to the waveguide axis, i.e. E-plane in the Fig. 5.4. Our goal is to design a well-directive antenna in order not to lose power when working at high power microwave. For this, the HPBW in the E- and H-planes should be as narrow as possible. An array of this SWA is proposed to achieve this goal and radiate in a pencil shape pattern.

95
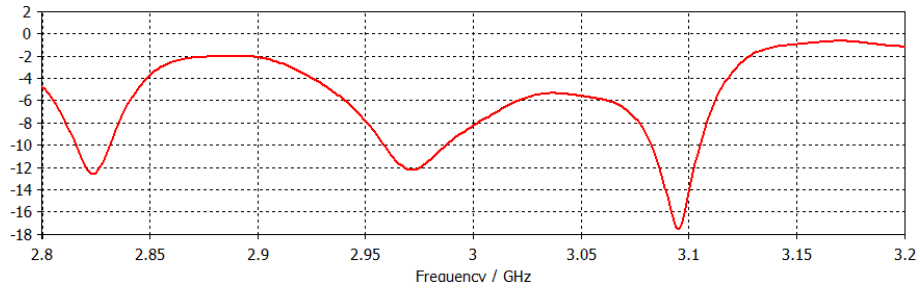
Figure 5.3: Reflection Coefficient of coaxial-fed SWA with elliptical slots

(a)   (b)
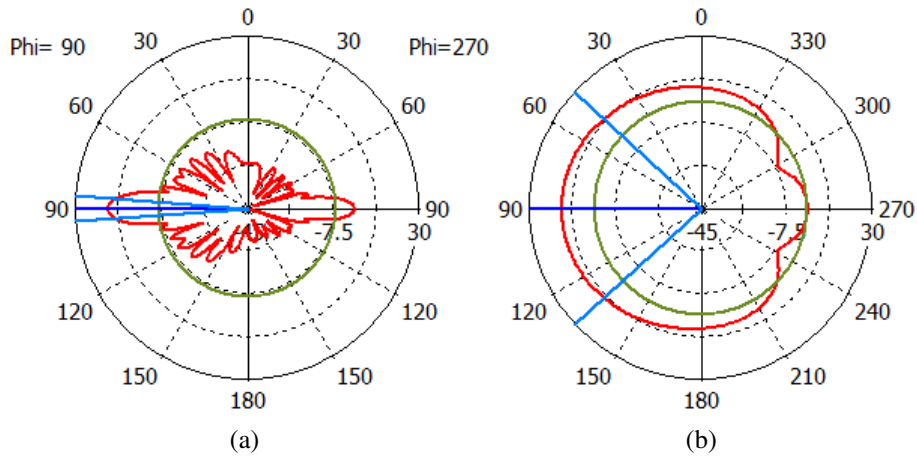
Figure 5.4: 2D radiation pattern of the single SWA, (a) H-plane, (b) E-plane

(a)   (b)
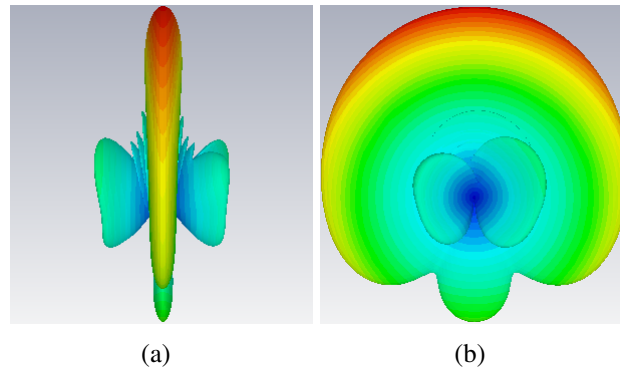
Figure 5.5: 3D radiation pattern of the single SWA, (a) H-plane, (b) E-plane

Table 5.2: Radiation Characteristics of a Single Element Coaxial-fed SWA

Elements	Phi = 90 H-Plane		Theta = 90 E-Plane		SLR	3D Gain
	HPBW	Main Lobe	HPBW	Main Lobe		
1	8.6°	15.4 dB	85.1°	15.4 dB	21.5 dB	15.4 dB

96

5.3 Slotted Waveguide Antenna Arrays

5.3.1 Two Elements Slotted Waveguide Antenna Array

An investigation of the HPBW, sidelobe level ratio, and gain of only 2 parallel elements SWA array is conducted in this section. The effect of the distance separating the two SWAs on the total gain and radiation pattern has been also studied, for which it was observed through simulations that the highest gain of 16.12 dB is achieved when the two SWAs are attached to each other with no spacing in between. For this value of separation, the 2D radiation patterns in both E- and H-planes are shown in Figs. 5.6. In order to compare the results of 2 elements SWA array to single element SWA, Table 5.3 examines the major differences in radiation characteristics of both arrays.
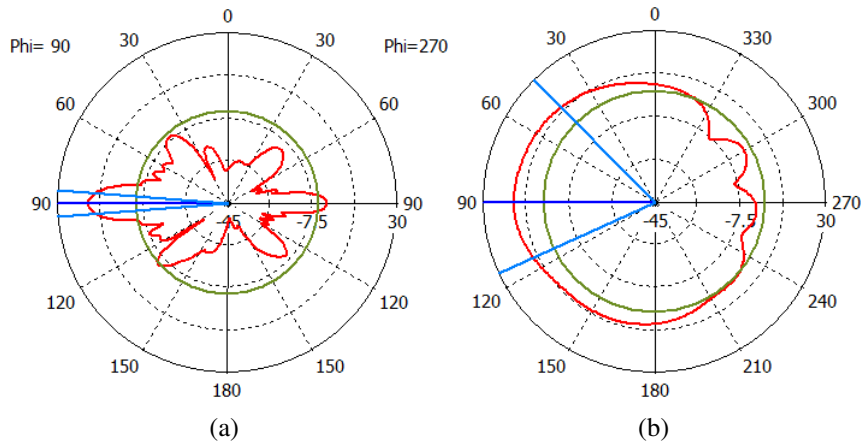
Figure 5.6: 2D Radiation pattern of the two parallel elements SWA array, (a) H-plane, (b) E-plane

As can be indicated from Table 5.3, using 2 elements SWA array resulted in an increased gain from 15.4 dB with the single element to 16.1 dB with 2 elements. However, the important improvement between the two cases is in the HPBW in the E-plane, for which it decreased in the case having 2 elements SWA array from 85.1°

Table 5.3: A Comparison Between the Radiation Characteristics of Single and Two
Elements SWA Array

Elements	Phi = 90 H-Plane		Theta = 90 E-Plane		SLR	3D Gain
	HPBW	Main Lobe	HPBW	Main Lobe		
1	8.6°	15.4 dB	85.1°	15.4 dB	21.5 dB	15.4 dB
2	8.9°	16.1 dB	70°	16.1 dB	26 dB	16.1 dB

to 70°. This supports the idea of building an array in the objective to reach a pencil beam shape radiation. However, these values are still not preferable for high power microwaves, for which high losses will occur for theses radiation characteristics.

5.4 Two-dimensional Slotted Waveguide Antenna Arrays Introduction

Referring to the basic antenna theory, in order to increase the gain of an antenna and direct its radiated wave, an array constructed from several antennas of the same type might be used. The main objective of the thesis is to radiate a high power microwave signal with a pencil shape pattern. The advantage of stacking SWAs in our case is seen in Table 5.3 for which the result of adding one additional SWA improved the radiation performance of the antenna in terms of its gain, SLR, and HPBW. Hence, our main objective is the use of a number of SWA elements, known as branch-lines, large enough to radiate in a pencil shape pattern. The challenge, in this case, is the feeding mechanism of such systems, taking into account that a single feeder can be used to feed the array system. The conventional feeding technique used in such SWA systems uses an additional waveguide as the main feeder to the SWA elements (branch-lines) [102–108].

Two main configurations of this added feeder are found. The first one collects

the narrow wall of the feeder to the input of the SWA branch-lines stacked in parallel. An example is shown in Fig. 5.7. In order to feed the wave into the branches, cut on the narrow wall of the feeder are made. The usual cuts used are those of the inclined coupling slots, or edged slots.
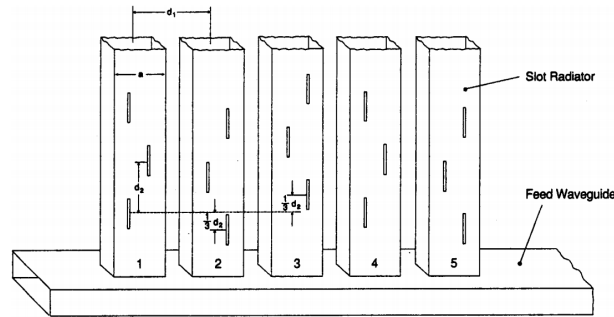
Figure 5.7: Geometry of the proposed antenna array [102]

The second configuration places the feeder on the non-radiating broad-wall faces of the SWA branch-lines. The conventional slots used in this configuration are the inclined coupling slots. An example of this type of feeding is shown in Fig. 5.8.
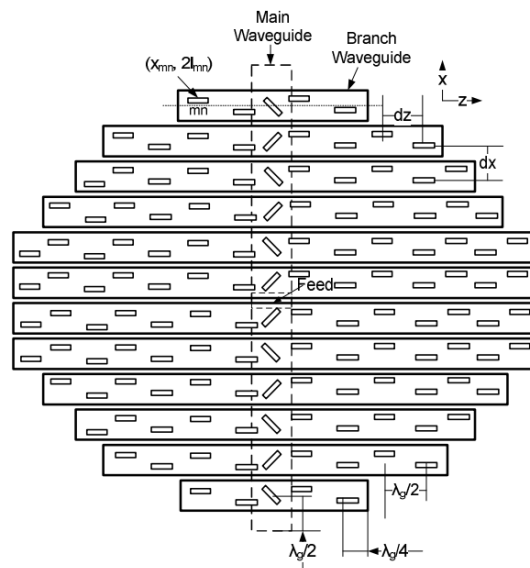
Figure 5.8: Planar slotted waveguide array antenna [107]

Designing the 2D SWA system array is performed in the next chapters. We

99

will start in Chapter 6 by applying the conventional method of feeding, which uses an added SWA as the main feeder, placed on the non-radiating broad-walls of the SWA branch-lines. The SWA branch-lines are designed using our procedural design proposed in Chapter 4. Next, in Chapter 7, a whole SWA system is designed using our procedural steps proposed in Chapter 4, for which the feeder used feeds the power using elliptical shunt slots rather than the conventionally used coupling slots or edge slots for feeding.

Chapter 6

Two-dimensional Slotted Waveguide Antenna Arrays with Inclined Coupling Slots

After investigating the design of one module Slotted Waveguide Antenna with a desired sidelobe level ratio in Chapter 4, this chapter investigates the use of inclined coupling slots in the added feeder. A simple procedure is illustrated for which the rotation angle of each inclined slot is optimized to obtain an overall low value of sidelobe levels.

6.1   Introduction

Inclined coupling slots have found their interest as the radiating elements used in the main feeder to couple the power to the SWA branch-lines in two-dimensional (2D) SWA array systems. Based on the procedure described by Elliott in [68], Bhatti *et al.* designed a planar slotted waveguide array antenna for X-band radar applica-

tions [107]. The antenna consists of multiple branch-line waveguides with broadwall radiating shunt slots. The inclined coupling slots are used on the main waveguide used to feed the branch waveguides, as shown in Fig. 5.8. The antenna feed point is located at the center of the main waveguide.

The same feeding technique has been used by Li *et al.* in [106]. The geometry of the proposed antenna array is shown in Fig. 6.1, which consists of two feeding waveguides, twelve feeding slots, twelve radiating waveguides, 20×12 radiating slots and a T-junction. Inclined feeding slots are also used to couple the wave incident from feeding port and fed into the radiating waveguides before it radiates into free space. The T-junction feeds equal amplitude and equal phase energy to the two feeding waveguides, with the center-fed configuration used to increases the operation bandwidth. On the broadwall of the rectangular waveguide, a staggered-slot is used as the feeding slot. The coupling energy is determined by the inclination angle of every slot.
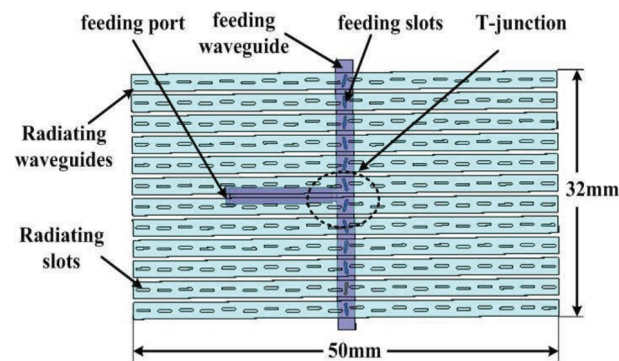
Figure 6.1: Geometry of the proposed antenna array [106]

Moreover, Sekretarov *et al.*, proposed an approach to the synthesis of large-aperture slotted waveguide antennas [108]. The approach is based on a combined usage of a full wave simulation and physical properties of SWA, and was applied to the development of a large-aperture Ka-band antenna, using the same feeding mechanism, as shown in Fig. 6.2.
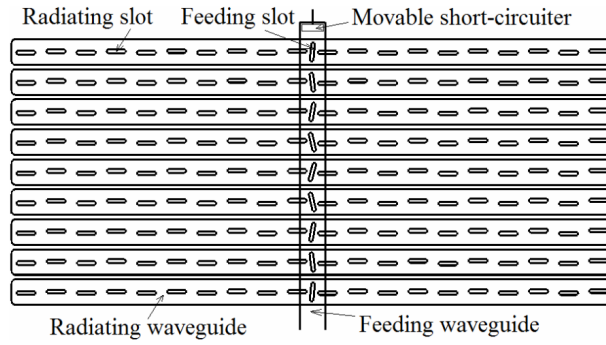
Figure 6.2: Geometry of the proposed antenna array [108]

The same feeding technique was also used by Hung and Chou who presented a design of X-band slotted waveguide antenna array that exhibits high directivity for a long-distance communication [103]. Their proposed antenna is shown in Fig. 6.3.
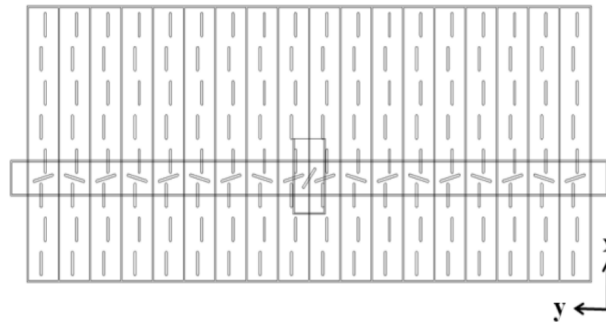
Figure 6.3: Geometry of the proposed antenna array [103]

Our objective is to use this type of feeding to feed a SWA array operating in the S-band. Care should be taken to the dimensions of the slots used in the feeder-waveguide, in addition to their rotation angle that determines the amount of power entering each element of SWA array.

This chapter presents an inventive simple procedure for the design of a two-dimensional (2D) SWA array system with a desired sidelobe level ratio, using inclined feeding slots and elliptical longitudinal radiating slots. The system consists of multi-ple branch-line waveguides with broadwall radiating shunt slots. A main waveguide is used to feed the branch waveguides through a series of inclined coupling slots with

well-defined rotation angles for low SLLs. For a specified number of identical longitudinal slots, our described procedure finds the slots length, width, locations along the length of the waveguide, and displacements from the center-line for each branch waveguide. Furthermore, for a specified number of branch waveguides, the method finds the rotation angle of each of the coupling slots.

To explain the controllable-sidelobe 2D SWA design procedure, an SWA with 8×8 elliptical slots, designed for an SLR around 20 dB, is taken as an example. An 8-element 1D SWA with a desired SLR is designed first. Eight identical SWAs are then attached side by side. The proper design of the 1D SWAs ensures having the desired SLR in one principal plane. To enforce the same SLR over the whole 3D pattern, special care should be given to the design of the feed SWA, whose slots should power the radiating SWAs according to a correct distribution. For the taken example, the feed SWA should have 8 slots, separated consecutively by a distance related to the radiating SWA aperture width and wall thickness. The power fed by each slot in the feeder and fed to the branchline waveguide is controlled by the inclination angle of the coupling slot. Two 2D designs are studied, which differ in the design of the SWA branch-lines. The simulations results for both designs are reported and compared.

6.2   Feeder Design

According to the procedure described by Elliott in [71] and A. F. Stevenson in [67], for the inclined slot in the broad wall shown in Fig. 4.1(b), the real part of the coupling-slot impedance can be given by:

$$\frac{R}{R_0} = 0.131 \frac{\beta_{10}}{k} \frac{\lambda_0^2}{ab} [I(\theta) sin(\theta + \frac{\lambda_g}{2a} J(\theta) cos(\theta)]^2 \qquad (6.1)$$

where θ is the angle of tilt, and:

$$\left.\begin{array}{c} I(\theta) \\ \\ J(\theta) \end{array}\right\} = \frac{cos(\frac{\pi K_1}{2})}{1-K_1^2} \pm \frac{cos(\frac{\pi K_2}{2})}{1-K_2^2} \tag{6.2}$$

$$\left.\begin{array}{c} K_1 \\ \\ K_2 \end{array}\right\} = \frac{\beta_1 0}{k}cos\theta \mp \frac{\lambda_0}{2a}sin(\theta) \tag{6.3}$$

However, as can be inspected through the equations, the process of calculating the inclination angles using these equations is a bit complicated. Nevertheless, our simulations proved that, working with the branches and designing in a way to radiate with low sidelobe levels, is somehow sufficient to obtain a 2D system radiated wave of low sidelobe levels. In this work, we calculate the excitation coefficient in a first step based on the distribution and SLR needed, and then we use the basic definition of the inclination angle, for which the power radiated by the inclined slot is directly related to the square of the inclination angle, i.e. the angle between the center of the waveguide and the slot, to calculate the needed inclination angle for each slot.

6.2.1   Example: Binomial Excitation

Although it is not directly possible to use a binomial distribution to control the SLR, using binomial excitations can lead to very low SLL. The binomial coefficients are obtained from the binomial expansion given in Equation 4.16.

An SWA of 8 slots is used in our system. In a simple procedure, we will assume that the largest binomial coefficient, i.e. 35 at slots 4 and 5 (in the center of the SWA), is that of an inclination angle of 45°, or $sin^2(\theta_4) = sin^2(\theta_5) = (\sqrt{2}/2)^2 = 1/2$. The other angles corresponding to the binomial coefficients of 1, 7, and 21, can be calculated using simple proportionality. For example, for a binomial coefficient of 1, the power radiated by the slot should be proportional to $(1/2)/35 = 1/70$. Hence,

105

$sin^2(\theta_1) = sin^2(\theta_8) = 1/70$, and thus $\theta_1 = \theta_8 = sin^{-1}\sqrt{1/70} = 6.864°$. The values calculated for other binomial coefficients are listed in Table 6.1.

Table 6.1: Binomial Coefficients and Corresponding Slots Displacements

Slot Number	Binomial Coefficient	Inclination Angle (°)
1	1	6.864
2	7	18.435
3	21	33.211
4	35	45
5	35	45
6	21	33.211
7	7	18.435
8	1	6.864

6.3 Branches Design

The feeder designed is used in two different SWA array systems, which are differentiated through the design of the SWA branch-lines used to radiate the wave in each system.

6.3.1 Two-dimensional Slotted Waveguide Antenna Arrays with Inclined Coupling Slots - Same Branch-lines

The first SWA branch-lines design is built through stacking 8 SWA modules of the same design, designed to operate at a frequency of 4.021 GHz, with 20 dB chebyshev distribution used to calculate the slots displacements using Equation 4.11. The corresponding chebycheb coefficients and slots displacements are listed in Table 6.2.

Table 6.2: Chebyshev Distributions and Corresponding Slots Displacements

Slot Number	Chebychev Coefficient	Displacement (in mm)
1	1	4.460
2	2.420	7.040
3	4.094	9.327
4	5.220	10.674
5	5.220	10.674
6	4.094	9.327
7	2.420	7.040
8	1	4.460

6.3.1.1 Results

Figs. 6.4(b) and 6.4(c) show a comparison of the gain patterns for the following 2 cases: Case 1 where the radiating slots have a uniform displacement and the coupling slots have a uniform rotation angle; and Case 2 where the radiating slots have non-uniform displacements and the coupling slots have non-uniform rotation angles as per the design procedure. As inspected, the SLR increased from 12.1 dB in case of uniform displacements and rotation angles to more than 20 dB with the non-uniform displacements and inclinations calculated using the presented simple design procedure.

6.3.2 Two-dimensional Slotted Waveguide Antenna Arrays with Inclined Coupling Slots - Different Branch-lines

NEW In the second system, two designs of 8 SWA branchlines each are studied. These two designs differ from design 1 in the length of the waveguide branchlines, for which the system takes an hexagonal shape, and hence different number of slots cut are needed in the branchlines. Designs 2-a and 2-b differ in the slots displacements. In Design 2-a the same displacements are adopted on all branchlines. In Design 2-b the displacements are re-calculated for each branchline according to the variations in

length and number of slots cut needed on each. This is shown through inspecting the displacements values of Designs 2-a and 2-b in Tables 6.3 and 6.4. Simulating both designs, a comparison of the radiation characteristics results of Design 1, 2-a, 2-b, and a uniform case having uniform slots displacements and inclination angles, is summarized in Table 6.5.

Table 6.3: Design 2-a Corresponding Slots Displacements

SWA Branchline & Slot Displacements							
1	2	3	4	5	6	7	8
-	-	-	4.460	4.460	-	-	-
-	-	7.040	7.040	7.040	7.040	-	-
-	9.327	9.327	9.327	9.327	9.327	9.327	-
10.674	10.674	10.674	10.674	10.674	10.674	10.674	10.674
10.674	10.674	10.674	10.674	10.674	10.674	10.674	10.674
-	9.327	9.327	9.327	9.327	9.327	9.327	-
-	-	7.040	7.040	7.040	7.040	-	-
-	-	-	4.460	4.460	-	-	-

Table 6.4: Design 2-b Corresponding Slots Displacements

SWA Branchline & Slot Displacements							
1	2	3	4	5	6	7	8
-	-	-	4.460	4.460	-	-	-
-	-	5.692	7.040	7.040	5.692	-	-
-	8.712	9.672	9.327	9.327	9.672	8.712	-
18.860	14.899	12.379	10.674	10.674	12.379	14.899	18.860
18.860	14.899	12.379	10.674	10.674	12.379	14.899	18.860
-	8.712	9.672	9.327	9.327	9.672	8.712	-
-	-	5.692	7.040	7.040	5.692	-	-
-	-	-	4.460	4.460	-	-	-

6.3.3   Results Discussion

Inspecting Table 6.5, one can see that Design 1 proposed achieves very low SLLs in both E- and H-planes compared to the case of having uniform inclined coupling slots. Design 2, having planar hexagonal shape, has lower SLL in H-plane (plane of interest) and lower HPBW in E-plane, but with a relatively higher SLL in E-plane, higher

Table 6.5: Compared Gain Pattern Results of 2D Design 1 and Design 2 With Both Configurations (2-a and 2-b)

Design	Gain (*dB*)	SLR (*dB*)		HPBW (°)	
		E-Plane	H-Plane	E-Plane	H-plane
Uniform	25.09	19.3	12.1	9.2	9.2
Design 1	23.7	22.5	28.6	12.6	10.6
Design 2-a	22.7	20.4	29.6	12	14.9
Design 2-b	22.11	19.3	32.4	12.1	15.7

HPBW in H-plane, and a lower gain. Hence, no major added values are seen as a result of transforming the all 8×8 SWA array system to the planer hexagonal one. Comparing the two configurations of Design 2, one having the same slots displacements between the branchlines and the second having different slots displacements according to the length and number of slots of each SWA branch, it is seen that both designs resulted in similar gain results, with a relatively higher gain, lower SLL in E-plane, and lower HPBW, for configuration 2-a having same slots displacements. Hence, the use of different displacements of slots between SWA branchlines in such configurations has no valuable improvements. The increment of HPBW in the three designs is higher than that of the uniform, and this is normal because of the decrement in the SLL values.
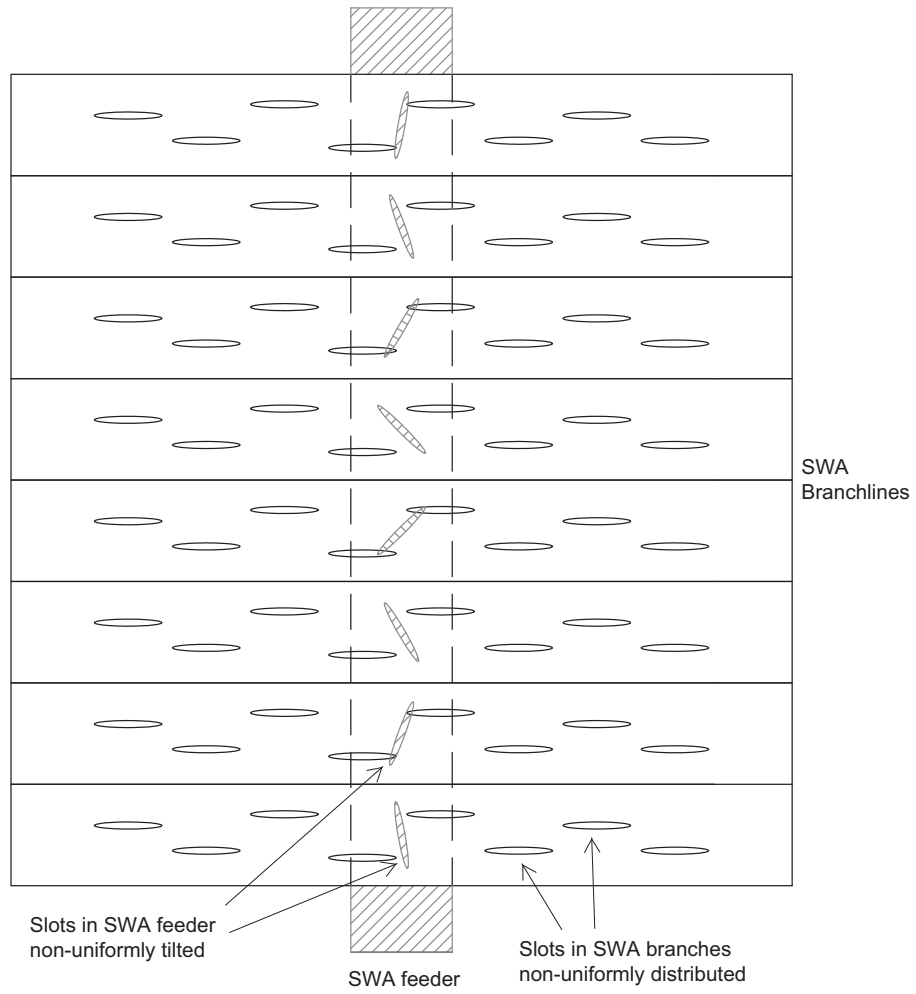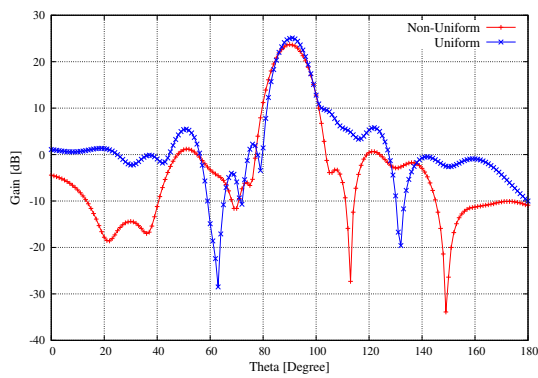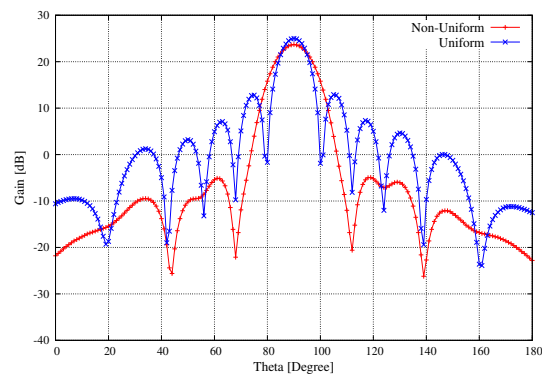
Figure 6.4: (a) 2D System, Compared gain pattern results of the uniform and non-uniform displacements and rotation angles design cases: (b) E-plane, (c) H-plane
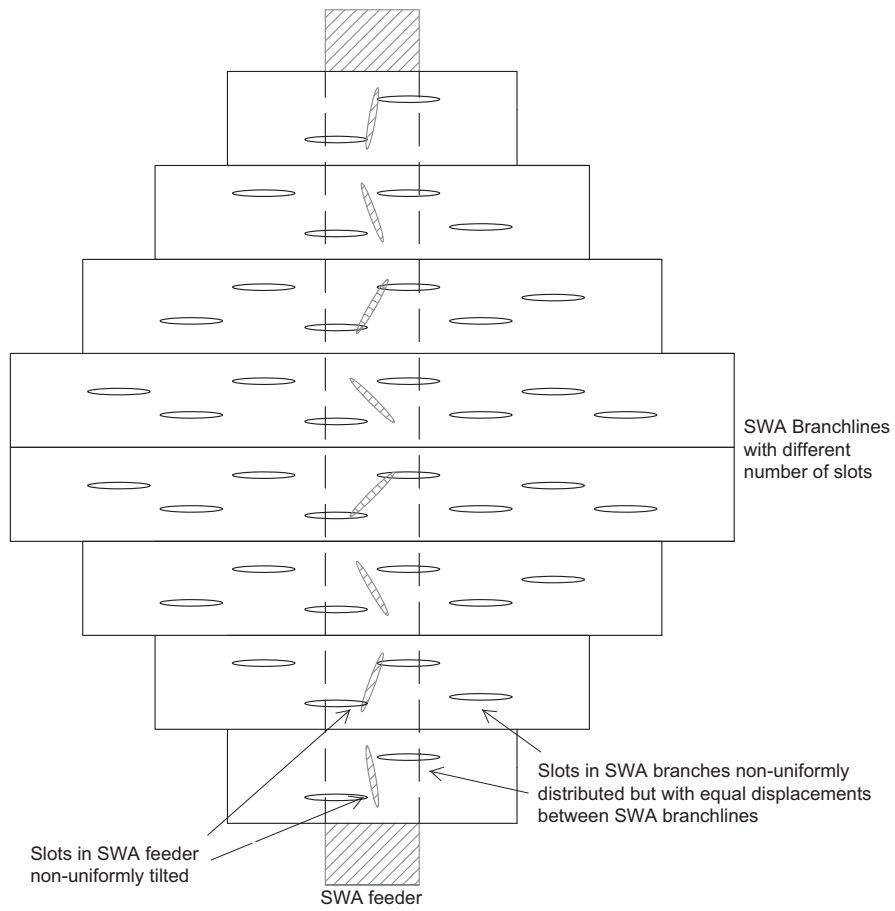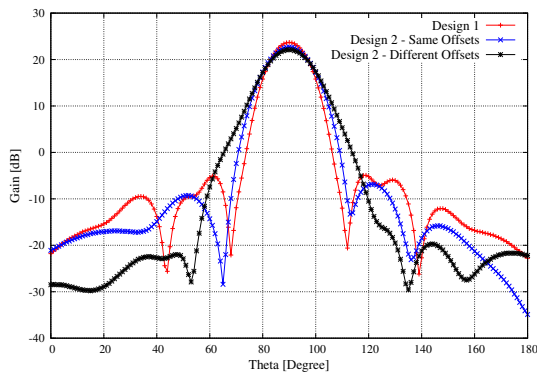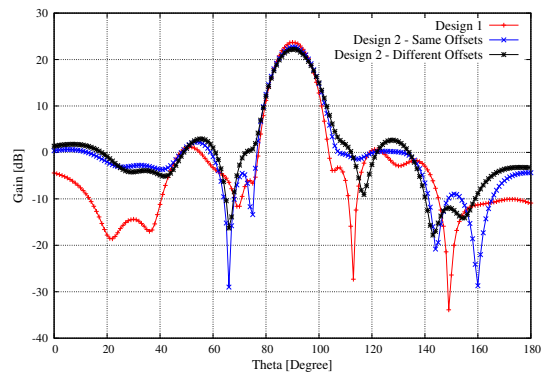
Figure 6.5: (a) 2D System, compared gain pattern results of 2D design 1, and design 2 with both configurations: (b) E-plane, (c) H-plane

6.4 Conclusion

This chapter presented a simple procedure for the design of 2D slotted waveguide antenna arrays with desired SLRs, using inclined coupling slots in the main feeder. Multiple SWA branches are used as radiating antennas, with a main SWA used in a as the feed. The procedure was illustrated through two examples designs of 8×8-elliptical-slot SWA arrays with SLR higher than 20 dB.

Most of the work in this chapter has been published by the author in [109].

Chapter 7

Two-dimensional Slotted Waveguide Antenna Arrays with Longitudinal Shunt Slots

This chapter presents an inventive and simple procedure for the design of a two-dimensional (2D) Slotted Waveguide Antenna (SWA) having a desired sidelobe level ratio (SLR) and a pencil shape pattern, using longitudinal elliptical slots in both branches and feeder SWAs. The 2D array is formed by a defined number of one-dimensional (1D) broadwall SWAs, which are fed using an extra broadwall SWA. For specified number of identical longitudinal slots in both dimensions, the desired SLR and the required operating frequency, this procedure finds the slots length, width, locations along the length of the waveguide, and offsets from its center-line. This is done for the radiating SWAs as well as the feed SWA. Two examples of SWA systems with 8×8 elliptical slots and 10×10 are designed using this procedure for an SLR higher than 20 dB. Design results are outlined and obtained data are given and explained.

113

7.1 Introduction

In this part of the thesis, a two-dimensional (2D) SWA array is designed for a pattern with a desired sidelobe level ratio (SLR). It consists of multiple branch-line waveguides with broadwall radiating shunt slots. A main waveguide is used in a novel way to feed the branch waveguides through a series of coupling slots. The conventional feeding mechanism as seen in previous chapters is based on the use of inclined broadwall coupling slots [107]. A second mechanism employs inclined or non-inclined slots in the narrow wall [72, 74]. For the procedure presented in this thesis, longitudinal broadwall slots are proposed for the feeding.

To explain the controllable-sidelobe 2D SWA design procedure, an 8×8 SWA is taken as an example, but the procedure may apply to any dimension using the steps presented by the authors in [99] for the 1D SWA case. This part of the thesis starts with the design of an 8-element 1D SWA with the same desired SLR. Eight identical such SWAs are required for the 2D SWA, where they are attached side by side. The proper design of the 1D SWAs ensures having the desired SLR in one principal plane. To enforce the same SLR over the whole 3D pattern, special care should be given to the design of the feed SWA, whose slots should power the radiating SWAs according to a correct distribution. For the taken example, the feed SWA should have 8 slots, separated consecutively by a distance related to the radiating SWA aperture width and wall thickness. Since this distance can be different from a half-guide wavelength, additional steps are taken to design the feed SWA using the procedure in [99], but without added complexity. Elliptical slots are also used in the example since they are more robust for high-power applications.

7.2 Design Procedure

The complete SWA system consists of 8 branch-line SWAs, each with 8 broadwall radiating shunt slots, and an 8-slot feed SWA. All SWAs, main and branch-lines, are designed to have a minimum SLR value of 20 dB, using the procedure described by the author in [99]. The design is done for the 3.952 GHz frequency to ensure the branch-line SWAs have each a total length of 50 cm.

7.2.1 Branch-line Slotted Waveguide Antennas Design

WR-229 waveguides ($a = 2.29$ in, $b = 1.15$ in) are used for the branch-line SWAs. The 8 slots are distributed as follows: the center of the first slot and the last slot are placed at a distance of quarter guide wavelength ($\lambda_g/4$), or $3\lambda_g/4$, from the waveguide feed and the waveguide short-circuited side respectively; and the distance between the centers of two consecutive slots is $\lambda_g/2$. The calculated slots displacements for each SWA branch using the procedure described by the authors in [99] from a Chebyshev taper are listed in Table 7.1. The length of the elliptical slot, optimized to obtain a low reflection coefficient S_{11} at 3.952 GHz, is found to be 41 mm. The slot width is equal to 4 mm. According to the used antenna orientation, each branch-line SWA has a broadside SWA in the E-plane, and an SLR higher than 20 dB in the H-plane.

7.2.2 Feed Slotted Waveguide Antenna Design

The main SWA has to be designed to feed the branch-line SWAs with a power distribution that results in an SLR not lower than 20 dB in the E-plane. The feed SWA is designed in a similar way to the radiating SWAs, with 8 elliptical slots made to the broadwall. The major difference is the spacing between the slots. To position each slot

at the center of each branch-line SWA, the distance between neighboring feed slots is equal to $a + 2w$, where w is the branch waveguide wall thickness. This is different from the conventional $\lambda_g/2$ distance assumed in [69] and [99], and would affect the operating frequency of the feed SWA if not addressed properly.

To overcome this issue, the waveguide dimensions for the feed SWA should be selected such that half the guide wavelength of the feed SWA is as close as possible to $a + 2w$ of the branches, or $\lambda_{g(feed)} \simeq 2 \times (a_{branch} + 2w_{branch})$. For this example, $a_{branch} + 2w_{branch} = 62.23$ mm, and the closest standard waveguide having $\lambda_{g(feed)}/2 \simeq 62.23$ mm is the WR-187 waveguide, with $\lambda_{g(feed)}/2 = 62.96$ mm. If standard waveguide dimensions do not provide a satisfactory solution, non-standard ones (for the feed or even the branch-line SWAs) should be used. The length of the required WR-187 feed waveguide is 624.5 mm. The slots displacements calculated by the authors in [99] from a Chebyshev taper are listed in Table 7.1. The width of the elliptical slots of the feed is 3.3 mm. The optimal length for the standalone feed SWA for resonance at 3.952 GHz is 41.7 mm.

Table 7.1: Slot Displacements in Branch and Feed SWAs

Slot Number	Displacement (mm)	
	SWA Branch (WR-229)	SWA Feeder (WR-187)
1 & 8	4.26	1.88
2 & 7	6.72	2.93
3 & 6	8.88	3.84
4 & 5	10.15	4.349

7.2.3 Two-dimensional Slotted Waveguide Antenna Arrays with Longitudinal Shunt Slots

The feed SWA is integrated with the branch SWAs by having identical slots cut into the back broadwall of each branch SWA to coincide with the feed slot. The combined

SWA system is shown in Fig. 7.1(a). Since the feed slots have different displacements from the feed waveguide center-line, and in order to have each at the exact middle of the back broadwall of the corresponding branch SWA (equidistant from slots 4 and 5), each branch SWA is moved according to the displacement of its own feed slot.

7.3 Simulations and Results

The design is simulated with the parameters listed in the previous section. Fig. 7.1(b) shows the reflection coefficient (S_{11}) of the branch, feed, and the 2D SWAs. The gain pattern plots of a 1D SWA and the complete 2D are given in Fig. 7.2. Comparing the 1D and 2D cases, the HPBW in the E-plane has decreased from $78°$ to $8.8°$, and the total gain has increased from 15.3 dB to 24 dB. The SLR for the 2D SWA is 20 dB in the E-plane, and 23.5 dB in the H-plane.

In addition, the breakdown capability if this antenna array has been studied, for which the maximum value of voltage has been calculated on the slot responsible for the maximum radiation. The slots that give the maximum radiation are the slots found in the middle of the array system: having the maximum fed power input from the SWA feeder, and the maximum displacements from the SWA branchline centerline where the slots are located. Simulating the design taking a high input power to the SWA feeder of a 6.25 MW, the maximum voltage on these slots is found to be equal to 5.55×10^5 V/m. This maximum voltage is still lower than the onset of air breakdown $3 \times 10^6 V/m$ that can cause the air to begin to break down. A lower value of this maximum voltage, and hence a higher value of power radiated, can be attained using larger slot width value.

SWA Branchlines

SWA branches moved according to feeding slots displacements

Slots in SWA feeder non-uniformly distributed

SWA feeder

Slots in SWA branches non-uniformly distributed
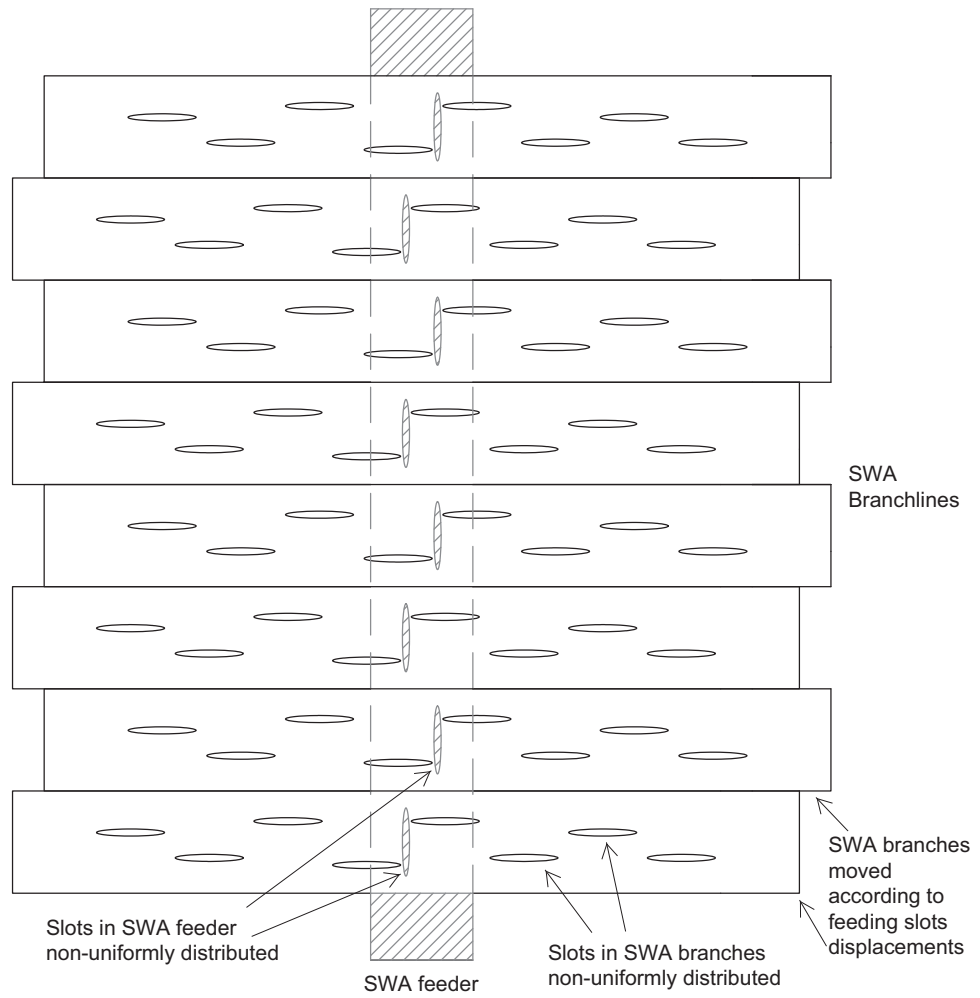
(a)
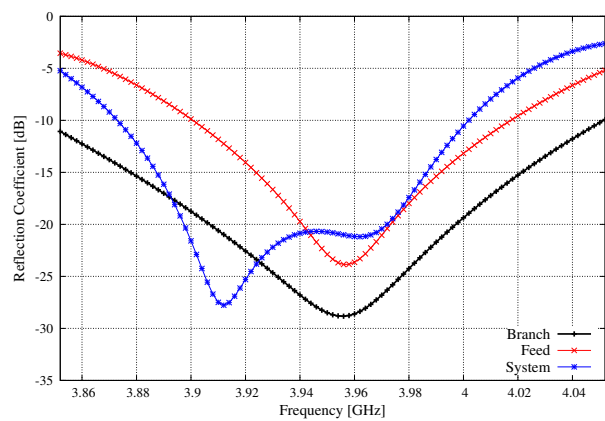
(b)

Figure 7.1: (a) Design of 2D SWA, (b) S_{11} for the branch, feed, and 2D SWAs, computed using ANSYS HFSS
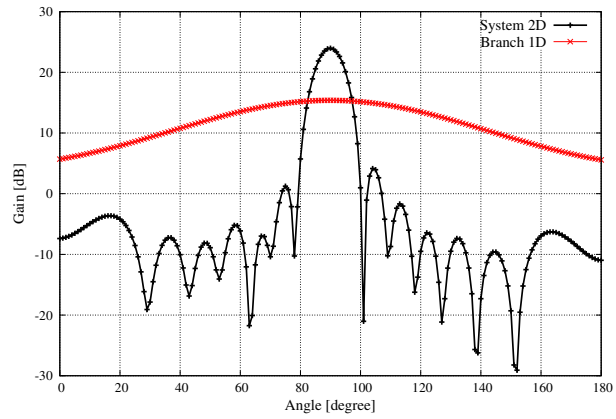
(a) E-plane
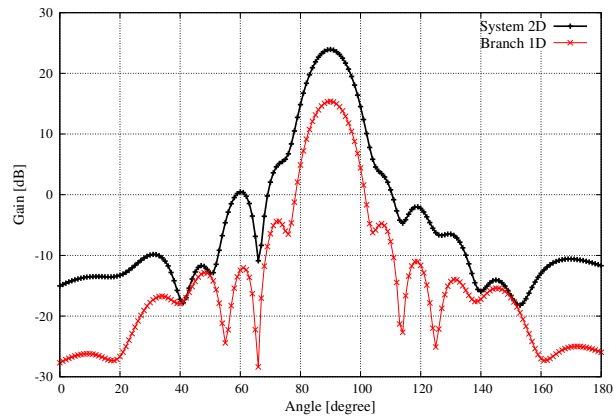
(b) H-plane

Figure 7.2: Rectangular gain pattern comparison of 1D and 2D SWAs, (a) E-plane, (b) H-plane, computed using ANSYS HFSS

7.4 Second Example

In the second example, a 10×10 SWA array is designed using the same design procedure described in this chapter. The system operates at 2.9 GHz, with the simulated polar gain patterns and 3D gain patterns, shown in Figs. 7.3 and 7.4 respectively. The radiation characteristics are also listed in Table 7.2. As can be seen, a pencil shape pattern has been obtained, validating our thesis objective.
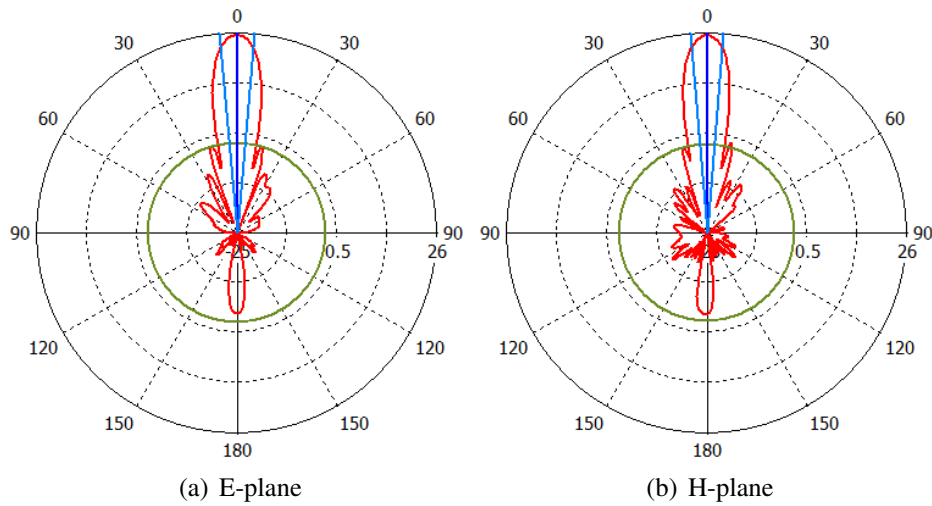
(a) E-plane   (b) H-plane

Figure 7.3: Polar gain pattern comparison of 10×10 2D SWA, (a) E-plane, (b) H-plane, computed using CST

Table 7.2: Gain Pattern Characteristics of the 10×10 2D SWA, Computed Using CST

Antenna	E-Plane		H-Plane		Gain
	HPBW°	SLR (dB)	HPBW°	SLR (dB)	
10×10 2D SWA	10	27.4	9.4	27.7	25.3 dB

7.4.1 Results Discussion

The 10×10 SWA array has been implemented to test the proposed method and validate the assumed improvements in this thesis. This is done through comparing the results
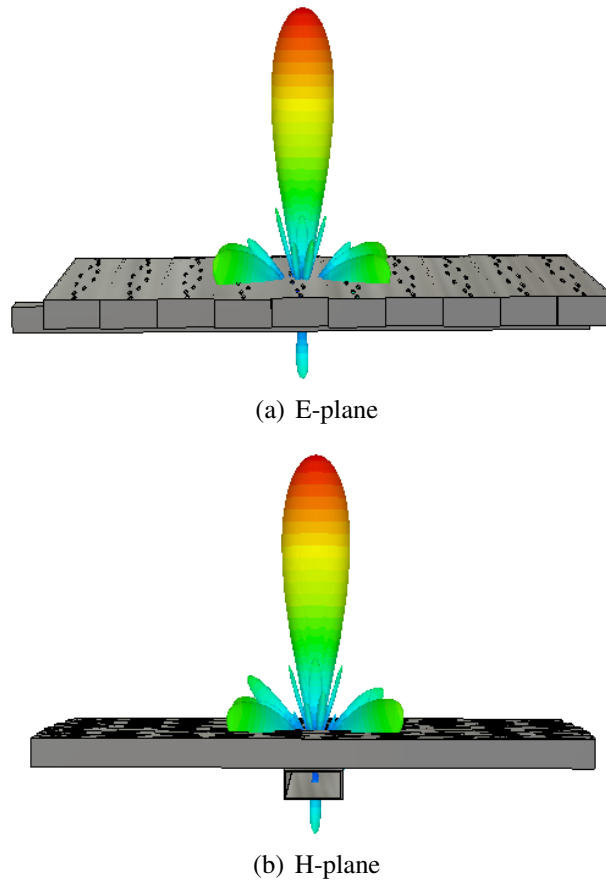
(a) E-plane

(b) H-plane

Figure 7.4: 3D gain pattern comparison of 10×10 2D SWA, (a) E-plane, (b) H-plane, computed using CST

achieved to a similar design proposed in [82], for which two proposed systems are found: a 10×10 SWA array with a main feeder connected as described in this thesis but using the conventional feeding mechanism of inclined coupling slots, and four arrays attached to each other in a rectangular shape each constructed each from 10×10 SWA branchlines with a main feeder, having a total of 40 SWA branchlines, each having 10 slots, with 4 main feeders, with both systems operating at 2.856 GHz, which is close to the frequency of operation of the array proposed her, i.e. 2.9 GHz. The gain of the single module is the same as in our proposed design. Table 7.3 shows a comparison of our proposed antenna and the similar designs proposed in [82].

Inspecting the compared results, one can easily see that our proposed design

Table 7.3: Gain Pattern Characteristics Comparison of Our Proposed Antenna and Similar Designs in [82]

Antenna	SLR (dB)		Gain (dB)
	E-Plane	H-Plane	
Our Proposed Design 10×10	27.4	27.7	25.3
Single Array 10×10 in [82]	13.67	13.67	25.4
Four Arrays 10×10 each in [82]	22.2	22.72	31.4

outperforms the similar single module design and even the four modules array system proposed in [82]. The gain is the same compared to the similar single module design. The SLLs of our proposed design in both planes is lower by around 14 dB compared to the single module design, and by around 3 dB compared to four SWA arrays system. These results validate our design procedure, and assure achieving low SLL, while maintaining high gain values.

7.5 Conclusion

This chapter presented a simple procedure for the design of 2D slotted waveguide antenna arrays with desired SLRs. Multiple SWA branches are used as radiating antennas, with a main SWA used in a novel way as the feed. The procedure was explained through the example design of an 8×8-elliptical-slot SWA with SLR higher than 20 dB.

Most of the work in this chapter has been published by the author in [110].

Chapter 8

Conclusion

High Power Microwave technology has found its interest in various applications ranging from commercial to military applications, such as radar and communication systems, law enforcement, materials processing, and environmental protection. This thesis presented the main parts involved in HPM systems, starting with a brief description of the High Power Microwave generators, and then focusing on the design and improvement of two widely known antennas for such applications. The main objective in the antenna part was to design an antenna capable of radiating the high power generated wave in a pencil shape pattern, with high gain and low sidelobe levels.

In a summary of the chapters:

Chapter 1 introduced the idea behind the use of HPM and its main and widely known applications. It described the main components of an HPM system, and stated the main objectives of the thesis.

Chapter 2 investigated the major blocks of a high power microwave system, with a brief description of pulse forming lines and pulse forming networks, Blumlein transmission lines, Marx generator, and magnetrons, mainly used in such systems.

Chapter 3 investigated the first type of antennas studied and improved in this thesis,

the Vlasov antenna. The conventional Vlasov antenna was originally designed with a step cut made to one end of a circular waveguide, and has been improved by Nakajima who used a beveled cut instead of the step one. The bevel cut design gets rid of the sharp corners present in the former one, which makes the antenna supportive of higher microwave powers, but this came at the cost of reduced antenna gain and broader beam widths. In addition, the maximum radiation of these two antennas is shifted by some angle in the $\phi = 90°$ plane, assuming the antenna is directed along the +Z axis. In this chapter, an improved shape with curved cuts for High Power Microwaves applications has been suggested, leading to higher gain, decreased HPBW, and decreased sidelobe levels. In addition, two optimized reflectors, one with enhanced position, and the second with additional shape enhancement having curved edges, have been proposed, with the ability to radiate the maximum radiation back to the waveguide axis and further decrease the HPBW. This concept has been validated using the bevel- and step-cut Vlasov antenna, and with the new curved cut proposed in this thesis.

The second part of the improved antenna concerned the Slotted Waveguide Antenna systems:

Chapter 4 presented a simple procedure for designing SWAs with specified SLRs. General guidelines for the slots width, length, and longitudinal positions were first given. The offsets of the slots positions with respect to the waveguide centerline, which determine the SLR, were then obtained from well-known distributions. An intuitive rule regarding the used distribution was deduced, which was to select a distribution with an SLR 15 dB higher than the desired SWA SLR. This procedure was implemented using a Python computer program. Illustrative examples showing the distribution coefficients, slots displacements, resulting patterns and S_{11} plots were given. A prototype antenna was fabricated and tested, and the results were presented.

In fabrication and measurement procedure, the waveport will be transformed into a

coaxial port to be able to feed the fabricated system and measure its parameters. For this, Chapter 5 studied the SWA designed antenna in the presence of a coaxial feed instead of the wave port used in the simulations software. This chapter also served as an introduction to two-dimensional SWA system.

After investigating the design of one module Slotted Waveguide Antenna with a desired sidelobe level ratio in Chapter 4, Chapter 6 investigated the use of inclined coupling slots in the added feeder. For this, a simple procedure for the design of 2D slotted waveguide antenna arrays with desired SLRs, using inclined coupling slots in the main feeder, has been presented. Multiple SWA branches are used as radiating antennas, with a main SWA used in a as the feed. The procedure was explained through two examples designs of 8×8-elliptical-slot SWA arrays with SLR higher than 20 dB. Adding our contributions on the SWA design procedures, Chapter 7 presented an inventive and simple procedure for the design of a 2D slotted waveguide antenna having a desired sidelobe level ratio (SLR) and a pencil shape pattern, using longitudinal elliptical slots in both branches and feeder SWAs. The 2D array is formed by a defined number of 1D broadwall SWAs, which are fed using an extra broadwall SWA. For specified number of identical longitudinal slots in both dimensions, the desired SLR and the required operating frequency, this procedure finds the slots length, width, locations along the length of the waveguide, and offsets from its centerline. This is done for the radiating SWAs as well as the feed SWA. Two examples of SWA systems with 8×8 elliptical slots and 10×10 are designed using this procedure for an SLR higher than 20 dB, where the design results are also reported in this part of the thesis.

Nevertheless, in Appendix A, the basic definition and concept of the Method of Moment, previously used to numerically calculate the slots equations, has been presented.

Finally, future extensions and interesting research directions are currently un-

der study by the authors to further improve the designed antennas in terms of the sidelobe levels, frequency tunability, gain, and size.

Appendix A

The Method of Moment

The Method of Moment (MoM) is a very successful tool in solving complex geometry electromagnetic (EM) problems, and is considered as the first computational approach in solving these problems. This Appendix approaches MoM in a very simple way and aims to produce a valuable procedure to solving boundary value problems, especially n^{th} differential equations. Starting with the definition of the method, the problem is converted into its respective integral equation form, and then the unknown function is expanded into a sum of weighted basis functions, where the weight coefficients are to be found. The Galerkin method, which selects testing functions equal to the basic functions, is adopted. The problem then becomes a system of linear equations, which is solved analytically or numerically to find the needed weight coefficients. Two differential equation examples are considered to illustrate the application of the procedure, which can be used as well for the solution of other boundary-value problems, including the slotted waveguide antenna electric field calculations. The considered examples show the detailed calculation process and make it easier to understand the solution procedure.

A.1 Introduction

The design and analysis of electromagnetic devices and structures before the computer invention were largely depending on experimental procedures. With the development of computers and programming languages, researches began using them to solve the challenging electromagnetic problems that could not be solved analytically. This led to a burst of development in a new field called computational electromagnetics (CEM), for which powerful numerical analysis techniques, including the Method of Moment (MoM), have been developed in this area in the last 50 years [111]. Harrington in [112] describes the MoM as a simple numerical technique used to convert integro-differential equations into a linear system that can be solved numerically using a computer. When the order of the equation is small, MoM can analytically solve the problem in a general and very clear manner.

A large number of publications address the use of MoM in solving various problems. Djordjevic and Sarkar in [113] showed that the inner product involved in MoM is usually an integral, which is evaluated numerically by summing the integrand at certain discrete points. Newman in [114] has presented three simple examples on the use of MoM in electromagnetics. These examples deal with the input impedance of a short dipole, a plane wave scattering from a short dipole, and two coupled short dipoles. The use of MoM in electromagnetic field has been introduced by Serteller *et al.* in [115]. This is done by presenting examples and software program, and also by giving the curriculum needed to quickly learn the basic concepts of numerical solutions.

This chapter approaches MoM in a very simple way and aims to produce a valuable procedure to solving boundary value problems, especially differential equations. Starting with the definition of the method, the problem is converted into its

respective integral equation form, and then the unknown function is expanded into a sum of weighted basis functions, where the weight coefficients are to be found. The Galerkin method, which selects testing functions equal to the basis functions, is adopted. The problem then becomes a system of linear equations, which is solved analytically or numerically to find the needed weight coefficients. Two differential equation examples are considered to illustrate the application of the procedure, which can be used as well for the solution of other boundary-value problems, including the slotted waveguide antenna electric field calculations.

A.2   Method of Moments Solution Approach

As the Method of Moments is based on expanding the unknown solution of the differential equation into known expansion and testing functions that satisfy the boundary value constraints, it is advisable to first introduce this approach in the solution. Accordingly, the sough of solution is expanded into a sum of known function, each satisfying the boundary conditions of the problem, with unknown coefficients to be determined by the solution. This determination is done with the help of testing function chosen similarly as the expansion function for the simplicity of the solution. The resulting equation is then converted into a linear system of equations by enforcing the boundary conditions at a number of points. This resulting linear system is then solved analytically for the unknown coefficients. This approach is very simple and quite interesting when applied to differential equation of order less than 3, but it will get more complicated for equations of higher order.

Accordingly, it is advisable to start with some basic mathematical techniques for reducing functional equations to matrix equations. A deterministic problem is considered, which will be solved by reducing it to a suitable matrix equation, and hence

the solution could be found by matrix inversion. The examples that we will choose are simple and easily illustrate the theory without any complicated mathematics. Linear spaces and operators will be used in our solution. At first, it is recommended to introduce MoM and define some terms related to first order non-homogeneous differential equation. The choice of this equation is important only for better understanding of the solution.

A general n^{th} order linear differential equation, defined over a domain D, has the form:

$$a_n \frac{d^n f(x)}{dx^n} + a_{n-1} \frac{d^{n-1} f(x)}{dx^{n-1}} + ... + a_1 \frac{df(x)}{dx} + a_0 f(x) = g(x) \tag{A.1}$$

In Equation A.1, the coefficients $a_n, a_{n-1}, .. , a_1, a_0$ and $g(x)$ are known quantities, and $f(x)$ is the function whose solution is to be determined. Equation A.1 can be written in the form of an operator equation

$$L(f(x)) = g(x), \tag{A.2}$$

where L is the operator equation, operating on $f(x)$, and given by:

$$L = a_n \frac{d^n ...}{dx^n} + a_{n-1} \frac{d^{n-1} ...}{dx^{n-1}} + ... + a_1 \frac{d...}{dx} + a_0 ... \tag{A.3}$$

The solution of Equation A.1 is based on defining the inner product $\langle f, g \rangle$, a scalar quantity valid over the domain of definition of L, which is given by:

$$\langle f(x), g(x) \rangle = \int_D f(x) g(x) dx \tag{A.4}$$

Similarly, we define:

$$\langle L(f(x)), g(x) \rangle = \int_D L(f(x))g(x)dx \tag{A.5}$$

The first step in calculating the integral, using Method of Moments, is to expand f into a sum of weighted basis functions f_1; f_2; f_3; âĂȩ., in the domain of L, as:

$$f(x) = \sum_n \alpha_n f_n \tag{A.6}$$

Testing functions denoted w_1; w_2; w_3; ... are defined in the range of L. These testing functions are used for all values of n. Using the inner product defined in Equation A.5, we obtain:

$$\sum_n \langle w_m, L(f_n) \rangle = \langle w_m, g(x) \rangle \ for m = 1,2,3.... \tag{A.7}$$

Expanding A.7 over the values of m and $n = 1,2,3,$âĂȩ, the following matrix equation is then obtained

$$\begin{bmatrix} \langle w_1, L(f_1) \rangle & \langle w_1, L(f_2) \rangle & ... & \langle w_1, L(f_n) \rangle \\ \langle w_2, L(f_1) \rangle & \langle w_2, L(f_2) \rangle & ... & \langle w_2, L(f_n) \rangle \\ ... & ... & ... & \\ \langle w_m, L(f_1) \rangle & \langle w_m, L(f_2) \rangle & ... & \langle w_m, L(f_n) \rangle \end{bmatrix} \begin{bmatrix} \alpha_1 \\ \alpha_2 \\ ... \\ \alpha_n \end{bmatrix} = \begin{bmatrix} \langle w_1, g \rangle \\ \langle w_2, g \rangle \\ ... \\ \langle w_m, g \rangle \end{bmatrix} \tag{A.8}$$

In a simpler form,

$$[L_{mn}][\alpha_n] = [G_m], \tag{A.9}$$

131

and the solution for the unknown coefficients is then

$$[\alpha_n] = [L_{mn}]^{-1}[G_m] \tag{A.10}$$

In our calculations, we will choose the test function w_m equal to the basis function f_n, which is known as Garlekin method. The determination of matrix $[L_{mn}]$ is straightforward, and its inverse is easy to obtain either analytically or numerically. Once this is done, the α_n coefficients are obtained, and the solution for f is found.

It is good to note here that choosing the appropriate basis/test function is necessary to get fast to the accurate solution.

A.2.1   Example 1

Considering the following second order differential equation defined by:

$$\frac{d^2 f(x)}{dx^2} = x^2 \tag{A.11}$$

defined over the domain $D = [0,1]$ with the following boundary conditions $f(0) = f(1) = 0$. Starting by choosing the basis function, let us choose

$$f_n = x - x^{n+1} \tag{A.12}$$

It is clear from A.12, that the chosen basis functions meet the boundary conditions and can be considered as a solution to the problem. Substituting A.12 into A.6, the left-hand side elements of A.7, which are the elements of the matrix $[L_{mn}]$, are found to be:

$$
\begin{aligned}
L_{mn} = \quad &\langle w_m, L(f_n)\rangle = \int_0^1 (x - x^{m+1})\left(\frac{-d^2(x - x^{n+1})}{dx^2}\right) dx \\
= \quad &\int_0^1 (x - x^{m+1})(n(n+1)x^{n-1})dx \\
= \quad &\frac{mn}{n+m+1}
\end{aligned}
\tag{A.13}
$$

In the same manner, we compute the elements of the matrix $[G_m]$, defined in A.7, which are found to be:

$$
G_m = \langle w_m, g\rangle = \int (x - x^{m+1})x^2 dx = \frac{m}{4(m+4)}
\tag{A.14}
$$

Then, we start by choosing $N = 1$, for which $n = m = 1$ in L_{mn} and G_m, hence $L_{11} = 1/3$; $G_1 = 1/20$, $\alpha_1 = 3/20$, and $f(x)$ is given by:

$$
f(x) = \frac{3}{20}(x - x^2)
\tag{A.15}
$$

It is clear from A.1, that the function $f(x)$ does not meet the original differential equation defined in A.11. Accordingly, we need to increase the value of N.

Let $N = 3$, and calculating the values of L_{mn}, G_m, and α_n:

$$
\begin{bmatrix} L_{11} & L_{12} & L_{13} \\ L_{21} & L_{22} & L_{23} \\ L_{31} & L_{32} & L_{33} \end{bmatrix}
\begin{bmatrix} \alpha_1 \\ \alpha_2 \\ \alpha_3 \end{bmatrix}
=
\begin{bmatrix} g_1 \\ g_2 \\ g_3 \end{bmatrix}
$$
$$
\Downarrow
$$
$$
\begin{bmatrix} 1/3 & 1/2 & 3/5 \\ 1/2 & 4/5 & 1 \\ 4/5 & 1 & 9/7 \end{bmatrix}
\begin{bmatrix} \alpha_1 \\ \alpha_2 \\ \alpha_3 \end{bmatrix}
=
\begin{bmatrix} 1/20 \\ 1/12 \\ 3/28 \end{bmatrix}
\tag{A.16}
$$

Hence, α_n could be calculated as:

$$
\begin{bmatrix} \alpha_1 \\ \alpha_2 \\ \alpha_3 \end{bmatrix} = \begin{bmatrix} 0 \\ 0 \\ 1/12 \end{bmatrix} \tag{A.17}
$$

Finally, calculating $f(x)$:

$$
f(x) = \sum_n \alpha_n f_n = \alpha_1 f_1 + \alpha_2 f_2 + \alpha_3 f_3 = 1/12(x - x^4) \tag{A.18}
$$

The function $f(x)$ given in Equation A.18 meets the boundary conditions defined in Equation A.11, and accordingly it is the correct solution of the problem.

A.2.2 Example 2

Considering the following second order differential equation defined by:

$$
\frac{d^2 f(x)}{dx^2} = 8x^2 + 2x \tag{A.19}
$$

defined over the domain $D = [0,1]$ with the following boundary conditions $f(0) = f(1) = 0$. Starting by choosing the basis function, it was noted that the basis function used in Example 1 could also be used here:

$$
f_n = x - x^{n+1} \tag{A.20}
$$

The chosen basis functions meet the boundary conditions and can be considered as a solution to the problem. $[L_{mn}]$ is calculated as in Example 1, since the same basis function is used, and it is given by:

$$L_{mn} = \frac{mn}{n+m+1} \tag{A.21}$$

In the same manner, we compute the elements of the matrix $[G_m]$, defined in Equation A.21, which are found to be:

$$G_m = \langle w_m, g \rangle = \int (x - x^{m+1})(8x^2 + 2x)dx = \frac{m(8m+26)}{3(m+3)(m+4)} \tag{A.22}$$

Then, we start again by choosing $N = 1$ for which $n = m = 1$. Accordingly, $L_{11} = -1/3$; $G_1 = 17/30$, $\alpha_1 = 21/30$, and $f(x)$ is given by:

$$f(x) = \frac{21}{30}(x - x^2) \tag{A.23}$$

It is clear from Equation A.23, that the function $f(x)$ does not meet the original differential equation defined in Equation A.19. Accordingly, we need to increase the value of N.

Let $N = 3$, and calculating the values of L_{mn}, G_m, and α_n:

$$\begin{bmatrix} L_{11} & L_{12} & L_{13} \\ L_{21} & L_{22} & L_{23} \\ L_{31} & L_{32} & L_{33} \end{bmatrix} \begin{bmatrix} \alpha_1 \\ \alpha_2 \\ \alpha_3 \end{bmatrix} = \begin{bmatrix} g_1 \\ g_2 \\ g_3 \end{bmatrix}$$
$$\Downarrow \tag{A.24}$$
$$\begin{bmatrix} 1/3 & 1/2 & 3/5 \\ 1/2 & 4/5 & 1 \\ 4/5 & 1 & 9/7 \end{bmatrix} \begin{bmatrix} \alpha_1 \\ \alpha_2 \\ \alpha_3 \end{bmatrix} = \begin{bmatrix} 17/30 \\ 14/15 \\ 24/21 \end{bmatrix}$$

135

Hence, α_n could be calculated as:

$$\begin{bmatrix} \alpha_1 \\ \alpha_2 \\ \alpha_3 \end{bmatrix} = \begin{bmatrix} 0 \\ 1/3 \\ 2/3 \end{bmatrix} \tag{A.25}$$

Finally, calculating $f(x)$:

$$f(x) = \sum_n \alpha_n f_n = \alpha_1 f_1 + \alpha_2 f_2 + \alpha_3 f_3 = 1/3(x - x^3) + 2/3(x - x^4) = 2/3x^4 + x^3/3 - x$$
$$\tag{A.26}$$

The function $f(x)$ given in Equation A.26 meets the boundary conditions defined in Equation A.19, and accordingly it is the correct solution of the problem.

A.3 Conclusion

This Appendix presented, in simplified steps, the procedure of using the Method of Moments in solving simple differential equations of different orders. The considered examples show the detailed calculation process and make it easier to understand the solution procedure. As can be seen, this approach could be easily used to solve mathematical problems and equations. According to the type of the equation, the solution of the Moment Method will vary to accommodate for the change in the given problem.

Most of the work in this chapter has been published by the author in [116–118].

Bibliography

[1] J. Emanuelson, "An introduction to nuclear electromagnetic pulse," B.S.E.E. Futurescience, LLC, Tech. Rep.

[2] M. Abrams, "The Dawn of the e-bomb," *IEEE Spectrum*, vol. 40, p. 24âĂŞ30, 2003.

[3] J. Benford, J. Swegle and E. Schamiloglu, *High Power Microwaves, Second Editions*. Taylor & Francis, 2007.

[4] R. Barker and E. S. (Eds.), *High-Power Microwave Sources and Technologies*. IEEE Press, 2001.

[5] P. Bhartia and I. J. Bahl, *Millimeter Wave Engineering and Applications*. Wiley, 1984.

[6] V. Gaponov-Grekhov and V. L. Granatstein, *Applications of High-Power Microwaves*. Artech House, 1994.

[7] R. J. Barker and E. Schamiloglu, *High-Power Microwave Sources and Technologies*. IEEE Press, 2001.

[8] S. T. Pai and Q. Zhang, *Introduction to High Power Pulse Technology*. World Scientific, 1995.

[9] M. Abrams, "The Dawn of the E-bomb," *IEEE Spectrum*, vol. 40, no. 11, p. 24âĂŞ30, November 2003.

[10] D. V. Girig, *High Power Electromagnetic Radiators: Nonlethal Weapons and Other Applications*.   Harvard University Press, 2004.

[11] H. K. Florigs, "The Future Battlefield: A Blast of Gigawatts?" *IEEE Spectrum*, vol. 25, no. 3, p. 50âĂŞ54, March 1988.

[12] F. Vega and F. Rachidi, "Remote Activation of Improvised Explosive Devices in Colombia using High Power Electromagnetic Sources," *4th Annual Vehicle Survivability*, Berlin, Germany, 2011.

[13] F. Vega and F. Rachidi, "Use of High Power Electromagnetic Radiation for Remote Activation of Improvised Explosive Devices in Colombia," *4th Annual Defeating IEDs Training Workshops*, Brussels, Belgium, 2011.

[14] Geneva International Center for Humanitarian Demining (GICHD), A Study of Manual Mine Clearancer, Book 5: Manual Mine Clearance Costings and Sensitivity Analysis, [Online], Available: http://www.gichd.org/fileadmin/pdf/publications/Manual_Mine_Clearance_Book5.pdf.

[15] G. S. Ling and C. W. Yuan, "Design of a Vlasov Antenna with Reflector," *International Journal of Electronics*, vol. 91, no. 4, pp. 253–258, 2004.

[16] R. A. Gilbert, "Waveguide Slot Antenna Arrays," *Ch. 9, in J.L. Volakis (ed.), Antenna Engineering Handbook, 4th Edition, McGraw-Hill*, 2007.

[17] A. Haddad and D.F. Warne, *Advances in High Voltage Engineering*.   Institution of Engineering and Technology, 2004.

[18] G. A. Mesyat, *Pulsed Power*.   Springer, 2005.

[19] Pulse Forming Network, Wikipedia, [Online], Available: http://en.wikipedia. org/wiki/Pulse_forming_network.

[20] M. Joler, C. G. Christodoulou, and E. Schamiloglu, "Limitations to Compacting a Parallel-Plate Blumlein Pulse-Forming Line," *International Journal of RF and Microwave Computer-Aided Engineering*, vol. 18, no. 2, pp. 176–186, 2008.

[21] M. Joler, C. G. Christodoulou, E. Schamiloglu, and J. Gaudet, "Effects of Dielectric Width Extension in a Parallel-Plate Blumlein Line," *Microwave and Optical Technology Letters*, vol. 46, no. 3, pp. 220–225, 2005.

[22] J. Benford and J. Swegle, *High-Power Microwaves*. Artech House, 1992.

[23] R. Verma, A. Shyam, and K. G. Shah, "Design and Performance Analysis of Transmission Line-Based Nanosecond Pulse Multiplier," *Sadhana*, vol. 31, no. 5, p. , 2006.

[24] R. E. Collin, *Foundations for Microwave Engineering*. 2nd ed., Wiley-IEEE Press, 2000.

[25] L. G. Maloratsky, *Passive RF and microwave integrated circuits*. Elsevier, 2004.

[26] Marx Generator, [Online], Available: http://hibp.ecse.rpi.edu/~leij/febetron/ marx.html.

[27] J. Lux, "Marx Generators," *High Voltage Experimenter's Handbook*, May 1998.

[28] J. Kronjaeger, "Marx generator," *Jochen's High Voltage Page*, 2003.

[29] "The 'Quick & Dirty' Marx generator," *Mike's Electric Stuff*, May 2003.

[30] Steve Jurvetson, Flickr, [Online], Available: http://www.flickr.com/photos/44124348109@N01/3582475427.

[31] H. Li and H.-J. Ryoo and J.-S. Kim and G.-H. Rim and Y.-B. Kim and J. Deng., "Development of Rectangle-Pulse Marx Generator Based on PFN," *IEEE Transactions on Plasma Science*, vol. 37, no. 1, pp. 190–194, January 2009.

[32] S. M. Turnbull, S. J. MacGregor, J. Harrower, and F. A. Tuema, "A PFN High Voltage Marx Generator," *IEE Colloquium on Pulsed Power*, March 1996.

[33] S. J MacGregor, S. M. Turnbull, F. A. Tuema, and J. Harrower, "The Performance of a Simple PFN Marx Generator," *Twenty-Second Internationl Power Modulator Symposium*, June 1996.

[34] E. Kuffel, W. S. Zaengl, and J. Kuffel, *High voltage engineering: fundamentals*. Newnes, 2000.

[35] Marx generator, Wikipedia, [Online], Available: http://en.wikipedia.org/wiki/Marx_generator.

[36] "A multiphysics approach to magnetron and microwave oven design," White Paper, CST AG, 2013.

[37] Magnetron Theory of Operation, Communication and Power Industries, Beverly Microwave Division, [Online], Available: http://www.cpii.com/docs/related/2/Mag%20tech%20art.pdf.

[38] Cavity magnetron, Wikipedia, [Online], Available: http://en.wikipedia.org/wiki/Cavity_magnetron#Radar.

[39] C. G. Montgomery, R. H. Dicke, and E. M. Purcell, *Principles of Microwave Circuits*. Peter Peregrinus Ltd., London, 1987, chap. 10.

[40] S. N. Vlasov, L. I. Sagryadskaya, and M. I. Petelin, "Transformation of a Whispering Gallery Mode, Propagating in a Circular Waveguide, into a Beam of Waves," *Radio Eng.*, vol. 12, no. 10, pp. 14–17, 1975.

[41] S. N. Vlasov and I. M. Orlova, "Quasioptical Transformer which Transforms the Waves in a Waveguide Having a Circular Cross Section into a Highly Directional Wave Beam," *Radiophysics and Quantum Electronics*, vol. 17, no. 1, pp. 115–119, 1974.

[42] S. N. Vlasov and I. M. Orlova, "Quasi-optical Transformer which Transforms the Waves in a Circular Waveguide to a Highly Directional Beam of Waves," *Radiophysics Quantum Electronics*, pp. 148–154, 1974.

[43] H. Zhou and X. Yang, "Design of Novel VLASOV-type Antennas for High Power Microwaves (HPM)," *IEEE 34th International Conference on Plasma Science*, p. 912, 2007.

[44] O. Wada and M. Nakajima, *EC6 Joint Workshop on ECE and ECRH*, 1987.

[45] B. G. Ruth, R. K . Dahlstrom, C. D. Schlesiger, and L. F. Libelo, "Design and Low-power Testing of a Microwave Vlasov Mode Converter," *IEEE MTT-S International Microwave Symposium Digest*, vol. 3, pp. 1277–1280, 1989.

[46] C. Vollaire, L. Nicolas, K. A. Conner, S .J. Salon, B. G. Ruth and L. F. Libelo, "Microwave radiation from slant cut cylindrical antennas-modeling an experiment," *IEEE Transactions on Magnetics*, vol. 34, no. 5, pp. 2712–2715, 1998.

[47] P. J. Sealy and R. J. Vernon, "Low-power Investigation of TE_{0n} and TM_{0n} Mode Vlasov Launchers (Gyrotron Applications)," *Antennas and Propagation Society International Symposium*, vol. 2, pp. 950–953, 1989.

[48] P. J. Sealyand and R. J. Vernon, "Equivalence-principle Model for Radiation from TE_{0n} and TM_{0n} Mode Step-cut and Slant-cut Vlasov Feeds," *Antennas and Propagation Society International Symposium*, vol. 3, pp. 1836–1839, 1991.

[49] R. K. Dahlstrom, L. J. Hadwin, B. G. Ruth, and L. F. Libelo, "Reflector Design for an X-Band Vlasov Antenna," *Antennas and Propagation Society International Symposium*, vol. 2, pp. 968–971, 1990.

[50] M. Fazaelifar and M. R. Fatorehchy, "Design, Fabrication and Test of Parabolic Cylinder Reflector and Horn for Increasing the Gain of Vlasov Antenna," *Progress In Electromagnetics Research Letters*, vol. 4, pp. 191–203, 2008.

[51] X. Zhang, Q. Wang, Y. Cheng and S. Wen, "Design of A 220GHz Vlasov Antenna Mode Converter," *International Workshop on Microwave and Millimeter Wave Circuits and System Technology*, pp. 1–2, 2012.

[52] J. A. Lorbeck and R. J. Vernon, "Singly Curved Dual-reflector Synthesis Technique Applied to a Quasi-optical Antenna for a Gyrotron with a Whispering-gallery Mode Output," *IEEE Transactions on Antennas and Propagation*, vol. 39, no. 12, pp. 1733–1741, 1991.

[53] B. Wang, C. -H. Du, P. -K. Liu, Z. -H. Geng and S. -X. Xu, "P3-12: Study of a Vlasov Mode Converter for 94GHz Whispering Gallery Mode Gyrotron," *IEEE International Vacuum Electronics Conference*, pp. 353–354, 2010.

[54] J. Braunstein, K. Connor, S. Salon, L. Libelo and C. D. Schlesiger, "Analysis of Flared end For Vlasov-type Antenna: Comparison of 2D Finite Element Analysis with Experiment," *IEEE Transactions on Magnetics*, vol. 30, no. 5, pp. 3120–3123, 1994.

[55] P. J. Sealy, R. J. Vernon and J. A. Lorbeck, "Vlasov feeds with corrugated flares for pattern enhancement," *Antennas and Propagation Society International Symposium*, vol. 1, pp. 714–717, 1995.

[56] A. D. R. Phelps, P. R. Winning and S. N. Spark, "Broadband Quasi-optical Mode Converters for High Power Microwaves," *IEEE Colloquium on Antenna and Propagation Problems of Ultrawideband Radar*, 1993.

[57] T. A. Spencer, C. E. Davis, K. J. Hendricks, R. M. Gilgenbach and M. J. Arman, "Long-pulse Hyrotron-backward-wave Oscillator Experiments," *IEEE International Conference on Plasma Science*, 1993.

[58] B. Wang, C. H. Du, P. K. Liu, Z. H. Geng and S. X. Xu, "Study of a Vlasov Mode Converter for 94GHz Whispering Gallery Mode Gyrotron," *IEEE International Vacuum Electronics Conference*, pp. 353–354, 2010.

[59] H. M. El Misilmani, M. Al-Husseini, K. Y. Kabalan, and A. El-Hajj, "Optimized Reflector Position for Vlasov Antennas," *Progress In Electromagnetics Research Symposium*, pp. 139–143, 2013.

[60] H. M. El Misilmani, M. Al-Husseini, K. Y. Kabalan and A. El-Hajj, "Improved Vlasov Antenna with Curved Cuts for High Power Microwaves," *International Conference on High Performance Computing and Simulation*, pp. 362–365, 2013.

[61] H. M. El Misilmani, M. Al-Husseini, and K. Y. Kabalan, "Improved Vlasov Antenna with Curved Cuts and Optimized Reflector Position and Shape," *International Journal of Antennas and Propagation*, vol. 2015, pp. 1–12, 2015.

[62] R. A. Gilbert, *Antenna Engineering Handbook.* McGraw-Hill, 2007, ch. Waveguide Slot Antenna Arrays.

[63] R. J. Mailloux, *Phased Array Antenna Handbook.* Artech House, 2005.

[64] W. Rueggeberg, "A Multislotted Waveguide Antenna for High-Powered Microwave Heating Systems," *IEEE Trans. Ind. Applicat.*, vol. IA-16, no. 6, pp. 809–813, 1980.

[65] R. S. Elliott and L. A. Kurtz, "The Design of Small Slot Arrays," *IEEE Trans. Antennas Propagat.*, vol. 26, pp. 214–219, March 1978.

[66] R. S. Elliott, "The Design of Traveling Wave Fed Longitudinal Shunt Slot Arrays," *IEEE Trans. Antennas Propagat.*, vol. 27, no. 5, pp. 717–720, September 1979.

[67] A. F. Stevenson, "Theory of Slots in Rectangular Waveguides," *Journal of Applied Physics*, vol. 19, pp. 24–38, 1948.

[68] R. S. Elliott, "An Improved Design Procedure for Small Arrays of Shunt Slots," *IEEE Trans. Antennas Propagat.*, vol. 31, pp. 48–53, January 1983.

[69] R. S. Elliott and W. R. O'Loughlin, "The Design of Slot Arrays Including Internal Mutual Coupling," *IEEE Trans. Antennas Propagat.*, vol. 34, pp. 1149–1154, September 1986.

[70] R. S. Elliott, "Longitudinal Shunt Slots in Rectangular Waveguide: Part I, theory," Rantec, Calabasas, CA, Rantec Report No. 72022-TN-1, Tech. Rep., November 1951.

[71] R. S. Elliott , *Antenna theory and Design. Revised Edition.* John Wiley & sons, 2003.

[72] Y.-M. Zhang, Z.-J. Zhang, X.-P. Lu, "Design of Ultralow Sidelobe Antenna Arrays with Inclined Slots in the Narrow Wall of Rectangular Waveguide," *Proceedings of the International Radar Conference*, pp. 437–441, 2003.

[73] D. Dogan, O. A. Civi, "Edge Wall Slotted Waveguide Antenna with Low Cross Polarization," *IEEE Antennas and Propagation Society International Symposium (APSURSI)*, pp. 1–4, July 2010.

[74] W. Wang, J. Jin, J.-G. Lu, and S.-S. Zhong, "An Untilted Edge-Slotted Waveguide Antenna Array Design," *3rd International Conference on Computational Electromagnetics and Its Applications*, pp. 208–211, 2004.

[75] C. E. Baum, "Sidewall Waveguide Slot Antenna for High Power," *Sensor and Simulation Note 503*, August 2005.

[76] M. Al-Husseini, A. El-Hajj, and K. Y. Kabalan, "High-gain S-band Slotted Waveguide Antenna Arrays with Elliptical Slots and Low Sidelobe Levels," *PIERS Proceedings*, Stockholm, Sweden, August 12-15, 2013.

[77] C. T. Tai, "Characteristics of liner antenna elements," in *Antenna Engineering Handbook*, H. Jasik, Ed. McGraw-Hill, 1961.

[78] A. A. Oliner, "The Impedance Properties of Narrow Radiating Slots in the Broad Face of Rectangular Waveguides," *IEEE Transactions on Antennas and Propagation*, vol. AP-5, no. 1, pp. 4–20, 1058.

[79] R. J. Stegan, "Longitudinal shunt slot characteristics," Hughes Aircraft Company, Technical Memorandum, No. 261, November 1951.

[80] R. J. Stevenson, "Theory of Slots in Rectangular Waveguide," *J. App. Phy.*, vol. 19, pp. 4–20, 1948.

[81] W. H. Watson, "Resonant Slots," *Journal of the Institution of Electrical Engineers - Part IIIA: Radiolocation*, vol. 93, pp. 747–777, 1946.

[82] W. Coburn, M. Litz, J. Miletta, N. Tesny, L. Dilks, C. Brown, and B. King, "A Slotted-Waveguide Array for High-Power Microwave Transmission," *Army Research Laboratory*, January 2001.

[83] A. L. Cullen, "Laterally Displaced Slot in Rectangular Waveguide," *Wireless Eng.*, pp. 3–10, January 1949.

[84] K. L. Hung and H. T. Chou, "A Design of Slotted Waveguide Antenna Array Operated at X-band," *2010 IEEE international Conference on Wireless Information Technology and System*, pp. 1–4, 2010.

[85] A. Safaai-Jazi, "A New Formulation for the Design of Chebyshev Arrays," *IEEE Trans. Antennas Propag.*, vol. 42, pp. 439–443, 1980.

[86] A. El-Hajj, K. Y. Kabalan, and M. Al-Husseini, "Generalized Chebyshev Arrays," *Radio Science*, vol. 40, RS3010, June 2005.

[87] T. T. Taylor, "One Parameter Family of Line-Sources Producing Modified Sin(π u)/ πu Patterns," *Hughes Aircraft Co. Tech.*, Mem. 324, Culver City, Calif., Contract AF 19(604)-262-F-14, September 4, 1953.

[88] C. A. Balanis, *Antenna Theory Analysis and Design*. Wiley, 2005.

[89] K. Y. Kabalan, A. El-Hajj, and M. Al-Husseini, "The Bessel Planar Arrays," *Radio Science*, vol. 39, no. 1, RS1005, Jan. 2004.

[90] J. M. Meek and J. D. Craggs, *Electrical Breakdown of Gases*. John Wiley and sons, 1978.

[91] A. Hong, "Dielectric Strength of Air," *The Physics Factbook*, 2000.

[92] G. F. Knoll, *Radiation Detection and Measurement, third edition.* John Wiley and sons, 2000.

[93] H, Jasik, *Antenna Engineering Handbook.* McGraw-Hill Book Co., 1961.

[94] J. L. Allen and B. L. Diamond, "Mutual coupling in array antennas," Lincoln Lab., MIT, Technical Report EDS-66âĂŞ443, October 4, 1966.

[95] H. Gruenberg, "Theory of Wave-Guide-Fed Slots Radiating into Parallel-Plate Regions," *Journal of Applied Physics*, vol. 23, no. 7, pp. 733–737, July 1952.

[96] A. L. Cullen, "Laterally Displaced Slot in Rectangular Waveguide," *Wireless Eng.*, pp. 3–10, January 1949.

[97] M. J. Ehrlich and J. Short, "Mutual Coupling Considerations in Liner-Slot Array Design," *Proc. IRE*, pp. 956–961, June 1953.

[98] I. P. Kaminow and R. J. Stegan, "Waveguide Slot Array Design," Hughes Aircraft Company, Technical Memorandum, No. 348, July 1954.

[99] H. M. El Misilmani, M. Al-Husseini, and K. Y. Kabalan, "Design of slotted waveguide antennas with low sidelobes for high power microwave applications," *Progress In Electromagnetics Research C*, vol. 56, pp. 15–28, 2015.

[100] H. M. El Misilmani, M. Al-Husseini, K. Y. Kabalan, and A. El-Hajj, "A Design Procedure for Slotted Waveguide Antennas with Specified Sidelobe Levels," *International Conference on High Performance Computing & Simulation*, pp. 828–832, 2014.

[101] Times Microwave Systems, [Online], Available: http://www.timesmicrowave. com/downloads/products/LMR-400.pdf/.

[102] U. Schulz, "A Flat Low-Cost Slotted Waveguide Antenna Array," *21st European Microwave Conference*, vol. 1, pp. 635–640, 1991.

[103] K.-L. Hung and H.-T. Chou, "A Design of Slotted Waveguide Antenna Array Operated at X-band," *IEEE International Conference on Wireless Information Technology and Systems (ICWITS)*, pp. 1–4, 2010.

[104] Z. Wasim, R. A. Bhatti, and J. K. Kayani, "Design, Fabrication and Testing of a Millimeter Wave Slotted Waveguide Antenna," *International Bhurban Conference on Applied Sciences Technology (IBCAST)*, pp. 55–57, January 2007.

[105] S. S. Sekretarov, D. M. Vavriv, "A Wideband Slotted Waveguide Antenna for SAR Systems," *European Microwave Conference (EuMC)*, pp. 232–235, 2009.

[106] X.-P. Li, S.-H. Zhang, Y.-B. Yang, and Z.-Y. Li, "Design and Thermal-analysis of A Slotted Waveguide Antenna Array for W-band Applications," *International Conference on Microwave and Millimeter Wave Technology (ICMMT)*, pp. 1–4, May 2012.

[107] R. A. Bhatti, B.-Y. Park, Y.-T. Im, and S.-O. Park, "Design of a Planar Slotted Waveguide Array Antenna for X-band Radar Applications," *Journal of the Korean Institute of Electromagnetic Engineering and Science*, vol. 11, no. 2, pp. 97–104, June 2011.

[108] S. S Sekretarov, A. V. Somov, and D. M. Vavriv, "Large-Aperture Slotted-Waveguide Antenna Arrays: Development and Fabrication Advances," *VIII International Conference on Antenna Theory and Techniques (ICATT)*, pp. 22–27, September 2011.

[109] H. M. El Misilmani, M. Al-Husseini, and K. Y. Kabalan, "Design Procedure for 2D Slotted Waveguide Antenna with Inclined Coupling Slots for Sidelobe Level Control," *Proc. Progress In Electromagnetics Research Symposium (PIERS)*, 2015.

[110] H. M. El Misilmani, M. Al-Husseini, K. Y. Kabalan, and A. El-Hajj, "Design Procedure for 2D Slotted Waveguide Antenna with Controllable Sidelobe Level," *Proc. IEEE International Symposium on Antennas and Propagation (APS)*, 2015.

[111] W. C. Gibson, *The Method of Moments in Electromagnetics*. Chapman & Hall/ CRC, Taylor & Francis group, 2008.

[112] R. F. Harrington, *Field Computation by Moment Methods*. Krieger Publishing Co., Inc, 1968.

[113] A. R. Djordjevic and T. K. Sarkar, "A Theorem on the Moment Method," *IEEE Transactions on Antennas and Propagation*, vol. 35, no. 3, pp. 353–355, March 1987.

[114] E. H. Newman, "Simple Examples of the Method of Moments in Electromagnetics," *IEEE Transactions on Education*, vol. 31, no. 3, pp. 193–200, August 1998.

[115] N. F. O. Serteller, A. G. Ak, G. Kocyigit, and T. C. Akinci, "Experimental Study of Moment Method for Undergraduates in Electromagnetic," *Journal of Electronics and Electrical Engineering*, vol. 3, no. 3, pp. 115–118, 2011.

[116] H. M. El Misilmani, K. Y. Kabalan, M. Abou Shahine, and M. Al-Husseini, "A Method of Moment Approach in Solving Boundary Value Problems," *Journal of Electromagnetic Analysis and Applications*, vol. 7, no. 3, 2015.

[117] H. M. El Misilmani, K. Y. Kabalan M. Abou Shahine, and M. Al-Husseini, "A Method of Moment Approach in Solving Boundary Value Problems," *Proc. the First Irbid International Engineering Conference (IIEC)*, Jordan, October 2014.

[118] H. M. El Misilmani, M. Abou Shahine, M. Al-Husseini, and K. Y. Kabalan, "A Simplified Method of Moment (MoM) Approach to solving nth Order Linear Differential Equations," *Int. Journal of Scientific & Engineering Research*, vol. 5, no. 6, 2014.